cience and Engineering Center
University of Wisconsin-Madison

A Final Report to
National Aeronautics and Space Administration
for
Atlantic Ocean Satellite Rain Maps for GALE

A REPORT from the

Cooperative Institute for Meteorological Satellite Studies

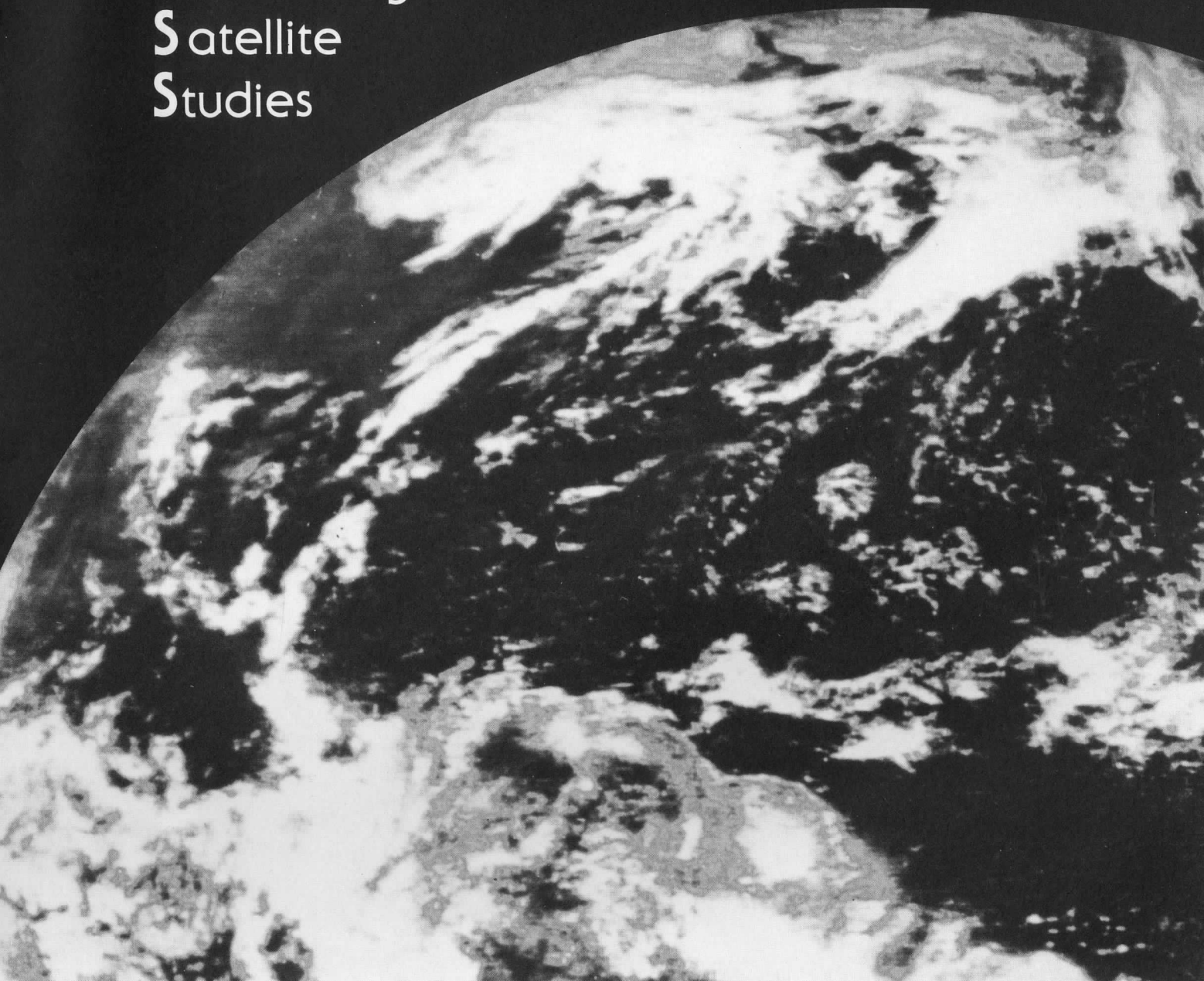

A Final Report to

National Aeronautics and Space Administration

for

Atlantic Ocean Satellite Rain Maps for GALE

A Final Report to

National Aeronautics and Space Administration

for

Atlantic Ocean Satellite Rain Maps for GALE

Contract #NAG5-742

University of Wisconsin Account #144X701

for the period of

1 October 1985 through 14 April 1988

submitted by

David W. Martin
Brian Auvine
Barry Hinton

Space Science and Engineering Center
at the University of Wisconsin-Madison
1225 West Dayton Street
Madison, Wisconsin 53706
(608)262-0544

April 1988

TABLE OF CONTENTS

I. INTRODUCTION

In support of GALE the Rain Studies Group at the University of Wisconsin - Madison has made two sets of maps of Atlantic Ocean rainfall. One set, which has been published in a quick look atlas (Martin and Auvine, 1987) concerns 24-hour rainfall. The other set, which has not been published previously, concerns 6-hour rainfall. Funding has limited both sets to parts of the GALE period. All of the maps are based entirely on information extracted from geostationary satellite images. This report presents a final set of both types of maps. It also describes the process by which the maps were made, assesses their accuracy, highlights the main features contained within them and recommends several possibilities for further work.

II. DATA

The maps are derived from digital infrared images of the GOES-6 satellite. Pixel resolution was 4 km at the subpoint of the satellite; about 5 km near the center of the map domain. Nominal time resolution was 1 hour. Very few of the processed images contained defects of any kind. From landmarks we estimate that absolute errors in pixel location are less than three pixels.

III. PROCESSING

Rainfall was estimated by the Global Precipitation Index (GPI) technique of Arkin (1983; also see Arkin and Meisner, 1987). This technique assumes that rainfall is linearly related to fractional cloud cover. 235 K is the threshold temperature for cloud. Ordinarily, the area, or box, for the measurement of GPI cloud cover is 2.5 degrees in

latitude and longitude and the interval between infrared images is 3 hours. In the present case a box is 1 degree in latitude and longitude and the image interval is 1 hour.

Fractional cloud covers (f) are averaged for the period of the estimate, then are related to rainfall ($\hat{R}$;mm) as

$$\hat{R} = k \bullet f$$

The coefficient $\underline{k}$ has a value of 72 mm d^{-1}.

Fields of rainfalls, consisting of one estimate for each box, were contoured by means of a standard microcomputer plot package (Plot 88 by Plotworks). For convenience the maps are presented in rectangular format. However, the area for which rain information actually is available is a trapezoid oriented northeast-southwest. Long-dashed lines mark the northwest and southeast sides of this trapezoid. A dotted line marks the southeast coast of the United States and Canada and islands of the western Atlantic.

The 19 daily maps are listed in Table 1 and presented in Appendix 1. Except for 21 and 22 January all maps are drawn from the Intensive Observing Periods. Nominally, days begin with the 00 UTC satellite image and end with the 23 UTC image.

Rainfall is contoured in units of millimeters. With one exception the increment between contours is 10 mm. The exception is the lowest contour, which marks values of 0.1 mm. This contour is dashed.

One correction has been made to the daily map set presented by Martin and Auvine (1987). The grid has been replotted to remove a scaling error in longitude (up to 2.5 degrees on the eastern edge, with the corrected image covering a broader strip of longitude) and repositioned to remove an offset (.5 degree in latitude and in

longitude, with the corrected image displaced to the north and east). Two changes also have been made. First, present maps for 21 and 22 January include a full set of GOES images. Second, the remaining seven maps which in the Martin/Auvine report contained less than 12 images have been dropped.

The 6-hour maps are identical to the 24-hour maps except in the following respects:

-- Their period spans the first two Intensive Observing periods and is continuous over the eleven days beginning at 00 UTC on 18 January;

-- In all but one case (1/18, 6-11 UTC, five images), maps are based on six infrared images.

IV. COMPARISONS WITH GAUGE RAINFALL

The coefficient we have used for these maps was derived for tropical marine regimes. Arkin (personal communication, 1986) predicted that its use in the present context would overestimate actual rainfall, that the overestimate would increase with latitude and that random errors would in general be larger than those to be expected in estimates of monthly tropical rainfall. In this section we compare satellite estimates with gauge measurements of rainfall.

A. PREMISES

Rainfall has variability in time and space. The scales of the variability depend upon the climatic regime as well as the specific synoptic situation producing it. Thus, it is possible to specify even the characteristic dimensions and durations of rain "events" only by glossing over much detail.

For the GALE data set, the a priori estimated characteristic time scale at a fixed geographic location and the characteristic spatial scale at a fixed time are the order of 1000 s and 10 kilometers respectively. This means that the rain value of each 1 degree latitude by 1 degree longitude by 6 hour resolution cell could be the mean of as many as 10^9 "independent events." However, if we account for the longer persistence of a rain system in a coordinate frame moving with the storm (at a speed the order of 5 ms^{-1}), the precipitation could cut entirely across the 1 degree by 1 degree spatial cell with a characteristic width of 10 km in six hours. Thus, a more realistic estimate of the number of independent rain "events" realized in a resolution cell would be the order of 10 for six hour accumulations. That this is the case will be verified later.

In the evaluation discussed below we first compare our estimates (in some instances interpolated to rain gauge locations) for a subset of the GALE data with the observations of individual rain gauges integrated over six hours. The rain gauge data is a "proxy" data set for true areal average rain. In view of this and the above paragraph, this comparison is a severe test. Consequently, for an alternative appraisal, it is appropriate to compare aggregated results with means formed from groups of the order of ten 6-hourly rain gauge observations. This simulates a more nearly ideal distribution of "truth data." There is no other practical approach in view of the very low density of rain gauges available--even with the special field program deployment.

B. COMPARISONS WITH INDIVIDUAL GAUGES

First we consider the statistical distributions of 6-hour rainfall both for the gauges and for the estimates. These are shown in Table 2.

Because rain is strictly non-negative, these are unsymmetrical and highly peaked at zero. The parts of the distribution for non-zero rain accumulation are well described by exponential, gamma or lognormal distributions as illustrated in Figs. 1 and 2.

The sharpness of the peak is reduced by any process which increases the integration (i.e., area, or time averaging), which accounts for part of the difference between the gauge observations and the estimates. Further difference may arise from the lack of discrimination of high rain rates by the estimation algorithm, which has absolute maximum 6-hourly accumulation of 18 mm. Thus, gauge observations are more skewed toward higher rain rates.

The selection of a specific analytic representation of the probability distributions is not required. The ones in the figures are for illustrative purposes only. However the parameter values for each are optimum for that particular distribution. Since the distributions of the rain estimates and the gauge data are not the same shape (i.e., similar in skewness and kurtosis) there is no elementary linear relation that will correctly transform rain rate determined by one into rate determined by the other for the entire range of rates, or even for the important range of rates. The main point to be made is that the gauge data especially are far from normally distributed, but would become more so, according to the central limit theorem, if each gauge "datum" were a more highly aggregated quantity, such as a mean value from several gauges, or averaged over a longer time period.

It is interesting to consider the instances in which the estimates indicate there is no rain, but gauge observations report rain (detection failure). The complementary failure in which the estimation suggests

rain, but there is no rain (false alarm), is not so easy to assess because of the inadequacy of the gauge network. Nevertheless the apparent false alarm rate is a useful quantity, since it provides an estimated upper limit on the true false alarm rate.

The cases are distributed among the four classes: (1) detection failure, (2) apparent false alarm rate, (3) success (rain-estimated and rain-observed), and (4) apparent success (no rain estimated and no rain observed). Elsewhere in this report we refer to classes (2) and (4) together as potential false alarm cases. The relative numbers of cases in each of the four classes are shown in Fig. 3.

Only the detection failure sector unambiguously points to a defect of the estimation scheme. The false alarm sector might well be due to the non-representativeness of the gauges. The "no rain estimated-no rain observed" case is alternatively not a measure of success since such a situation could arise from coincidental failure of the algorithm and inadequacy of the gauge network.

Quantitative comparisons are somewhat more interesting than the categorical comparison of Fig. 3. Consider Fig. 4, a simple scatter plot of interpolated estimates as a function of gauge observations. This figure manifests much of what was stated above: A concentration of points at low rain rates, a line of false alarms for various y-values at $x = 0$, a short row of points for various small x-values at $y = 0$, and a broad cloud of points. Together these points show a modest positive correlation ($r = 0.40$). It is easy to envision from this plot that, corresponding to any value of estimated rain, there is not a unique value of actual rain, rather there is a probability distribution of actual rain, from which the sample gauge observations are drawn. We

should not expect the points to lie along a simple curve, as would be the case if the two types of observation were connected by an elementary deterministic physical law. What we hope for then, is to discover the relationship of the mean of actual rain (approximated by the gauge observations) as a function of the estimated rain. Least-squares regressions are a suitable means of investigating this relationship.

The results of regression of the estimates on the gauges are shown in Table 3. This model consists of a constant plus a linear term. We note from the table that the constant term is surprisingly large, but rather poorly determined. On this ground, as well as our firm expectation that the mean rain rate ought to be nil when it is estimated to be so, we also present results for a second regression in Table 4. In this case we have constrained the constant to be zero. Note that r^2 in this case (Table 4) refers to the moment about 0, not about the mean, hence its much larger value. The salient result from Table 4 is that this model is about as good as the one incorporating the constant term.

In order for the significance test results shown in the table to be valid, the residuals must satisfy the normality assumption used in deriving the tests. Since the data themselves were seen to be very non-normal, it is worthwhile to verify this for the residuals. For this purpose we exhibit Fig. 5. The y-axis on these probability plots is scaled such that a normal distribution will lie along a straight line. Therefore, the plots show the poor approximation normality of the residuals.

It is interesting to consider the relation of gauge observations and the estimates when all potential false alarms are eliminated. That is, we only consider the cases for which gauge-recorded 6-hour rainfall

exceeds zero. In this circumstance the linear coefficient is somewhat larger (Table 5), especially if we choose the regression for which the constant term is zero (Table 6). There is no substantial difference between the standard errors of the two regressions, but the latter would be preferred on physical grounds. Additionally, the constant term is poorly determined and its "spread" includes zero. In any case, the regression of Table 6 results in a linear coefficient of 0.94. By eliminating the potential false alarms, the means (and other distribution parameters) of the gauges and estimates are brought somewhat more in accord, as shown in Table 7.

The locations of the array of gauge locations used for comparison are shown in Fig. 6. This illustrates that we have the order of one or two gauges per cell. Moreover, it is instructive to consider the gauge-gauge correlations (Table 8). The table suggests, because of many low gauge-gauge correlations, the possibility that the low value of the estimate-gauge correlation, mentioned above, might be attributable to the spatial variation of rain combined with the "point" nature of gauges. Thus comparisons with individual gauges may have only a little relevance to assessment of the estimation algorithm's skill for estimating area average rain over 1 degree squares, tending to give a somewhat pessimistic evaluation. Perhaps we should not ignore the "error" of the gauge measurements with respect to the desired area average.

This leads naturally to a reconsideration of the regression illustrated in Table 3. In this case the prescription is that the rain estimates $\hat{R}$ should be modified or replaced by a new estimate,

$$\tilde{R} = [a + b \cdot \hat{R}]$$

to achieve an improvement. The a,b are the regression coefficients from Table 3, or from Table 4 (for which a = 0). In either case, the regression line was obtained by minimizing the sum of the squares of the y-deviations only. This is equivalent to assuming that the gauge data are "perfect." However, they are <u>not</u> perfect measures of area average rainfall as indicated above.

If one wants to minimize the sum of the squares of the x-deviation plus the squares of the y-deviation, then it can be shown that the constant must be chosen so that the curve passes through the centroid of the data, and has a slope equal to the ratios of the standard deviations. This is the appropriate procedure if the gauges and estimation contribute equally to the scatter about the regression line.

There is yet a third logical possibility. Since the gauge data are intrinsically point measurements, while the GPI is intrinsically an area measurement, it is conceivable that the GPI estimate errors are much smaller than the gauge errors for area averaged rain. In this event one would minimize the sum of the squares of the x-deviations only. After considering the further possibility of aggregating, or averaging, gauge data, we shall illustrate how the assumed apportionment of error affects the regression curves.

C. COMPARISONS WITH AGGREGATED GAUGE MEASUREMENTS

The rhetorical question, "How big an area does a gauge represent when averaged over six hours?" can be investigated by considering the inter-gauge correlations, and especially their variation with distance. The correlations and distances are displayed in Table 8. A scatter plot, Fig. 7, is somewhat more instructive, however. The figure suggests that the inter-gauge correlation falls to the level of the

correlation between estimated rain and gauges at a distance of about 90 km. To view the gauge data as "truth" requires working at correlations such that the square of the gauge-gauge correlation is much greater than the square of the estimate-gauge correlation.

If we say that it is sufficient for the square of the gauge-gauge correlation to be at least three times the square of the estimate-gauge correlation, then we conclude that the gauge-gauge correlation should be 0.69, or more. This follows from the correlation of estimates to gauges of about 0.4 cited earlier. Thus, the gauge-gauge correlation should be the square root of $3 \cdot (0.4)^2 = 0.69$. Fig. 7 thus suggests no more than 30 km as a safe coverage zone radius for a rain gauge averaged over six hours. This is equivalent to about 10 to 12 evenly distributed rain gauges per one degree square near 30°N latitude. Thus the inter gauge correlation data support the estimate of about 10 gauges per one degree square given above.

Since the gauge data are linear, they can be added. The GPI algorithm is also linear because histograms "add" and rain is a linear function of histogram classes. Thus, one can average the rain estimates corresponding to 10 or 12 gauge observations and compare them with the average of the gauge observed rain, to simulate better an ideal truth data set, and obtain a better evaluation of the estimation algorithm.

One result of this procedure is displayed in Table 9, which gives regression results for a constant plus linear term. The table shows that the constant is very small and need not be included since it is also rather poorly determined. Thus we reran the regression excluding the constant term, obtaining the results in Table 10. Both regressions exhibit satisfactorily the normal distribution of deviations (Fig. 8),

since they are substantially the same. In either case the linear coefficient has value of about 0.81.

Why are the results better than for the comparisons of individual observations? The probable answer is that the aggregated data do not violate the normality assumption as strongly as the original data. The large peak of the data is pushed slightly away from zero, allowing for both positive and negative deviations of the estimated data from the gauge data. (Compare Fig. 5 with Fig. 9.) In the same way the skewness of the data distribution is reduced, which is more favorable. (For a linear regression to work perfectly, the distributions of both the dependent and the independent variable must have the same standardized skewness and kurtosis.)

Fig. 9 shows the range of relationships we have discussed between the gauge observed 6-hour rain accumulations and the estimates obtained from the infrared threshold algorithm.

While we leave the selection of the "best" relationship to the reader, our own preference is for (a), (c) or a compromise between them. In producing the maps curve (a) was selected.

V. PATTERNS

In spite of interruptions to the record, certain patterns do emerge in the daily maps. Overall, rainfall apparently is heavier in the north than in the south. Everywhere its preferred scale is distinctly larger than that of the estimation grid. Frequently the rain is banded from northeast to southwest.

Although not as extensive as the daily maps, the 6-hour maps have the advantage of continuity. Over the last half of January, at least,

their 6-hour interval is well suited to capturing the evolution of west Atlantic rain systems. In general systems move from west to east. Some of the stronger centers move in a northerly direction as well. Often the northern part of a band lags the southern part, with the result that the band tends to pivot cyclonically across the domain. There were two periods of what might be called pluviogenesis--the development of a well-marked, isolated rain system--18 through 19 January and 23 January. In addition, between 25 and 27 January a cyclonically curved rain band pivoted across the northern part of the domain. Intervening periods were relatively dry.

VI. CONCLUSIONS

For the GALE gauge data set the GPI calibration over-estimated rain by 44 percent. This is based on the mean values in Table 2. Accounting for the disagreement can be viewed in two ways: (1) the coefficient of rain rate for cloud colder than the threshold is too large, or (2) the coefficient is not too large, but the area covered by over-threshold cloud tends to be larger than the rain area. Because elimination of the potential false alarm cases reduces the disagreement to 24 percent as shown by the difference of the means in Table 7, we find (2) attractive.

Considering the technique as an area average measurement (Table 9), conclusions are less clear-cut. The aggregated results suggested a correlation > 0.58 between the estimates and the "truth." (This follows from the square root of the value 0.345 for r^2 at the bottom of Table 9.) They seemed to indicate that the sensitivity of the GPI was about 19 percent too large for this coastal zone data set, since the linear coefficient differs from one by 19 percent. Further, a constant term

≈ 0 was a natural consequence, not an artificial constraint. It is somewhat risky to give great weight to general conclusions from this very small data set, but since correlation value is similar to that found by Arkin and Meisner (1987) it seems that a consistent evaluation is becoming established.

Users might expect that these maps slightly underestimate peak rates and substantially overestimate the sizes of rain systems. Frontal rains may be offset to the east (P. Robertson, NASA Marshall, personal communication). Overall, rain rates probably are biased on the high side.

The gauge-satellite rainfall comparisons could profitably be extended. Even more useful would be comparisons over the ocean of satellite and radar rain rates. Once their quality has been established, the satellite estimates should be combined with gauge and radar measurements in a comprehensive mapping of GALE rainfall.

ACKNOWLEDGMENTS

Mrs. Delores Wade and the staff of the McIDAS facility created the GALE-rain GOES archive and performed initial data processing. Maps were made through the efforts of Gail Dengel, David Santek, Gary Krueger, and David Slezewski. Tom Mercer, GALE Project Office, provided PAM data. Jan Waite-Schuster typed the manuscript.

REFERENCES

Arkin, P. A., 1983: A diagnostic precipitation index from infrared satellite imagery. Tropical Ocean - Atmosphere Newsletter, 17, 5-7. (Available from JISAO, U. of Washington, AK-40, Seattle, WA 98105.)

Arkin, P. A., and B. N. Meisner, 1987: The relationship between large-scale convective rainfall and cold cloud over the Americas during 1982-84. Mon. Wea. Rev., 115, 51-74.

Martin, D. W., and B. Auvine, 1987: Quick look Atlantic Ocean Rain Maps for GALE. Report on Contract NAG5-742, Space Science and Engineering Center, Madison, WI 53706, 31 pp.

4/DWM/rpts/NAG5-742

Table 1. GOES-6 images for the daily maps. Crosses mark those images which actually were processed.

Month	January											February			March				
Date	18	19	20	21	22	23	24	25	26	27	28	11	14	27	1	8	9	12	14
IOP		1						2				5	6	10	11		12	13	
Time																			
00 UTC	X	X	X	X	X	X	X	X	X	X	X	X		X		X	X	X	X
	X	X	X	X	X	X	X	X	X	X	X	X		X		X	X	X	X
	X	X	X	X	X	X	X	X	X	X	X	X		X		X	X	X	X
03	X	X	X	X	X	X	X	X	X	X	X	X		X		X	X	X	X
	X	X	X	X	X	X	X	X	X	X	X	X		X			X		
	X	X	X	X	X	X	X	X	X	X	X	X		X		X	X	X	X
06	X	X	X	X	X	X	X	X	X	X	X	X		X	X	X	X	X	X
	X	X	X	X	X	X	X	X	X	X	X	X	X	X	X	X			
	X	X	X	X	X	X	X	X	X	X	X	X	X						
09	X	X	X	X	X	X	X	X	X	X	X	X		X	X	X	X	X	X
	X	X	X	X	X	X	X	X	X	X	X	X		X	X	X	X	X	X
	X	X	X	X	X	X	X	X	X	X	X	X	X	X	X	X	X	X	X
12	X	X	X	X	X	X	X	X	X	X	X	X	X	X	X	X	X	X	X
	X	X	X	X	X	X	X	X	X	X	X	X	X	X	X	X	X	X	X
	X	X	X	X	X	X	X	X	X	X	X	X	X	X	X	X	X	X	X
15	X	X	X	X	X	X	X	X	X	X	X	X	X	X	X	X	X	X	X
	X	X	X	X	X	X	X	X	X	X	X	X	X	X	X	X	X	X	X
	X	X	X	X	X	X	X	X	X	X	X	X	X	X	X	X	X	X	X
18	X	X	X	X	X	X	X	X	X	X	X	X	X	X	X	X	X	X	X
	X	X	X	X	X	X	X	X	X	X	X	X	X	X	X	X	X	X	X
	X	X	X	X	X	X	X	X	X	X	X	X	X	X	X	X	X	X	X
21	X	X	X	X	X	X	X	X	X	X	X	X	X	X	X	X	X	X	X
	X	X	X	X	X	X	X	X	X	X	X	X	X	X	X	X	X	X	X
	X	X	X	X	X	X	X	X	X	X	X	X	X	X	X	X	X	X	X

Table 2. Distribution parameters of six hour rain accumulation from gauge observations and the rain estimation algorithm, both the nominal grid point values and interpolated to the gauge locations.

Distribution Parameter	Gauge Data	Rain Estimation Algorithm Grid Pt.	Interp.
Sample size	112.000	112.000	112.000
Average	2.932	4.000	4.165
Median	0.508	2.000	2.270
Mode	0.000	0.000	0.000
Standard deviation	6.011	4.830	4.694
Minimum	0.000	0.000	0.000
Maximum	35.560	18.000	18.000
Range	35.560	18.000	18.000
Skewness	3.641	1.268	1.184
Standardized skewness	15.730	5.481	5.117
Kurtosis	15.078	0.653	0.500
Standardized kurtosis	32.573	1.412	1.08148

Table 3. Model fitting results for gauge accumulation as a function of interpolated estimates of rain.[1]

Term in regression	coefficient	std. error	t-value	sig. level
CONSTANT	0.796	0.700	1.13	0.25
LINEAR	0.512	0.111	4.58	0.00

95 percent confidence intervals for coefficient estimates

	Lower Limit	Upper Limit
CONSTANT	-0.591	2.184
LINEAR	0.290	0.734

Analysis of variance for the regression

Source	Sum of Squares	DF	Mean Square	F-Ratio	P-value
Model	643.125	1	643.125	21.0050	.0000
Error	3367.95	110	30.6177		
Total (Corr.)	4011.07	111			

R-squared = 0.160 Stnd. error of est. = 5.53
R-squared (Adj. for d.f.) = 0.152

[1]Standard errors in the upper division of the table (and similar tables to follow) are standard errors of the corresponding constant or coefficient of the regression term. For example, the standard error in determining the constant term in this regression is 0.700. The standard error given at the bottom of the table is that of the estimated variable.

Table 4. Model fitting results for gauge accumulation without a constant term

Term in regression	coefficient	std. error	t-value	sig. level
LINEAR	0.597	0.083	7.14	0.00

95 percent confidence intervals for coefficient estimates

	Lower Limit	Upper Limit
LINEAR	0.431	0.763

Analysis of Variance for the Full Regression

Source	Sum of Squares[1]	DF	Mean Square[1]	F-Ratio	P-value
Model	1566.58	1	1566.58	51.0310	.0000
Error	3407.54	111	30.6986		
Total	4974.12	112			

R-squared = 0.314946[2] Stnd. error of est. = 5.540
R-squared = 0.3149462 Stnd. error of est. = 5.540

[1]Taken about zero, not the mean.
[2]This is not the square of a true correlation for regressions in which the constant has been forced to zero. In these cases it is a moment about zero, rather than the mean. These remarks also apply to Tables 6 and 10.

Table 5. Model fitting results selecting cases for which the gauge accumulations are greater than zero.

Term in regression	coefficient	std. error	t-value	sig.level
CONSTANT	2.045	1.128	1.81	0.07
LINEAR	0.738	0.165	4.45	0.00

95 percent confidence intervals for coefficient estimates

	Lower Limit	Upper Limit
CONSTANT	-0.213	4.30
LINEAR	0.406	1.06

Analysis of Variance for the Full Regression

Source	Sum of Squares	DF	Mean Square	F-Ratio	P-value
Model	809.698	1	809.698	19.8427	.0000
Error	2366.74	58	40.8058		
Total (Corr.)	3176.44	59			

R-squared = 0.254 Stnd. error of est. = 6.38
R-squared (Adj. for d.f.) = 0.242

Table 6. Regression results after eliminating the potential false alarm cases and rejecting the constant term

Term in regression	coefficient	std. error	t-value	sig. level
LINEAR	0.9430	0.123	7.63	0.00

95 percent confidence intervals for coefficient estimates

	Lower Limit	Upper Limit
LINEAR	0.695	1.190

Analysis of Variance for the Full Regression

Source	Sum of Squares	DF	Mean Square	F-Ratio	P-value
Model	2473.23	1	2473.23	58.3476	.0000
Error	2500.89	59	42.3879		
Total	4974.12	60			

R-squared = 0.497 Stnd. error of est. = 6.51
R-squared (Adj. for d.f.) = 0.497

Table 7. Distribution parameters when potential false alarms are eliminated.

Distribution Parameter	Gauge Observation	Estimated Value
Sample size	60.000	60.000
Average	5.473	4.416
Standard deviation	7.337	5.106
Median	2.540	2.500
Mode	2.540	0.000
Minimum	0.254	0.000
Maximum	35.560	18.000
Skewness	2.766	1.208
Standardized skewness	8.748	3.821
Kurtosis	8.045	0.540
Standardized kurtosis	12.721	0.855

Table 8. Correlations and separation distances between pairs of rain gauges.

Sample Correlations (top), significance (middle), separation in km (bottom)

	Gauge1	Gauge2	Gauge3	Gauge4	Gauge5	Gauge6	Gauge7	Gauge8
Gauge1	1.0000							
	.0000							
	0							
Gauge2	.1137	1.0000						
	.6988	.0000						
	312	0						
Gauge3	.3468	.8103	1.0000					
	.2245	.0004	.0000					
	251	85	0					
Gauge4	.6809	.4120	.3028	1.0000				
	.0073	.1433	.2927	.0000				
	93	223	172	0				
Gauge5	.1078	.9853	.7295	.4461	1.0000			
	.7138	.0000	.0031	.1098	.0000			
	223	89	52	135	0			
Gauge6	-.2540	.0327	-.0737	-.2441	.0492	1.0000		
	.3808	.9118	.8024	.4004	.8674	.0000		
	131	202	168	44	122	0		
Gauge7	-.3303	-.2367	-.2712	-.5318	-.2431	.35921	1.0000	
	.2488	.4152	.3483	.0503	.4023	.2072	.0000	
	240	552	487	331	463	363	0	
Gauge8	.6243	.0339	-.0474	.5768	.0950	-.3254	-.3068	1.0000
	.0170	.9084	.8722	.0308	.7466	.2562	.2860	.0000
	74	285	241	70	201	83	284	0

Table 9. Regression model for grouped rain gauge observations.

Term in regression	coefficient	std. error	t-value	sig.level
CONSTANT	0.0294	1.46	0.020	0.98
LINEAR	0.812	0.338	2.40	0.04

95 percent confidence intervals for coefficient estimates

	Lower Limit	Upper Limit
CONSTANT	-3.35	3.41
LINEAR	0.03	1.59

Analysis of Variance for the Full Regression

Source	Sum of Squares	DF	Mean Square	F-Ratio	P-value
Model	17.0694	1	17.0694	5.76	.043
Error	23.7027	8	2.96283		
Total (Corr.)	40.7720	9			

R-squared = 0.418 Stnd. error of est. = 1.72
R-squared (Adj. for d.f.) = 0.345

Table 10. Model fitting results selecting gauge accumulations greater than zero with no constant term included.

Term in regression	coefficient	std. error	t-value	sig. level
LINEAR	0.818	0.118	6.92	0.00

95 percent confidence intervals for coefficient estimates

	Lower Limit	Upper Limit
LINEAR	0.550	1.085

Analysis of Variance for the Full Regression

Source	Sum of Squares	DF	Mean Square	F-Ratio	P-value
Model	126.232	1	126.232	47.9285	.0001
Error	23.7039	9	2.63376		
Total	149.936	10			

R-squared = 0.841 Stnd. error of est. = 1.62
R-squared (Adj. for d.f.) = 0.841

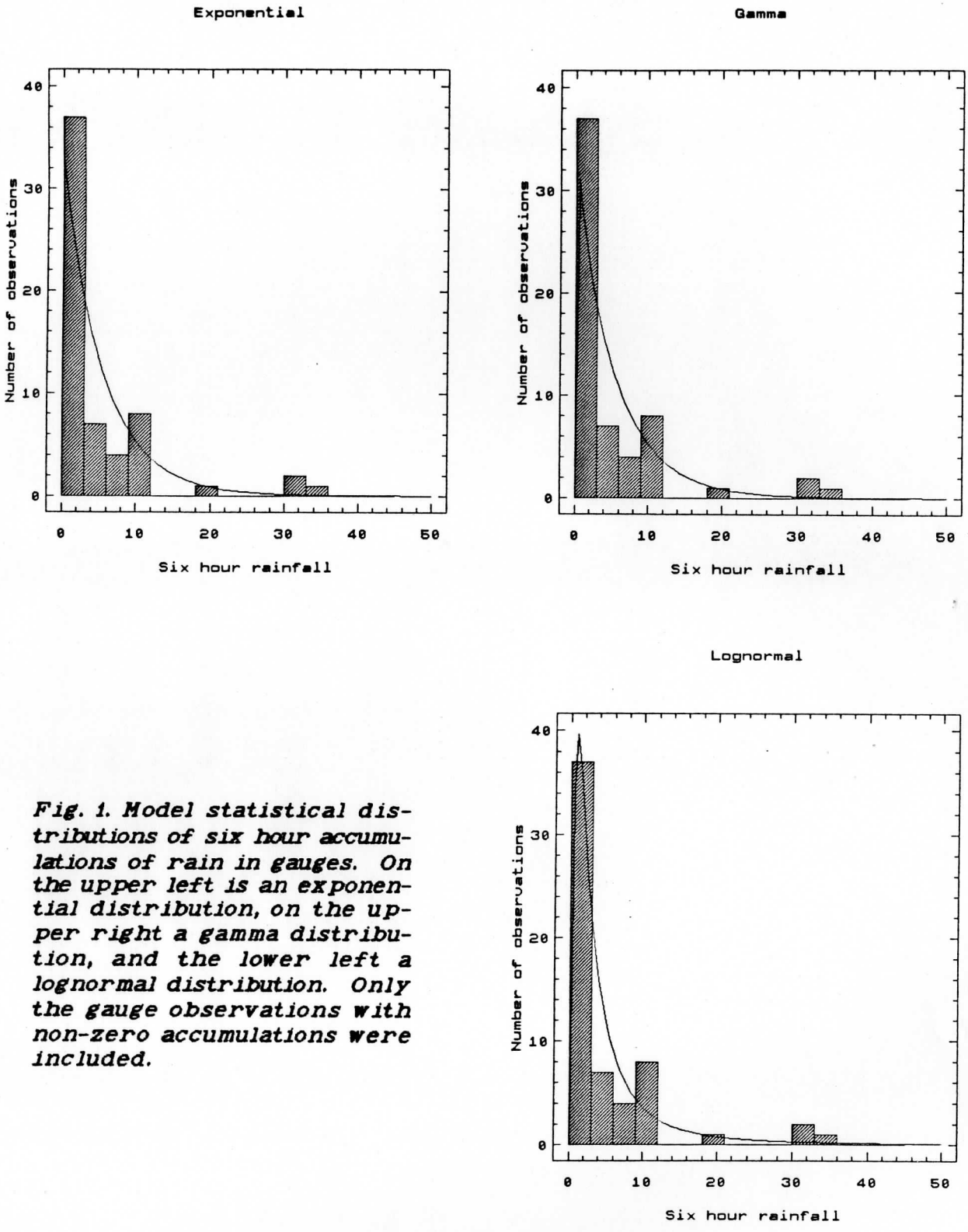

Fig. 1. Model statistical distributions of six hour accumulations of rain in gauges. On the upper left is an exponential distribution, on the upper right a gamma distribution, and the lower left a lognormal distribution. Only the gauge observations with non-zero accumulations were included.

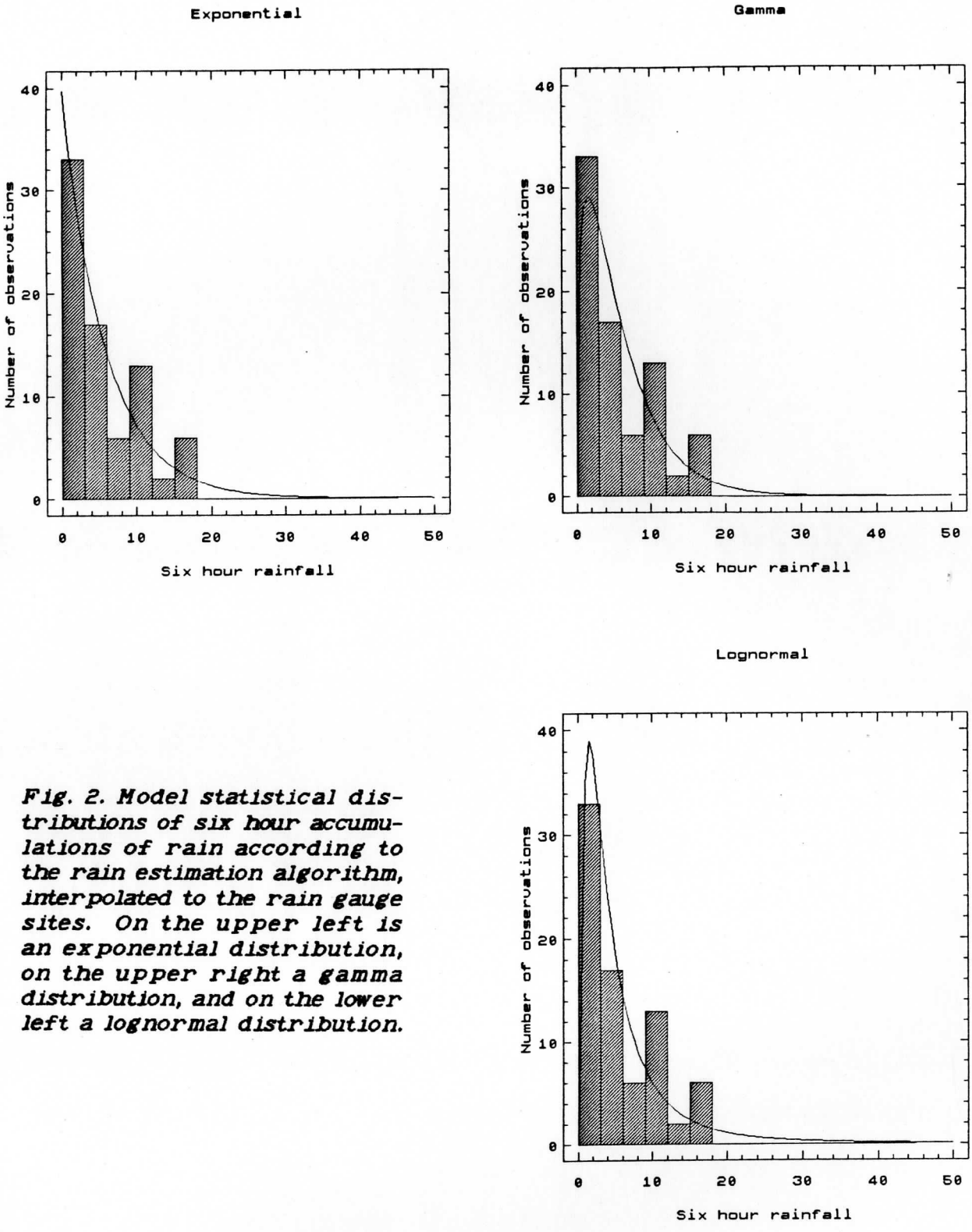

Fig. 2. Model statistical distributions of six hour accumulations of rain according to the rain estimation algorithm, interpolated to the rain gauge sites. On the upper left is an exponential distribution, on the upper right a gamma distribution, and on the lower left a lognormal distribution.

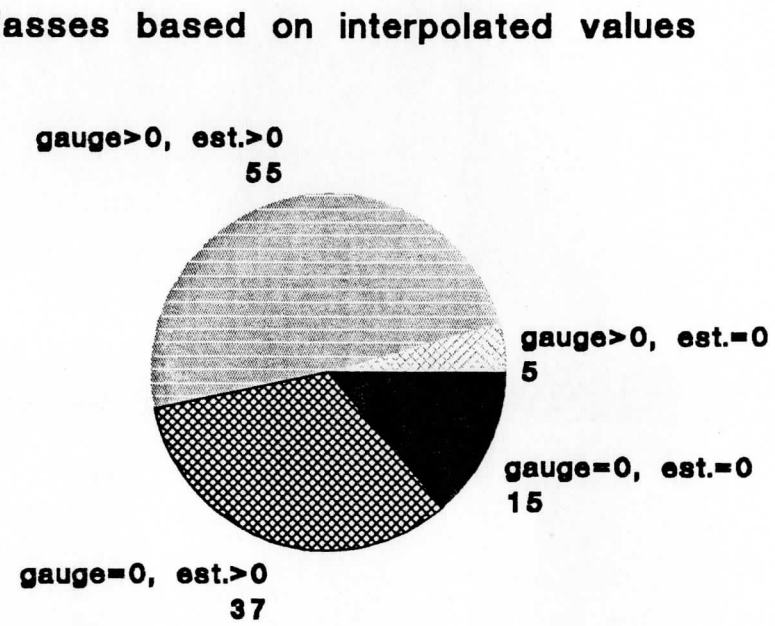

Fig. 3. Composition of the data set according to a classification scheme derived from the pairs of rain accumulation values (zero, or non-zero) obtained from the gauges and the rain estimation algorithm interpolated to the gauge locations. The numerals labeling each sector are numbers of cases in that class.

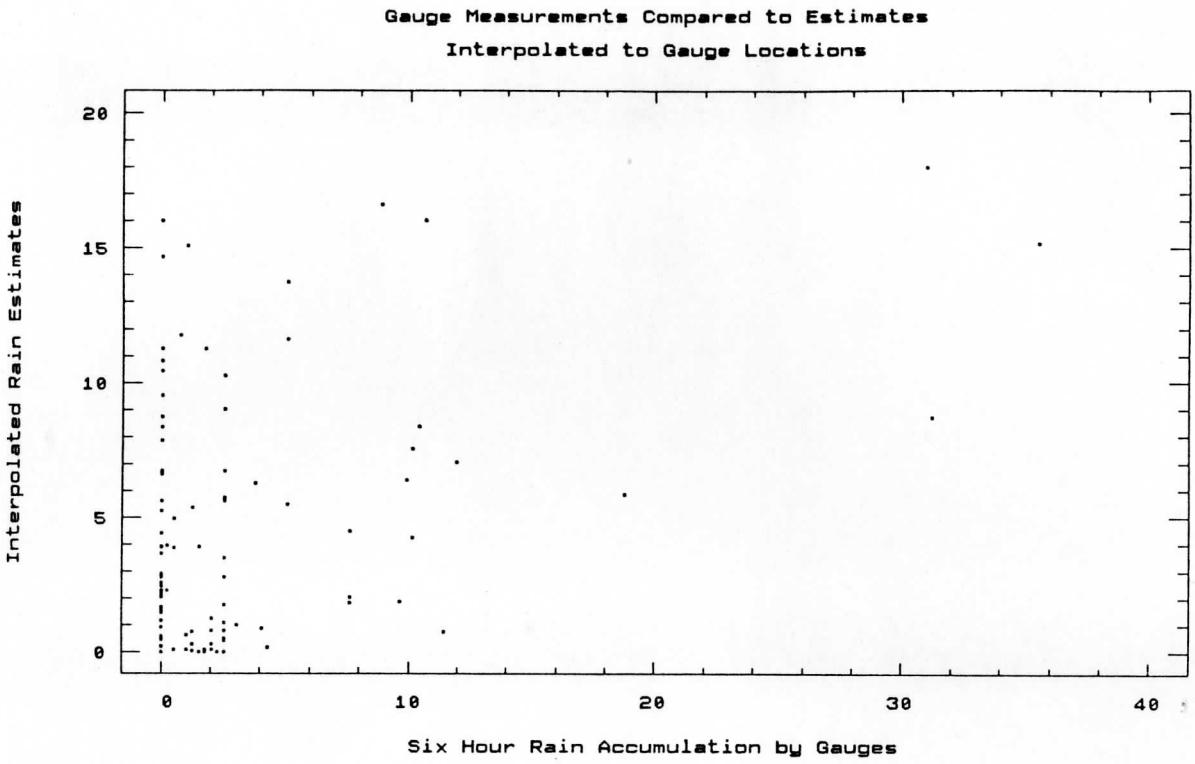

Fig. 4. Scatter plot of rain estimates (interpolated to the gauge sites) and the corresponding gauge observations. Values on both axes refer to six hour accumulations in mm.

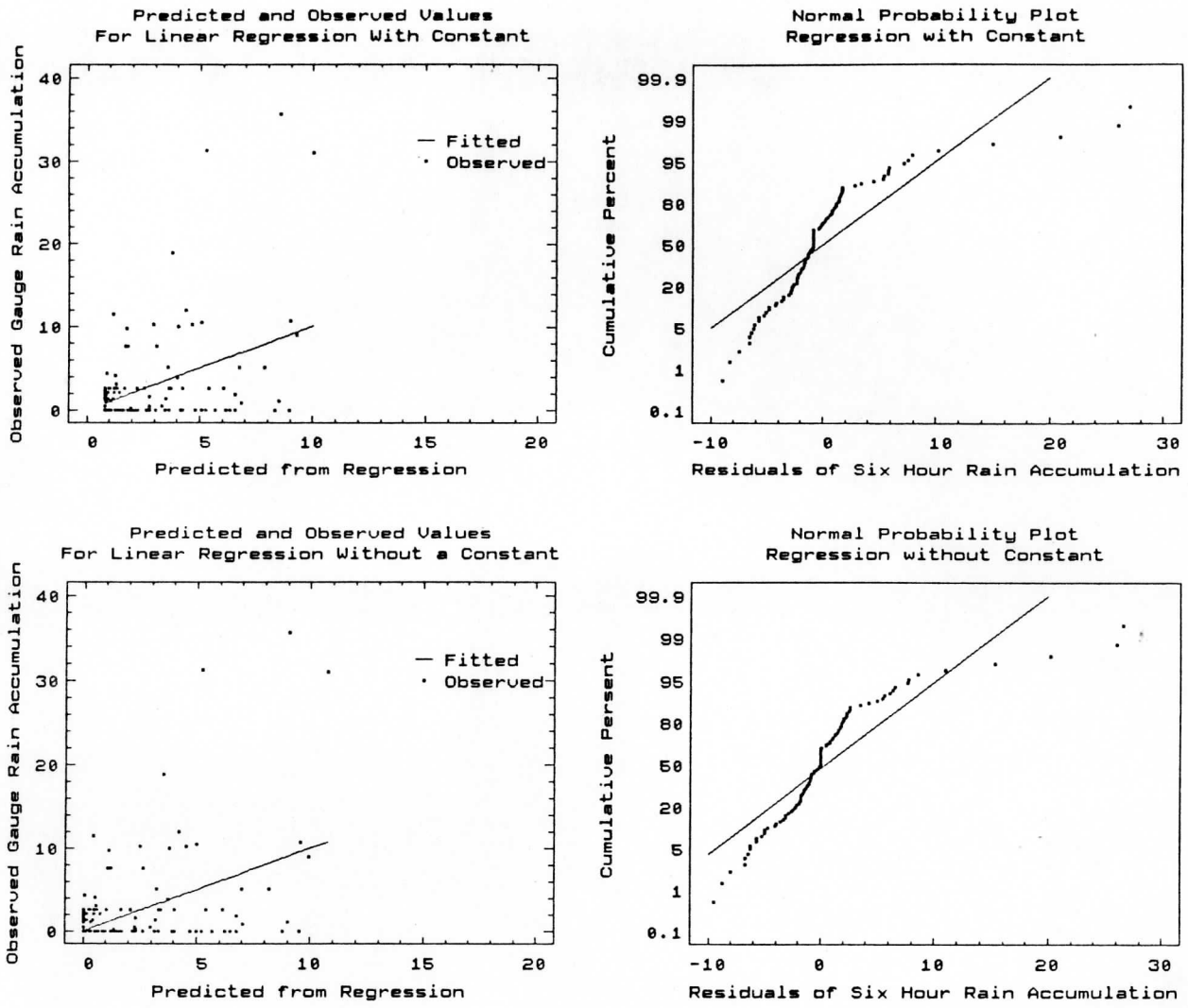

Fig. 5. Two regression curves with scatter plots of the data and normal probability plots of the residuals. The top two panels refer to the linear regression with a constant from Table 3, while the lower panels refer to that of Table 4 which has no constant term. An ideal normal distribution of residuals would appear along the lines shown in the right panels. The patterns shown indicate a marked departure from normality.

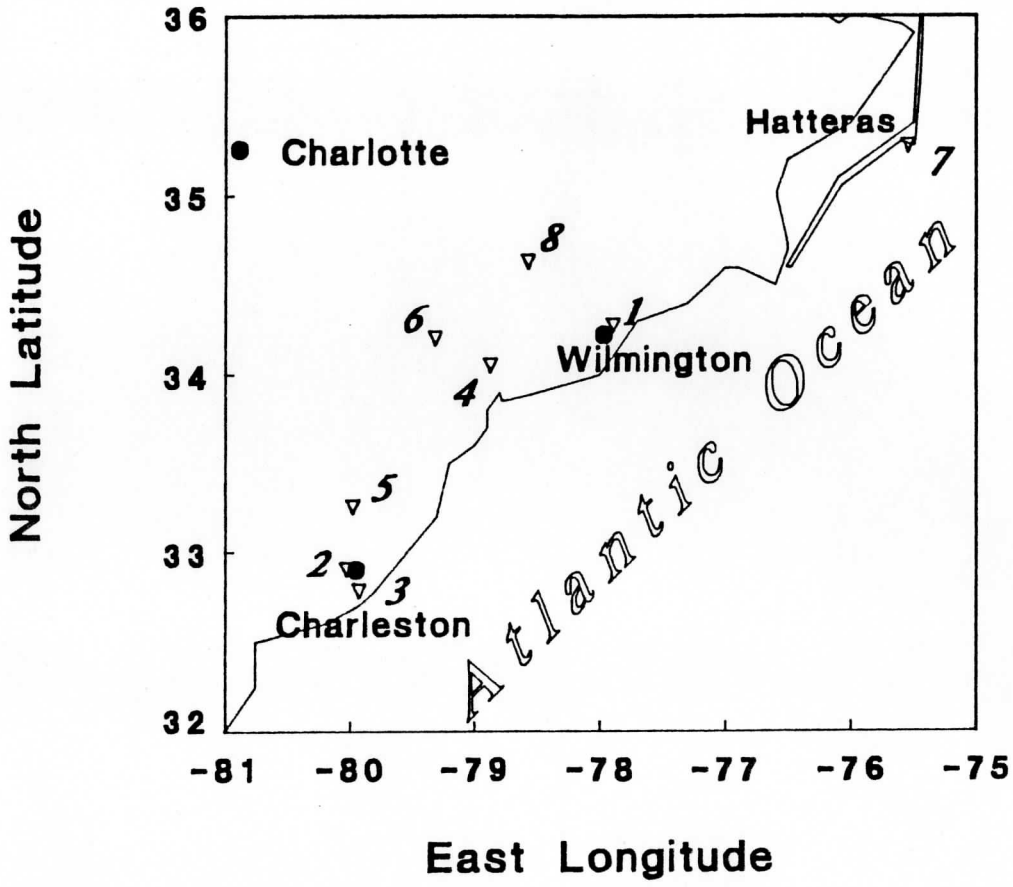

Fig. 6. Chart of the study area. Gauge locations are indicated by triangles. The numerals are used to identify individual gauges in Table 8.

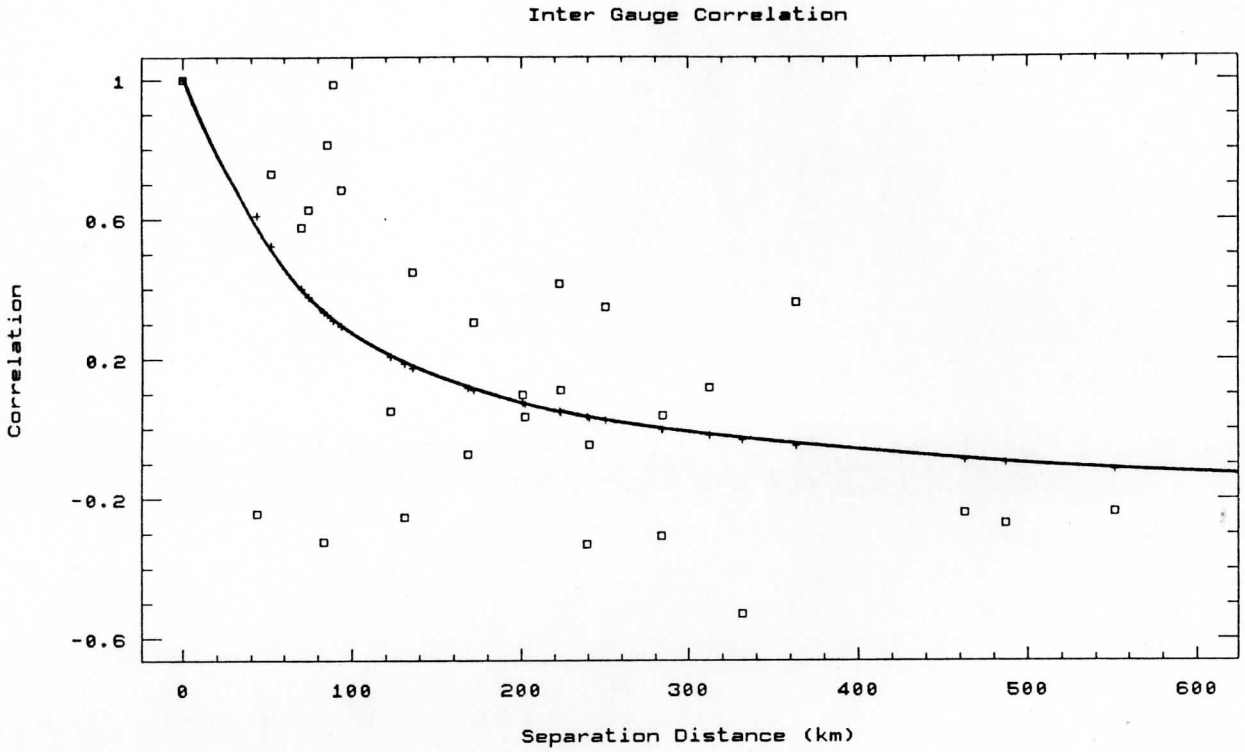

Fig. 7. Scatter plot of inter gauge correlations and a regression curve fitted to the points. The form chosen for the curve was a constant plus the square root of the separation distance. The zero crossing point is near 290 km, while the 0.7 correlation value (corresponding to $r_{ij}^2 = 0.5$) is located at a separation of about 25 km.

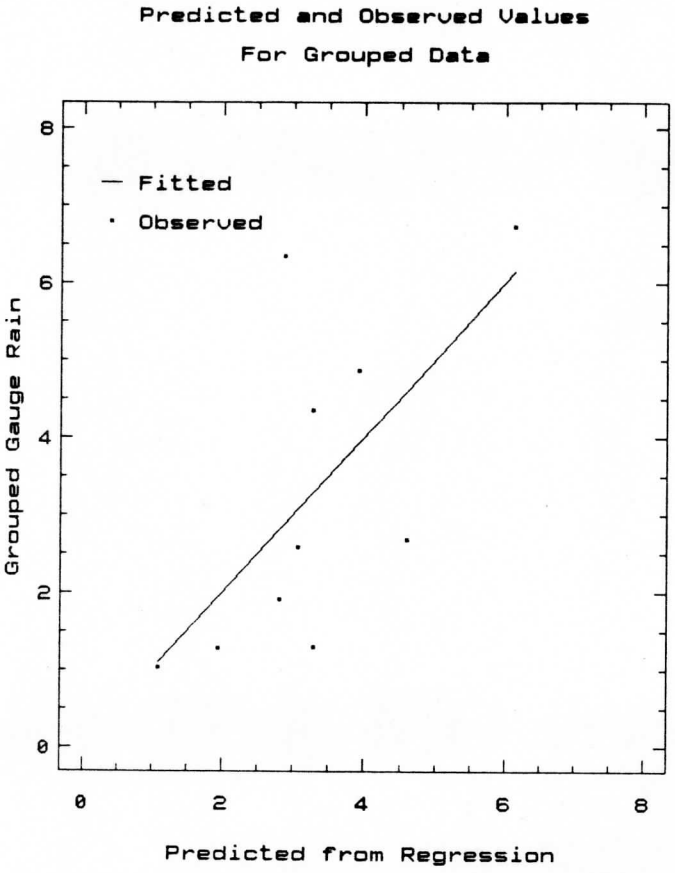

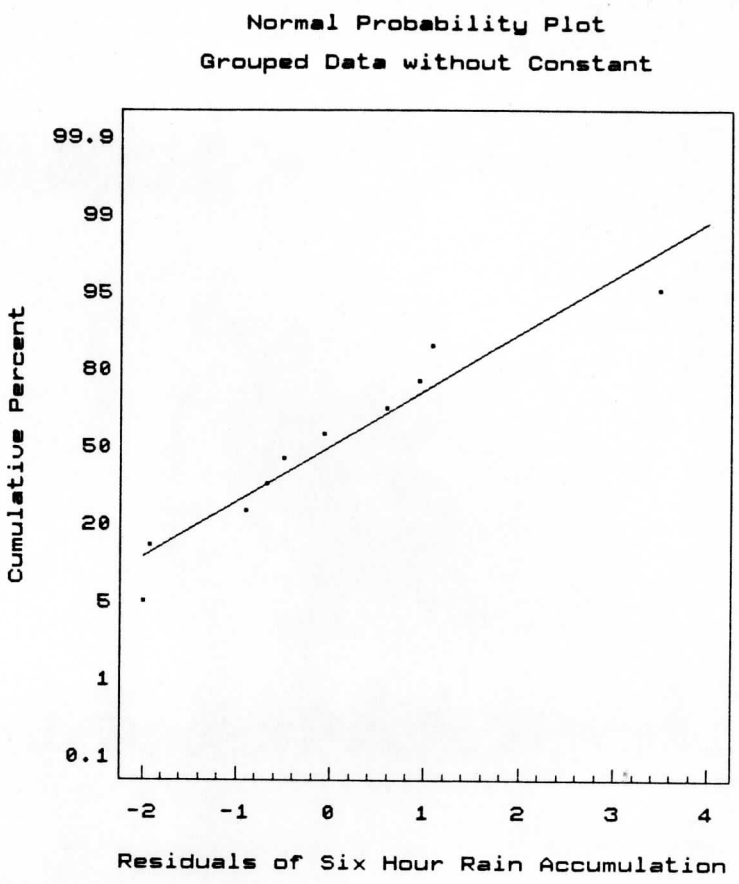

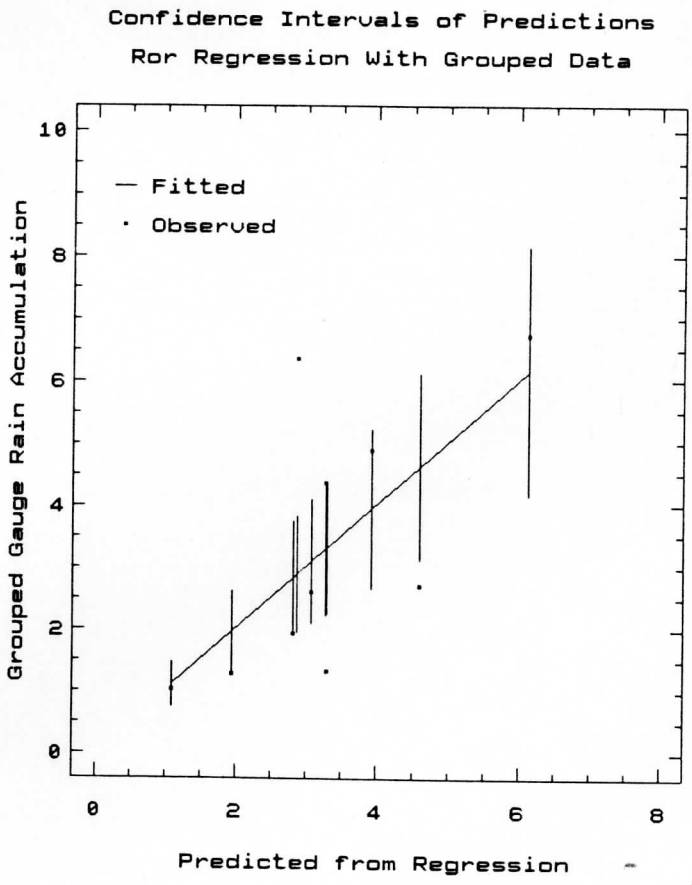

Fig. 8. Regression results for the grouped data. All three plots refer to the regression of Table 10, but the upper panels are indistinguishable from the corresponding results for the regression of Table 9. Clearly, grouping the data has improved the normality of the residuals as expected (upper right). The confidence intervals (lower left) reflect only the uncertainty due to the determination of the linear coefficient in the regression. The bars shown refer to the 95 % confidence level.

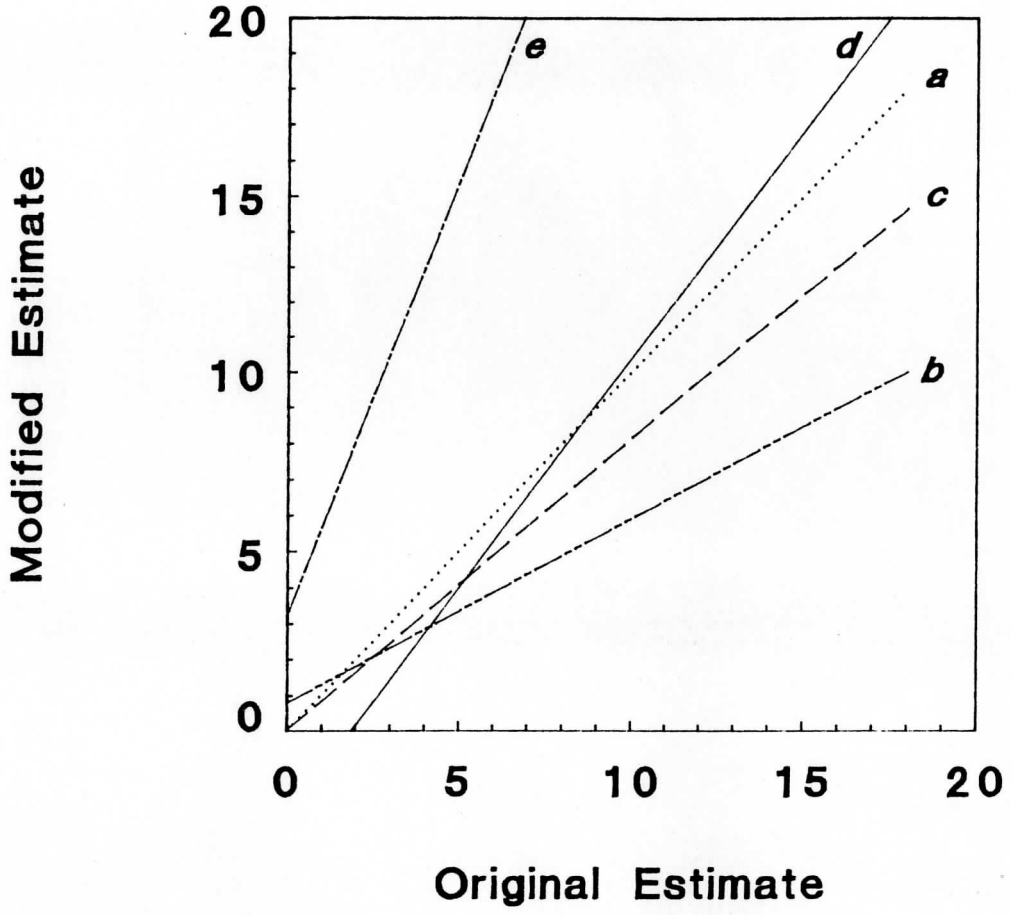

Fig. 9. Five possible relations between the original rain estimates and a retuned estimate based on comparisons with the gauges. Curve (a) corresponds to the original (unmodified) estimate. Curve (b) is the regression of Table 3, which assumes the gauges are perfect truth, and which incorporates a constant. Curve (c) denotes the regression of Table 10 for grouped data (the Table 9 case would be indistinguishable). Curve (d) results from assuming that the errors in the gauge measurements and the rain estimates have equal variance. A regression which excluded the false alarm cases, corresponding to the data summarized in Table 7, is not shown but would lie approximately mid way between (a) and (c). The left most curve, (e), would result from minimizing the x-deviations from the regression line, and represents an upper limit on a linear relation between the original estimates and a retuned one based on gauge data.

APPENDIX 1

TWENTY-FOUR HOUR MAPS

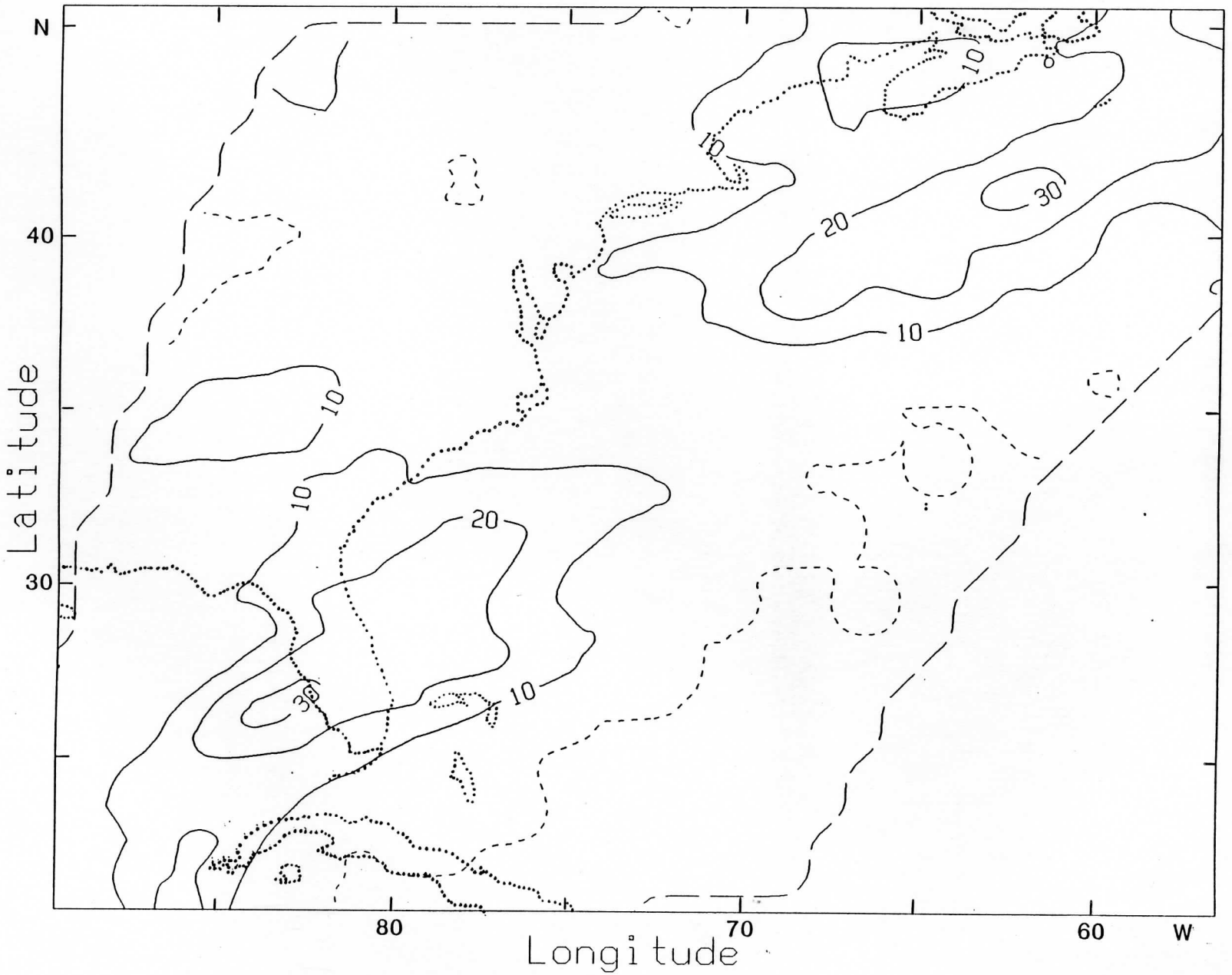
1/18
N
40
30
Latitude
80
70
60
W
Longitude
10
20
30

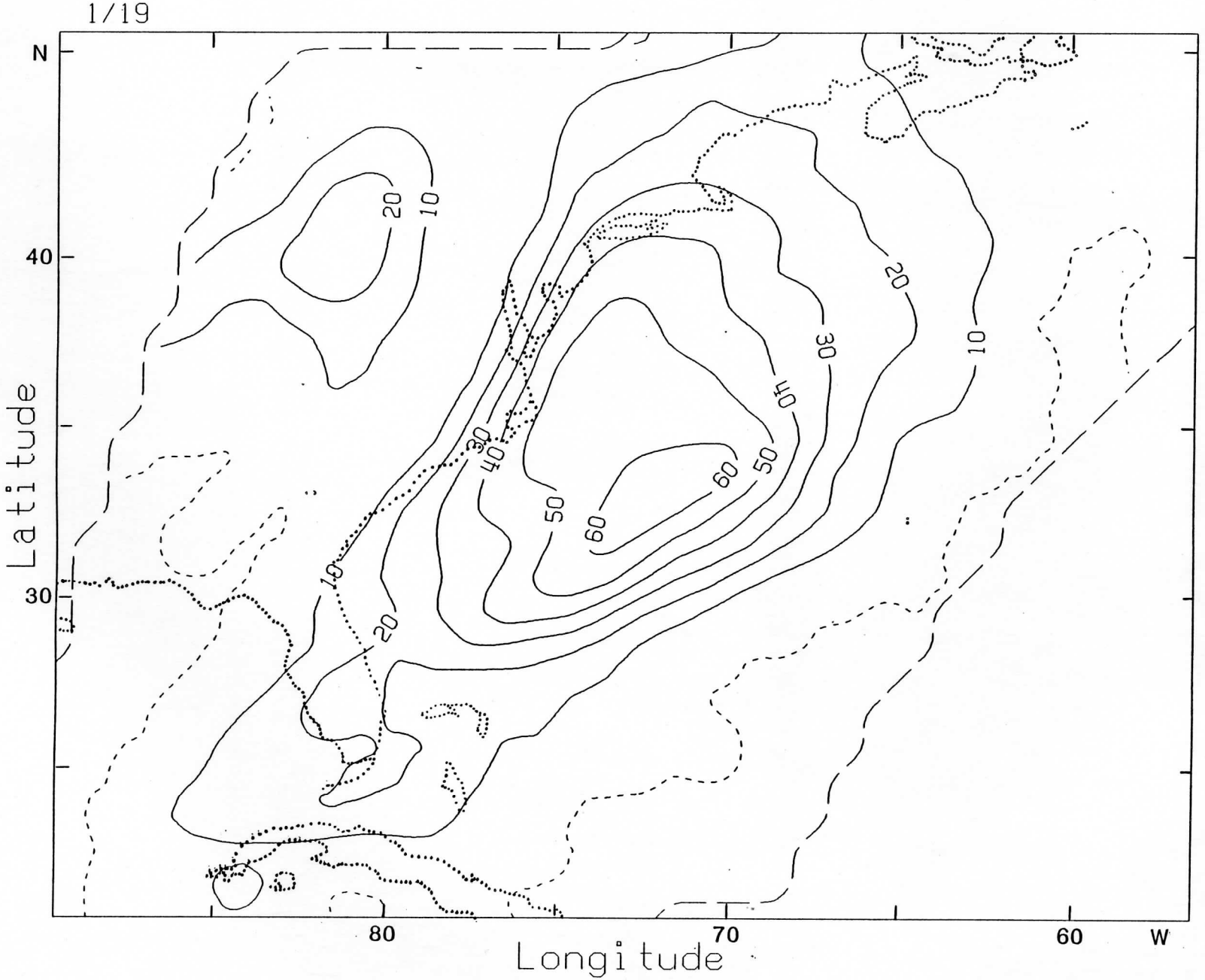
1/19
N
40
30
Latitude
80
70
60
W
Longitude
10
20
30
40
50
60

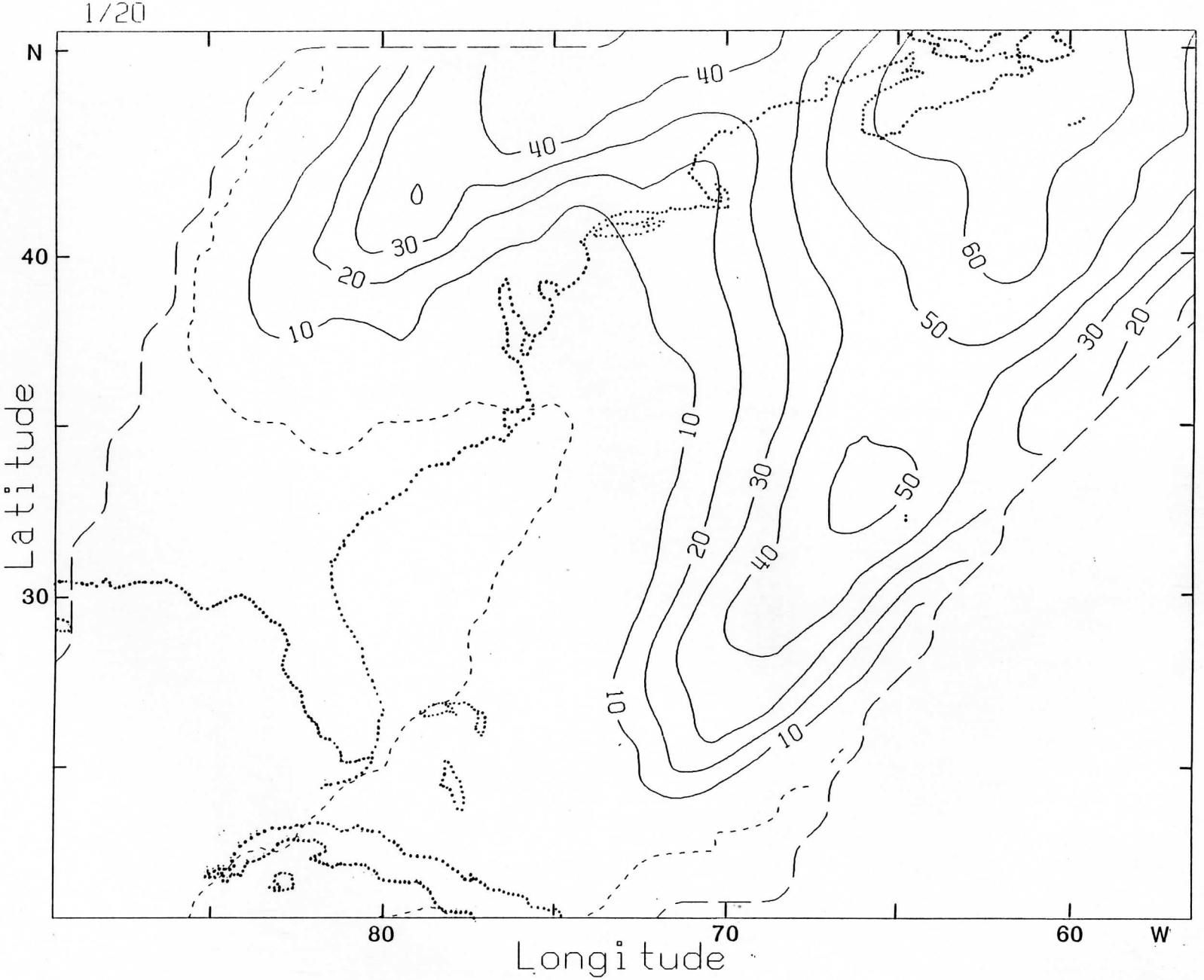
1/20
N
40
30
Latitude
80
70
60
W
Longitude
0
10
20
30
40
50
60

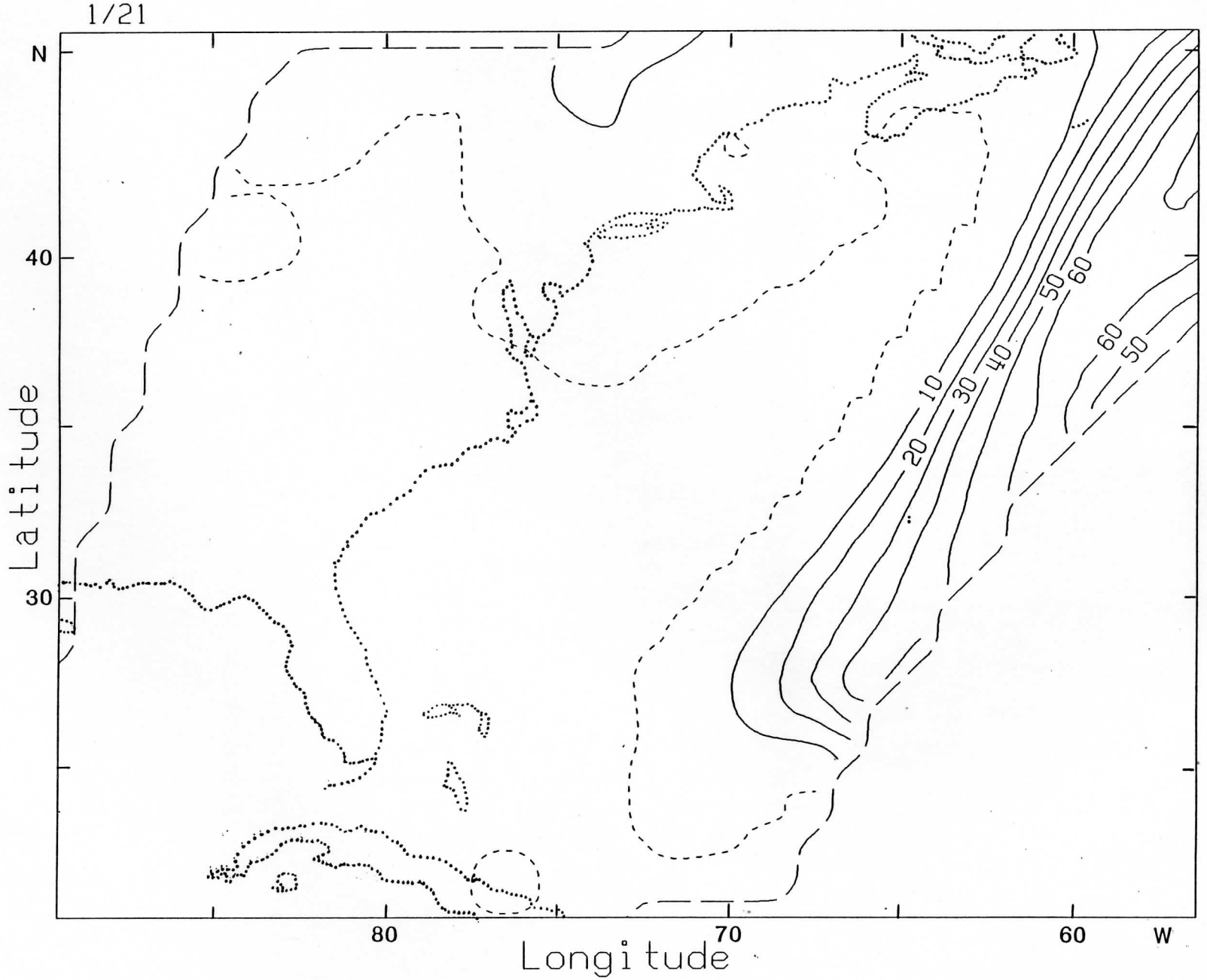
1/21
N
40
30
Latitude
80
70
60
W
Longitude
10
20
30
40
50
60
50
60

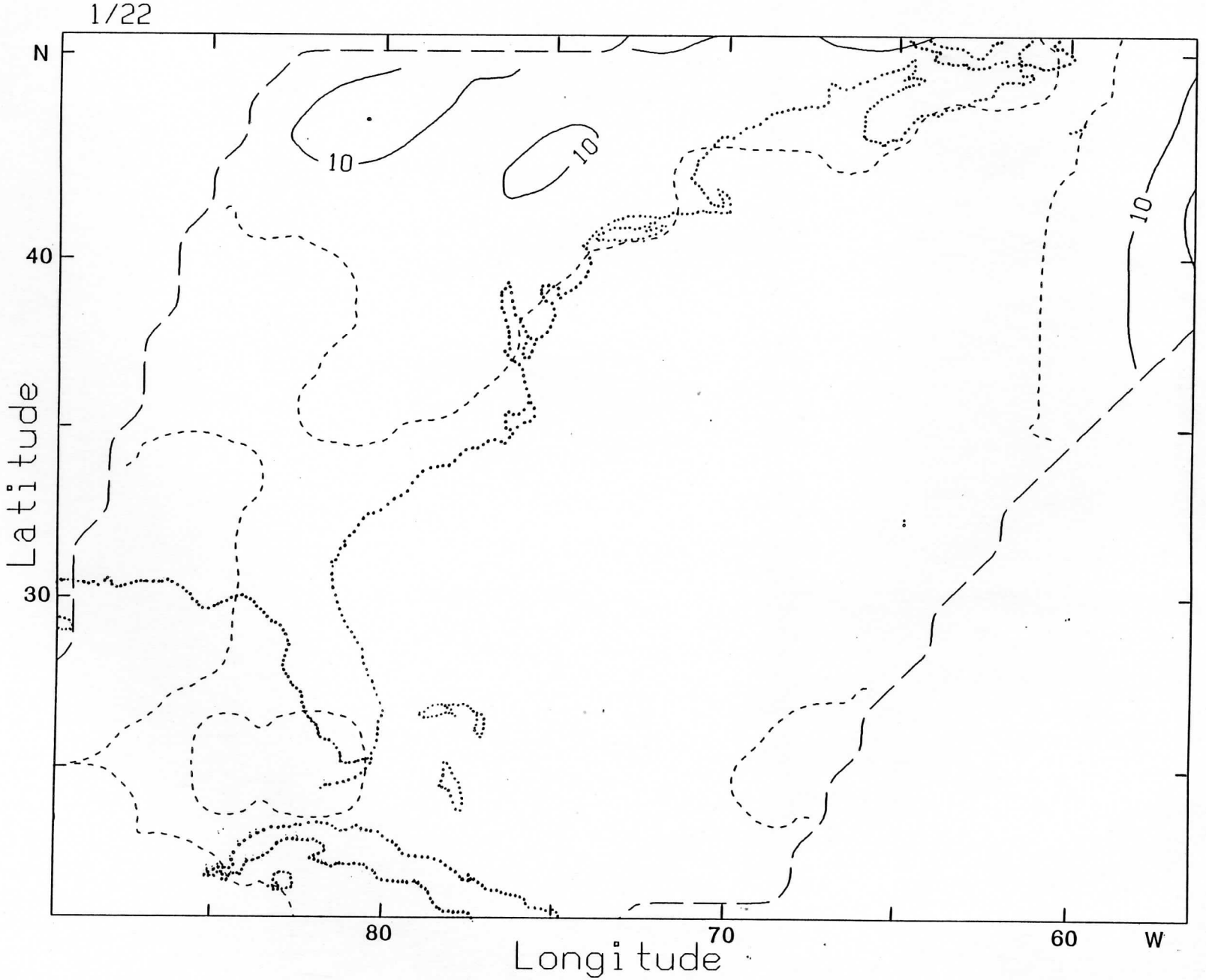
1/22
N
40
30
Latitude
10
10
10
80
70
60
W
Longitude

1/23

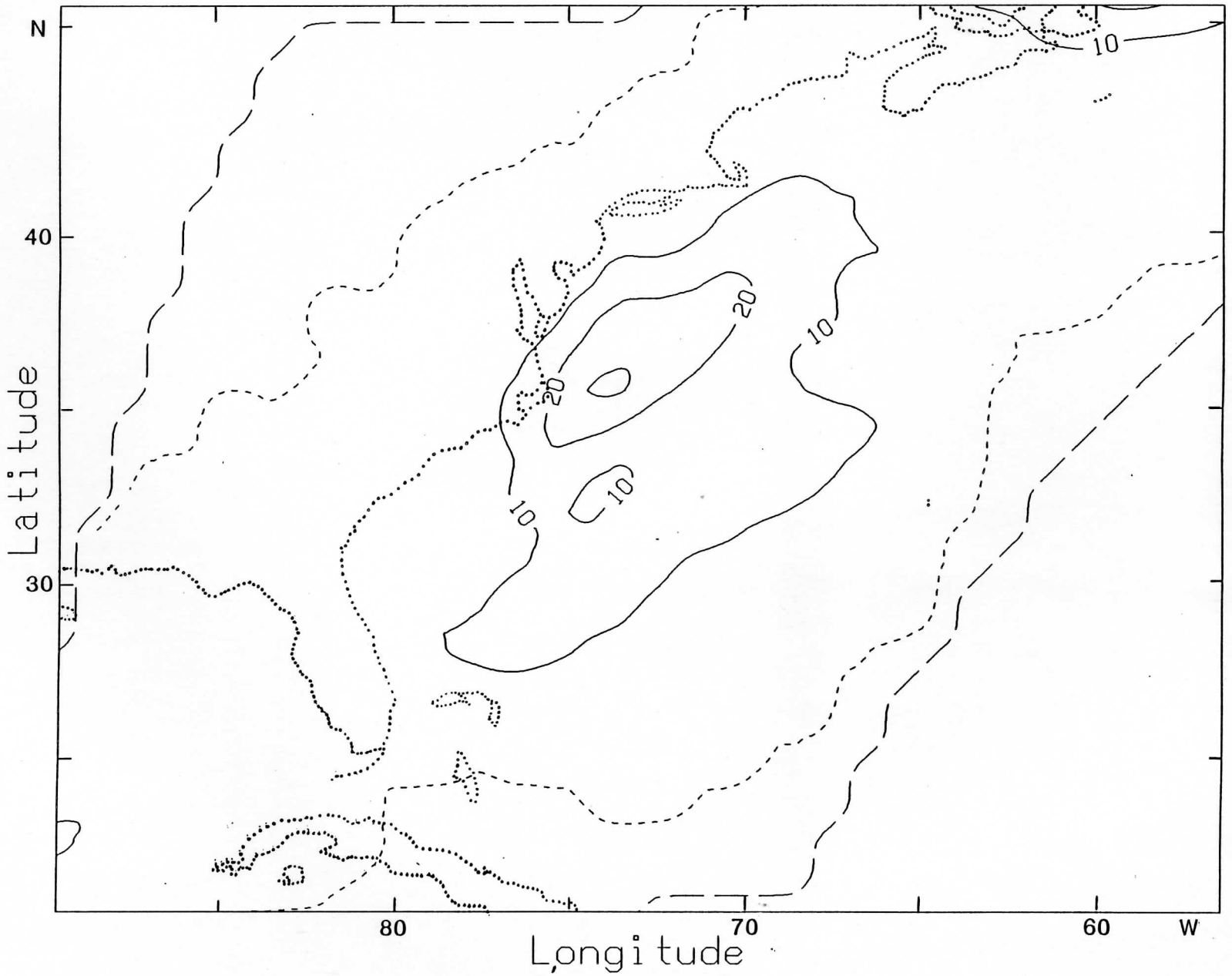

oh

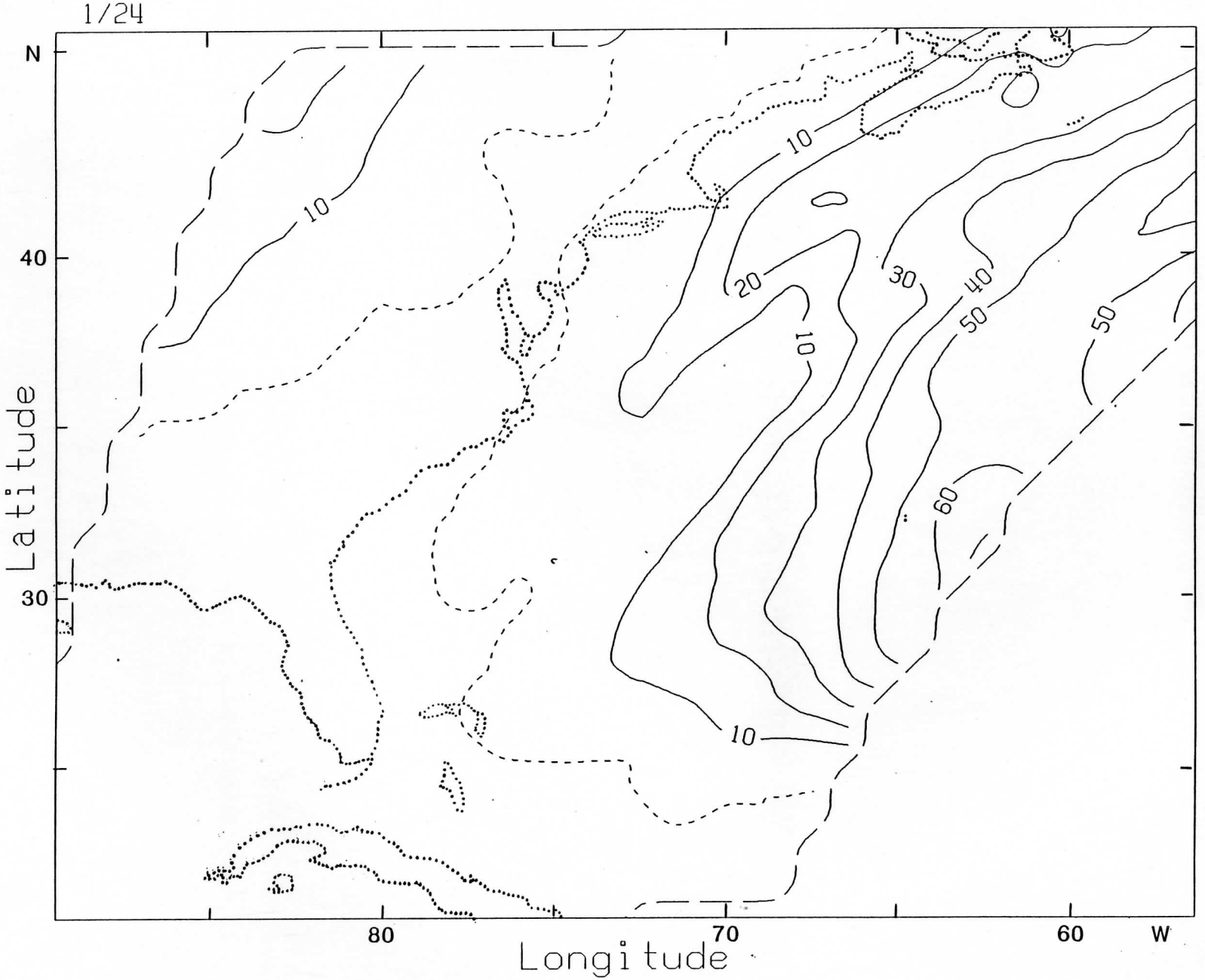
1/24
N
40
30
Latitude
80
70
60
W
Longitude
10
10
20
10
30
40
50
50
60
10

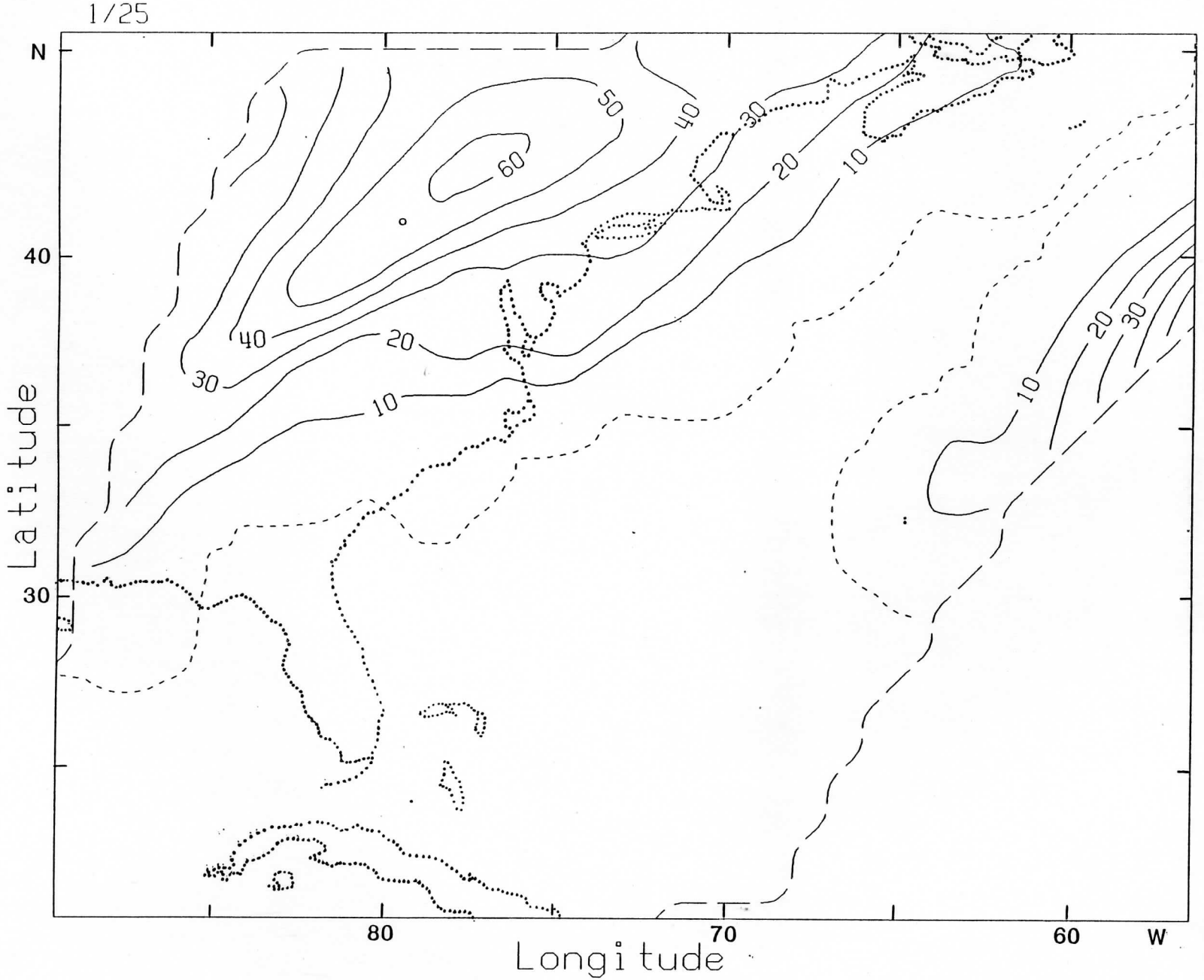
1/25
N
40
30
Latitude
80
70
60
W
Longitude
60
50
40
30
20
10
40
20
30
10
10
20
30

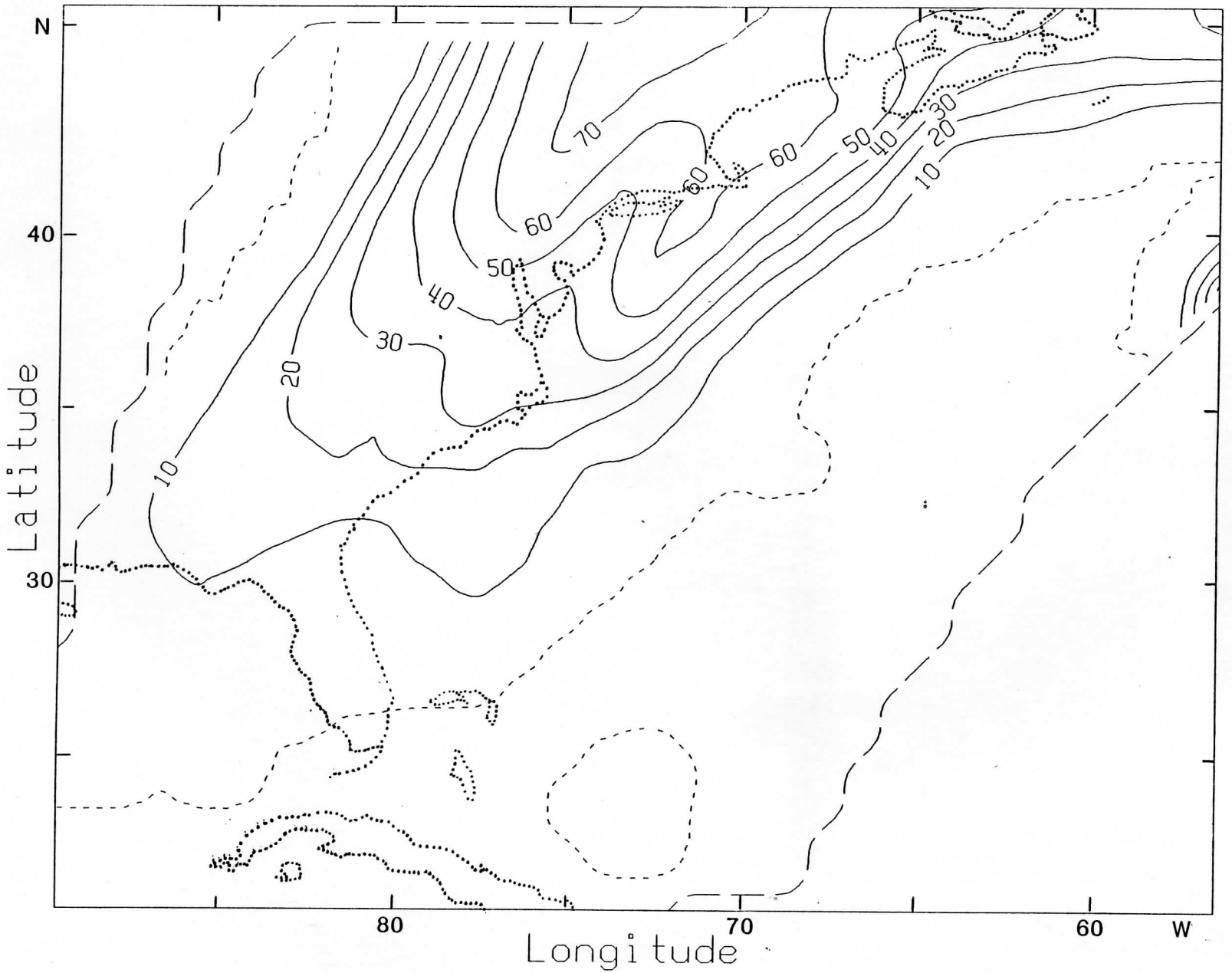
N
40
30
Latitude
80
70
60
W
Longitude
70
60
60
50
50
40
40
30
30
20
20
10
10

1/27

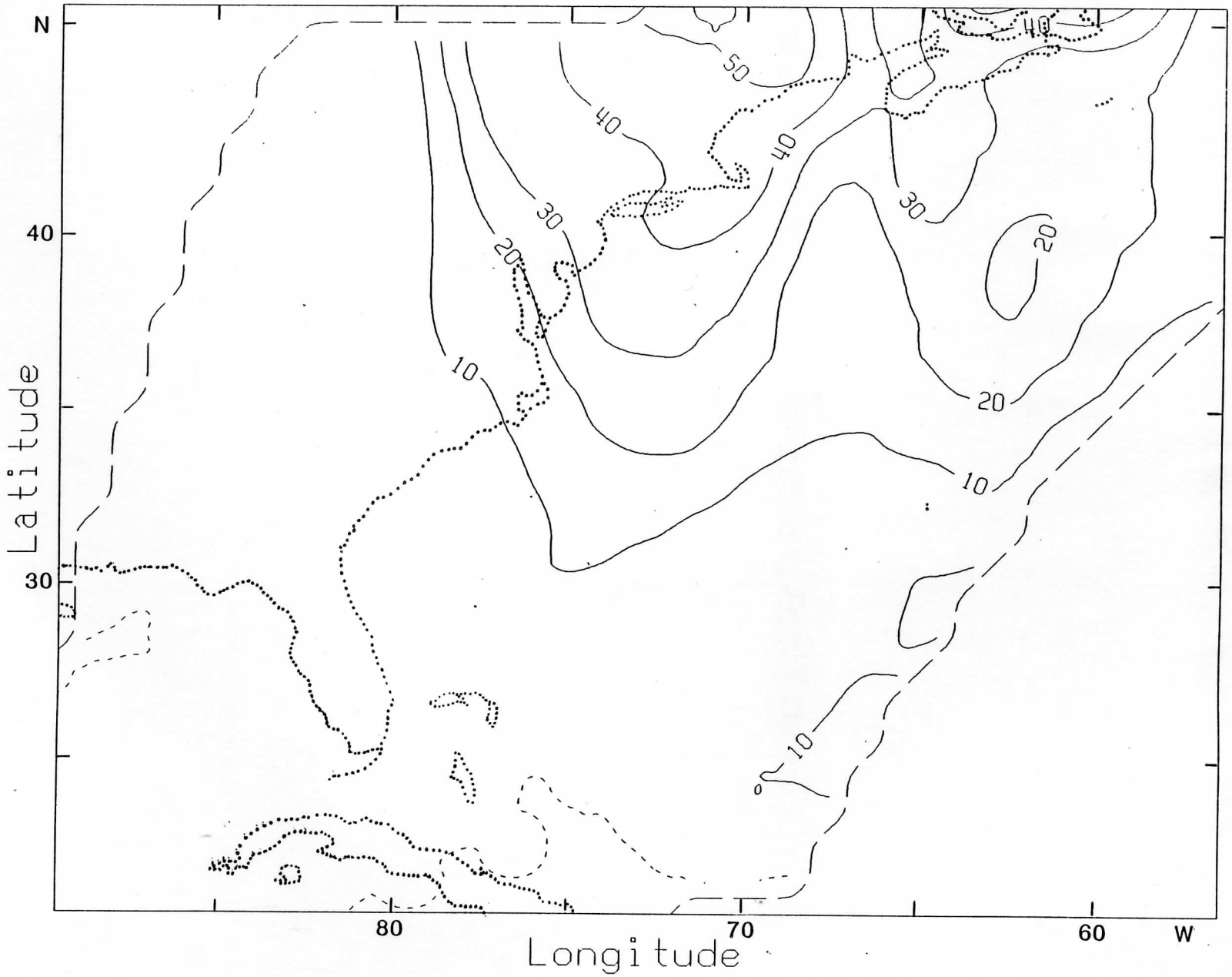
N
40
30
Latitude
80
70
60
W
Longitude
50
40
40
30
30
20
20
20
10
10
10
10

44

1/28

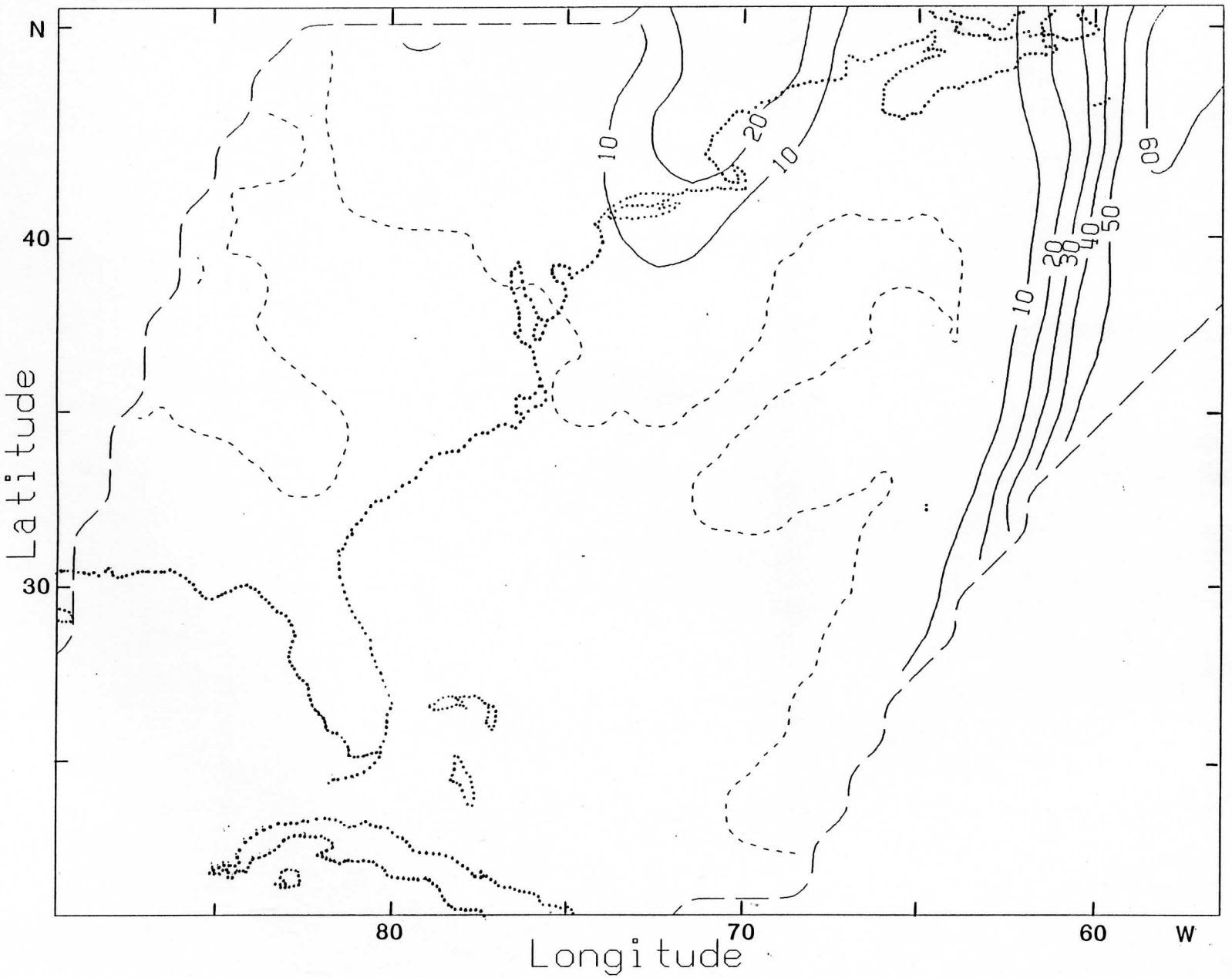

45

2/11

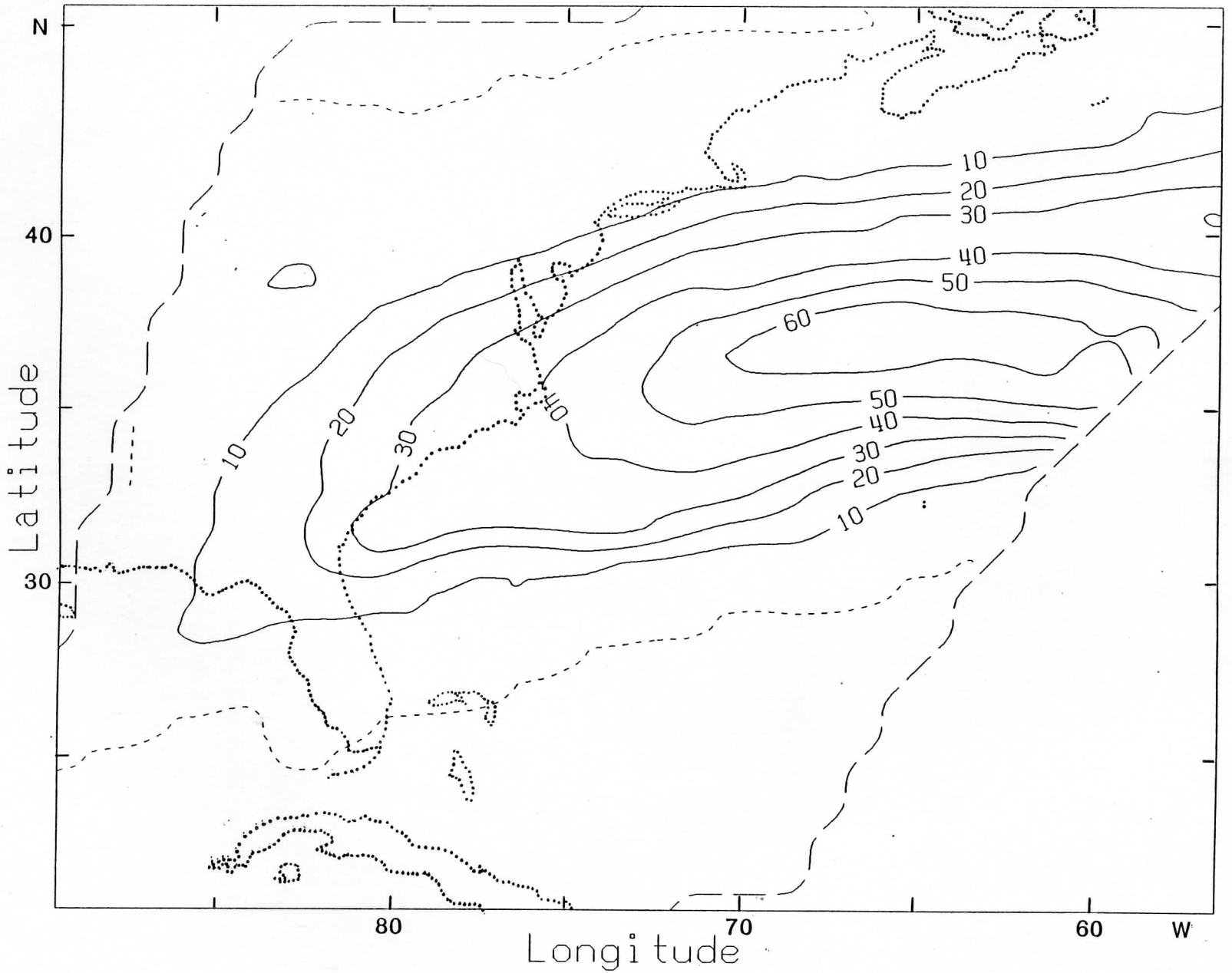
N
40
30
Latitude
10
20
30
40
50
60
50
40
30
20
10
80
70
60
W
Longitude

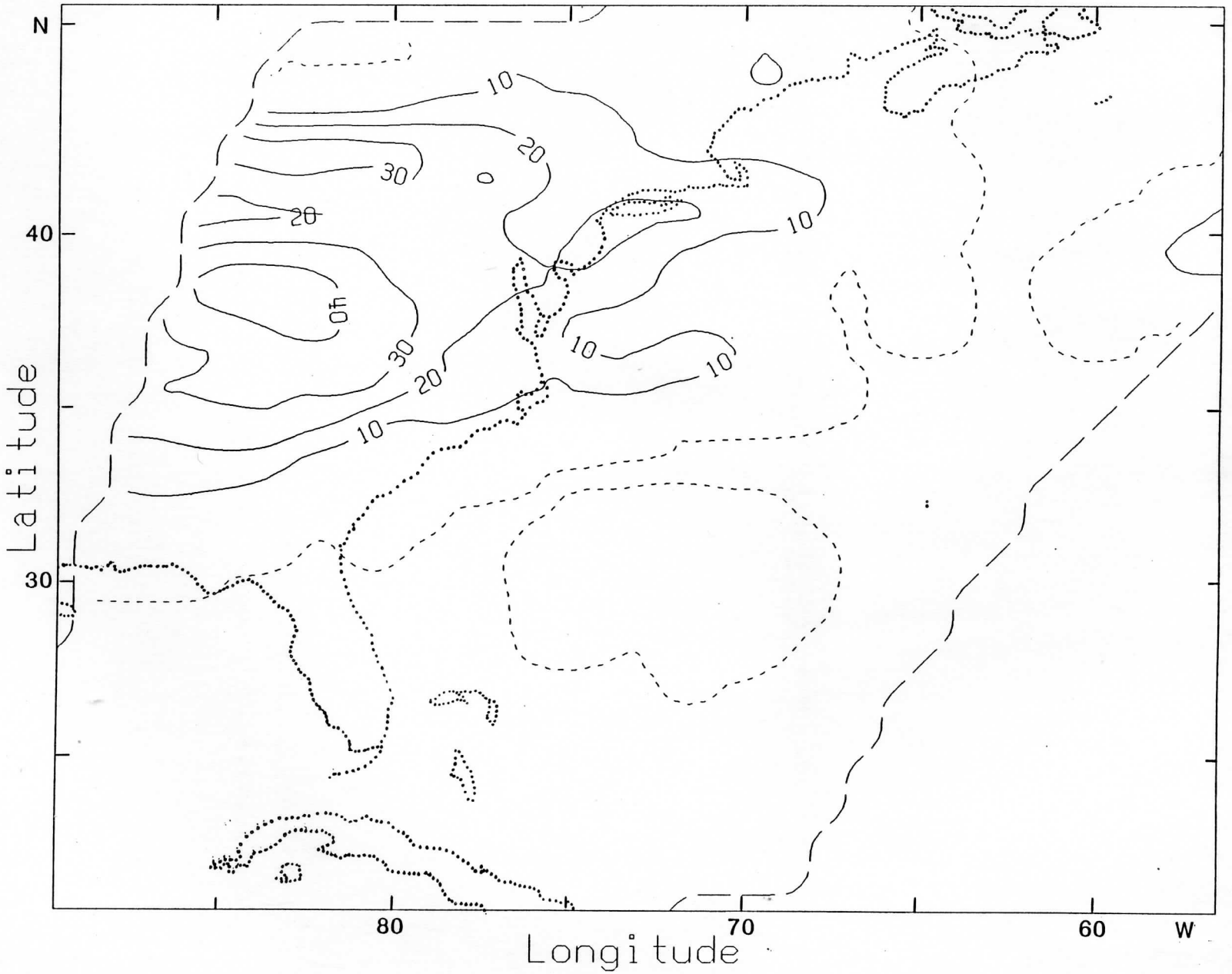
N
40
30
Latitude
10
20
30
0
20
10
30
20
10
10
10
10
80
70
60
W
Longitude

47

2/27

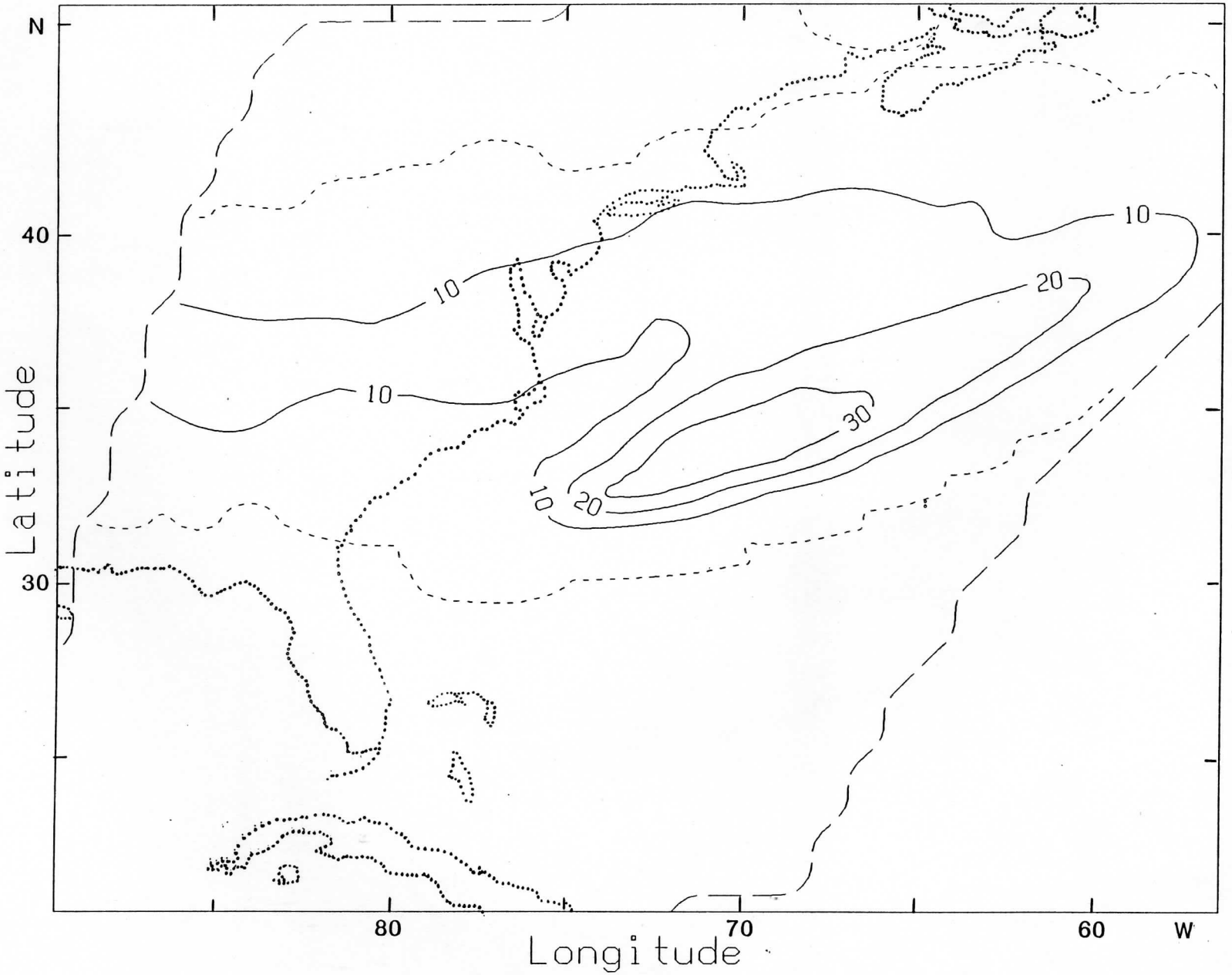

8h

3/1

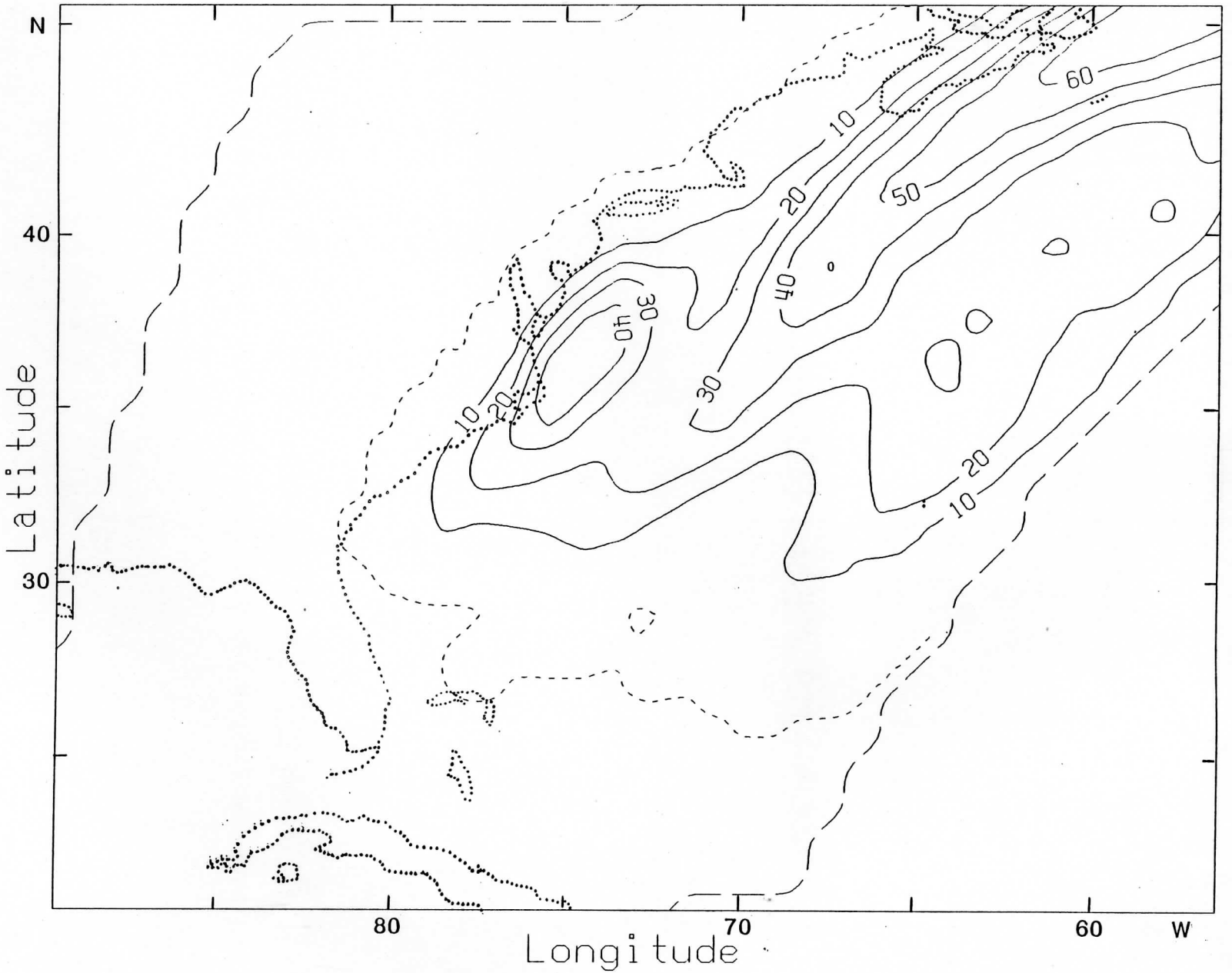

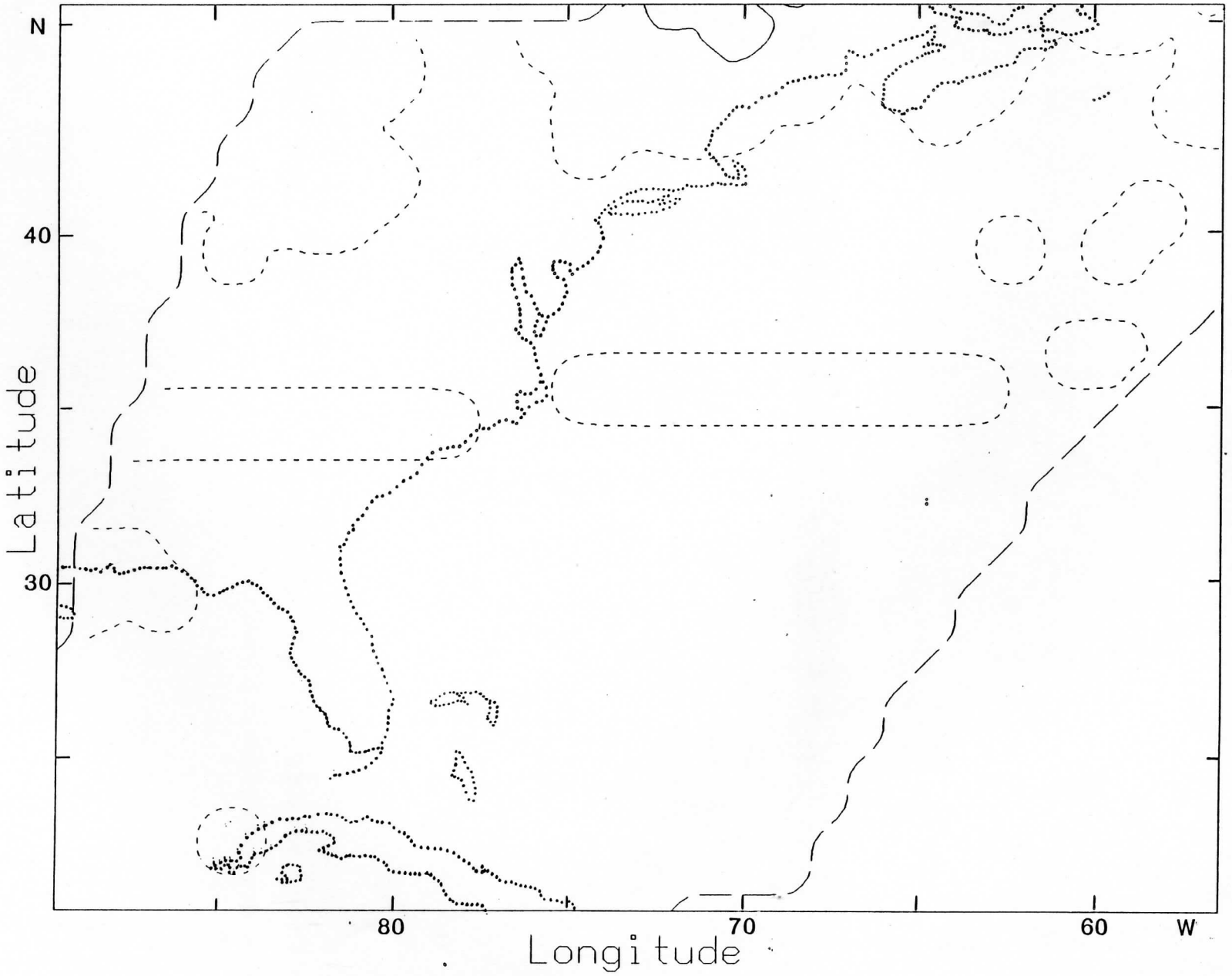
N
40
30
Latitude
80
70
60
W
Longitude

3/9

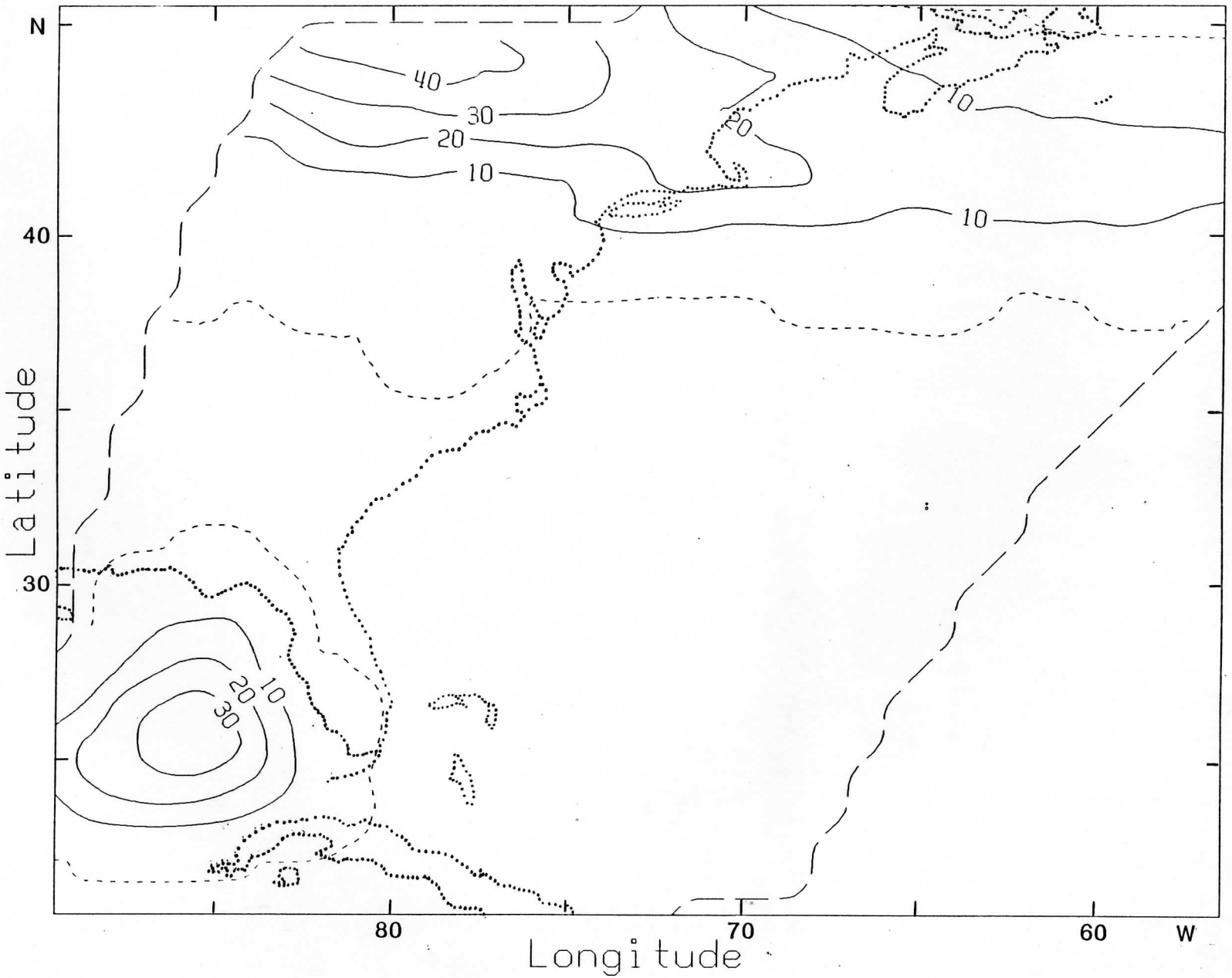

15

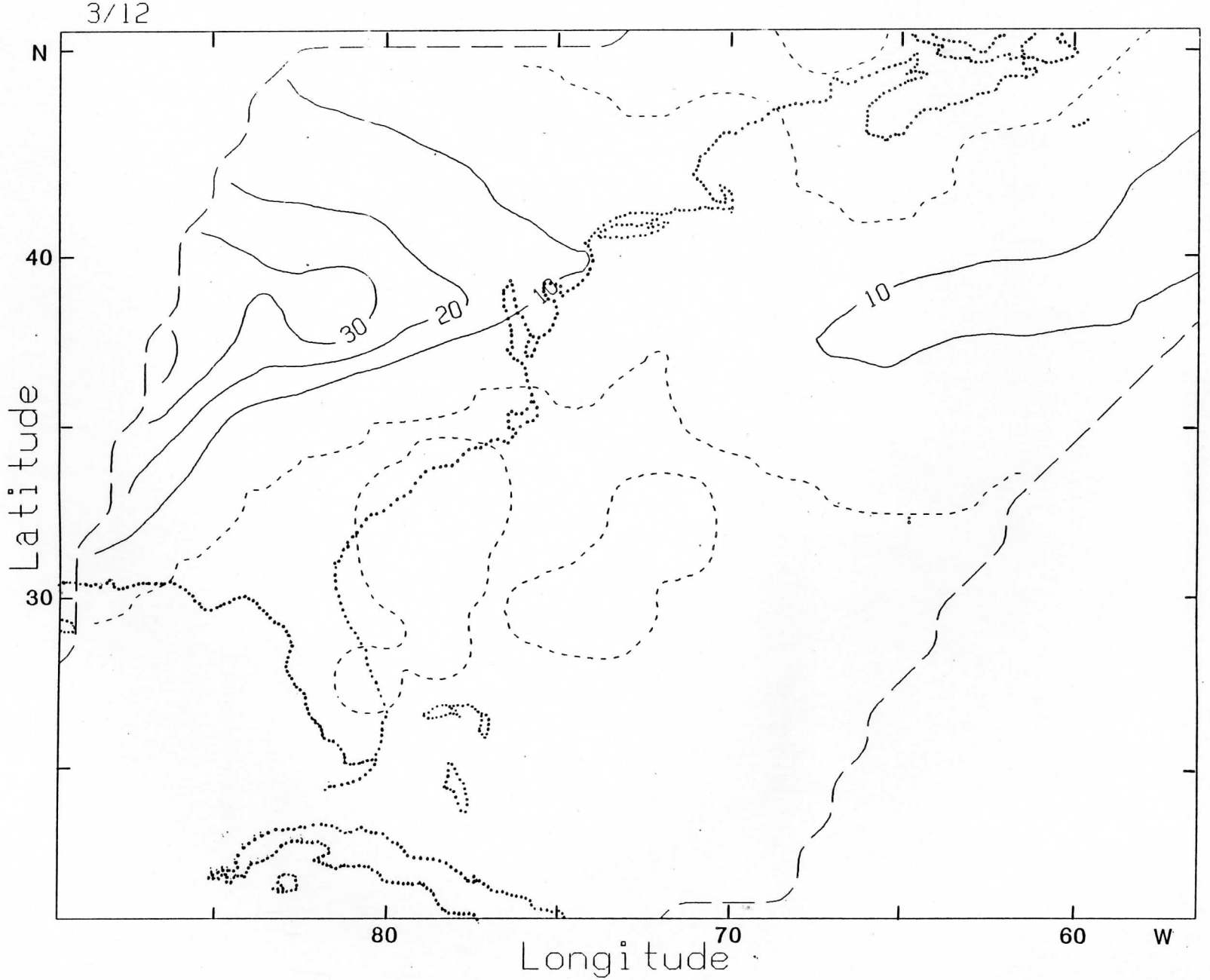
3/12
N
40
30
Latitude
30
20
10
10
80
70
60
W
Longitude

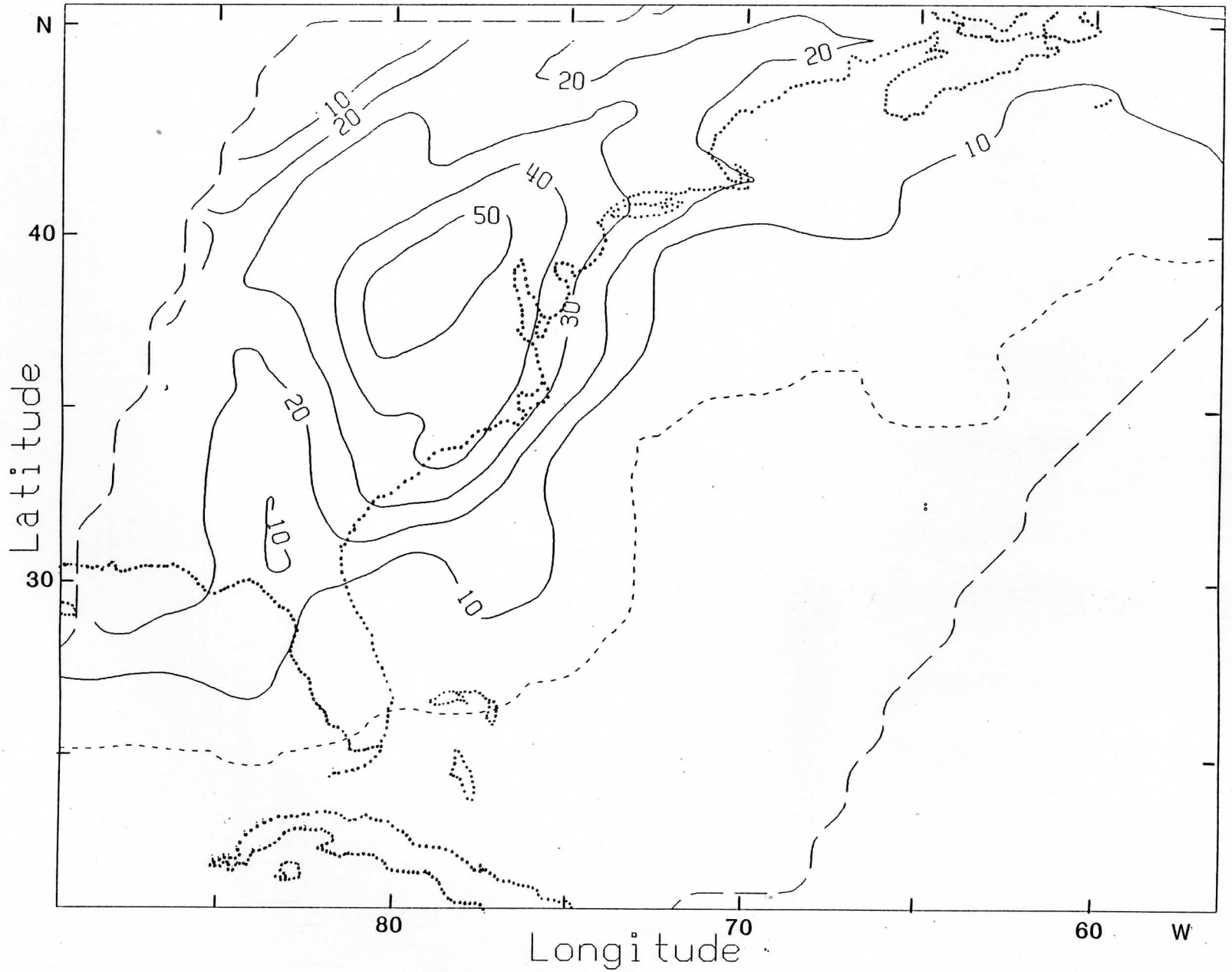
N
40
30
Latitude
80
70
60
W
Longitude
10
20
20
20
40
50
30
10
10
10

APPENDIX 2

SIX-HOUR MAPS

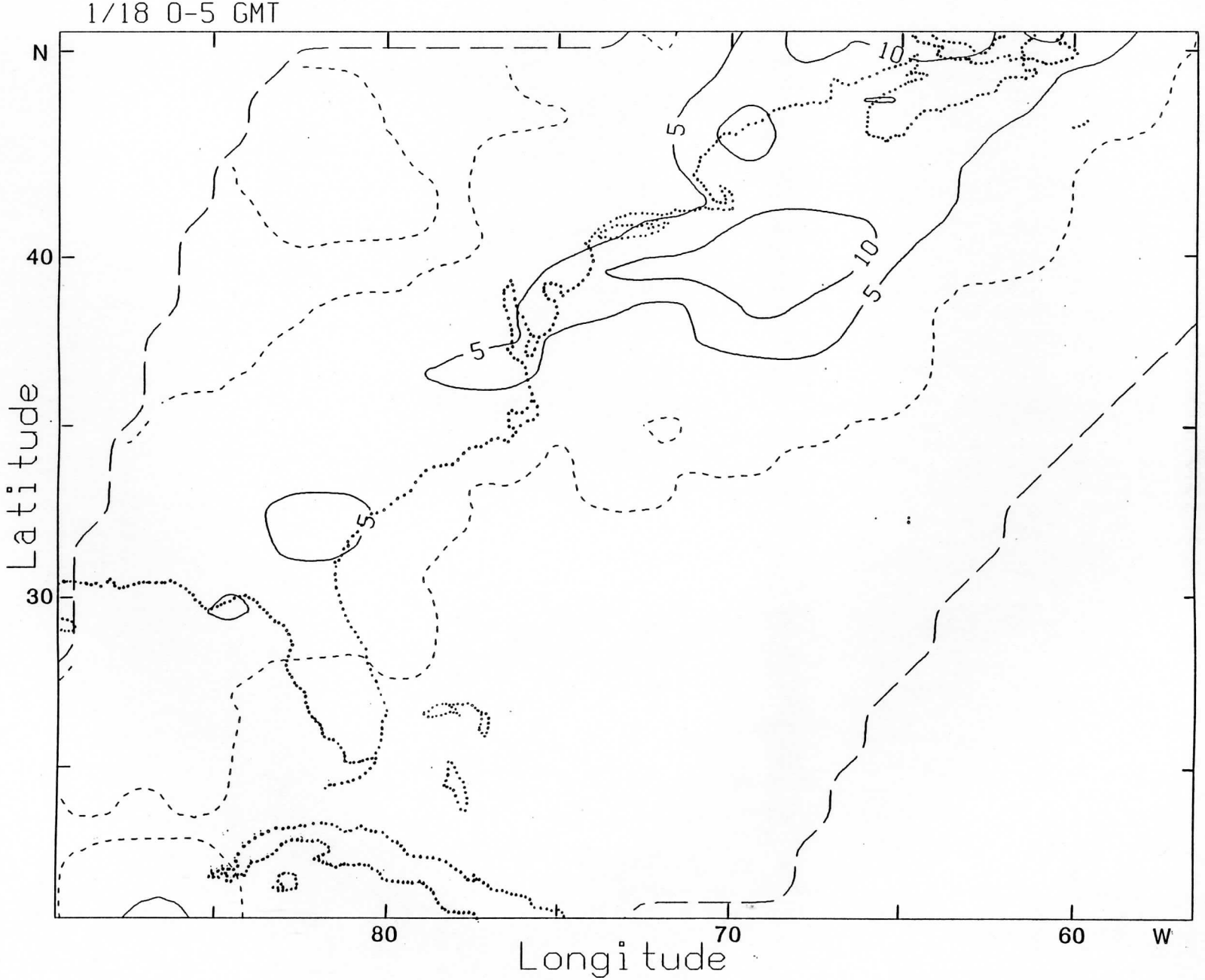

55

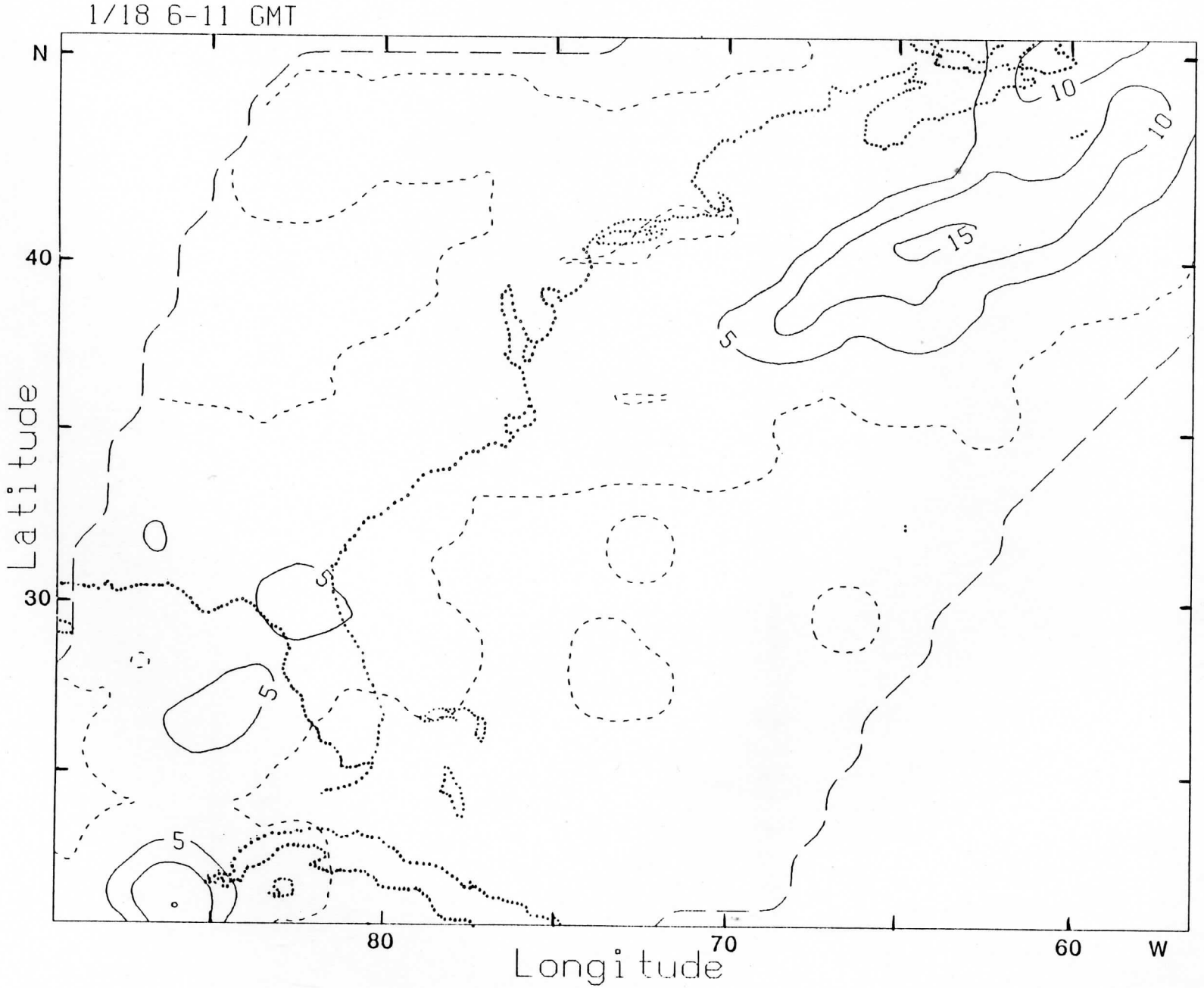

25

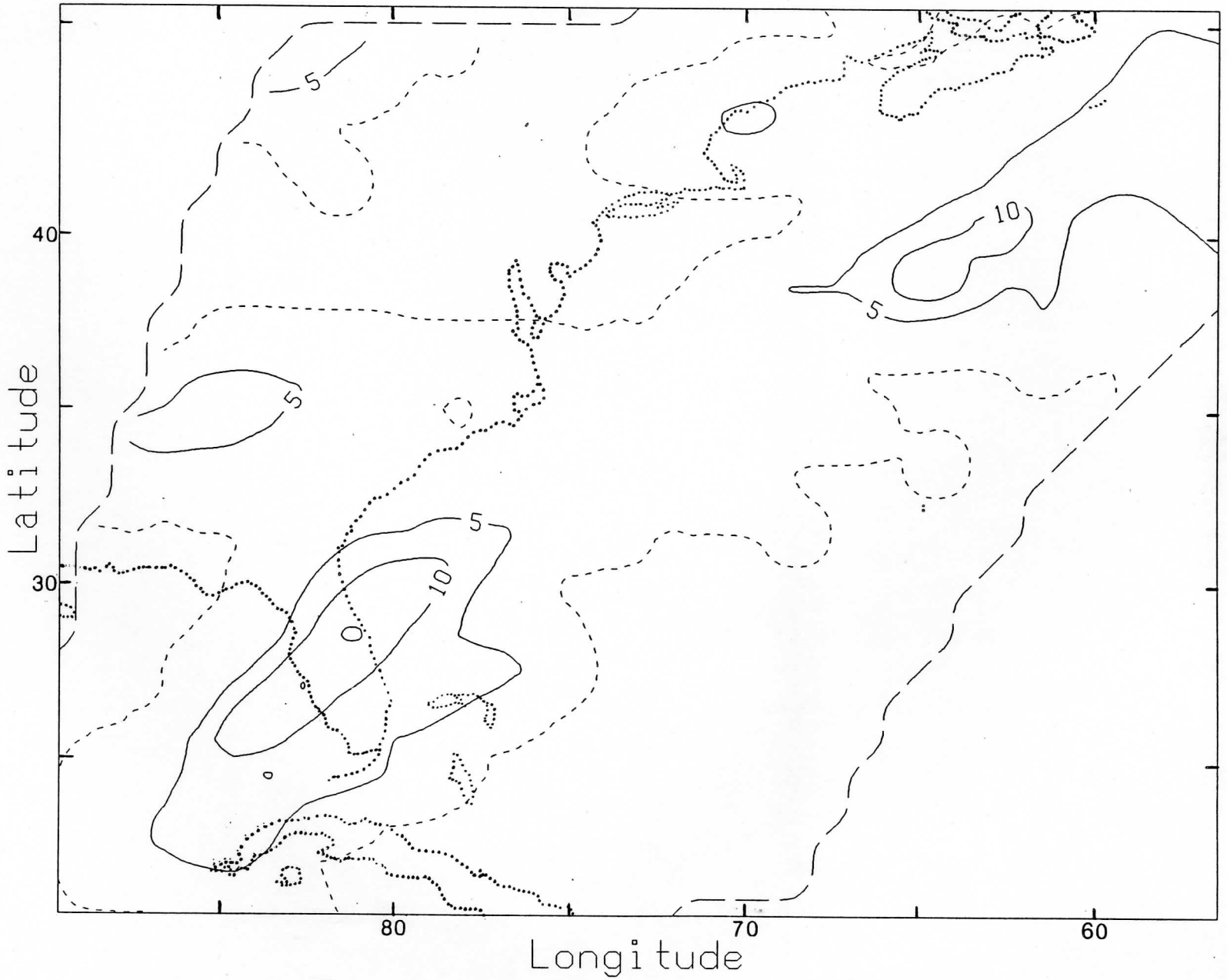

57

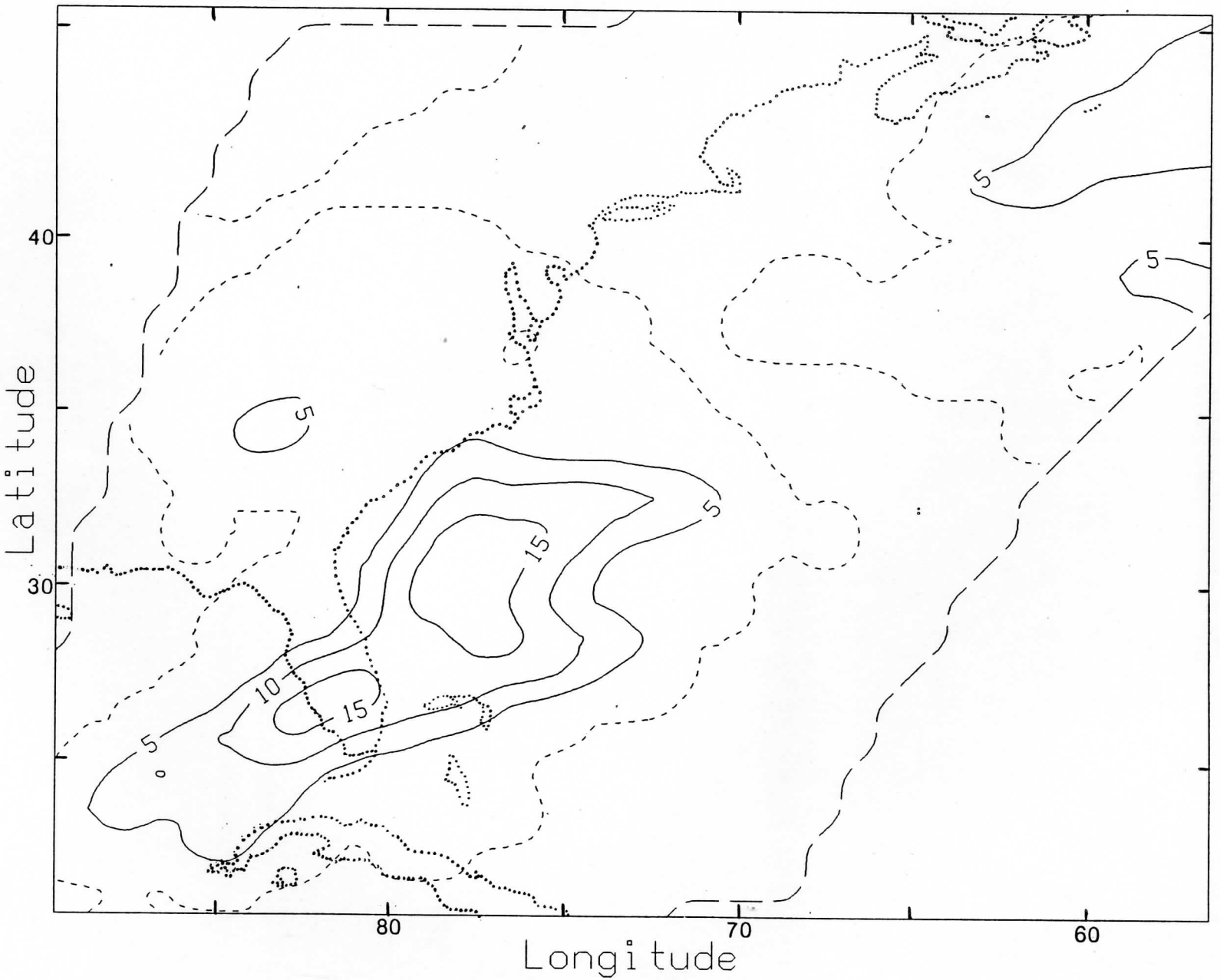
1/18 18-23 GMT
40
30
Latitude
80
70
60
Longitude
5
5
5
5
10
15
15

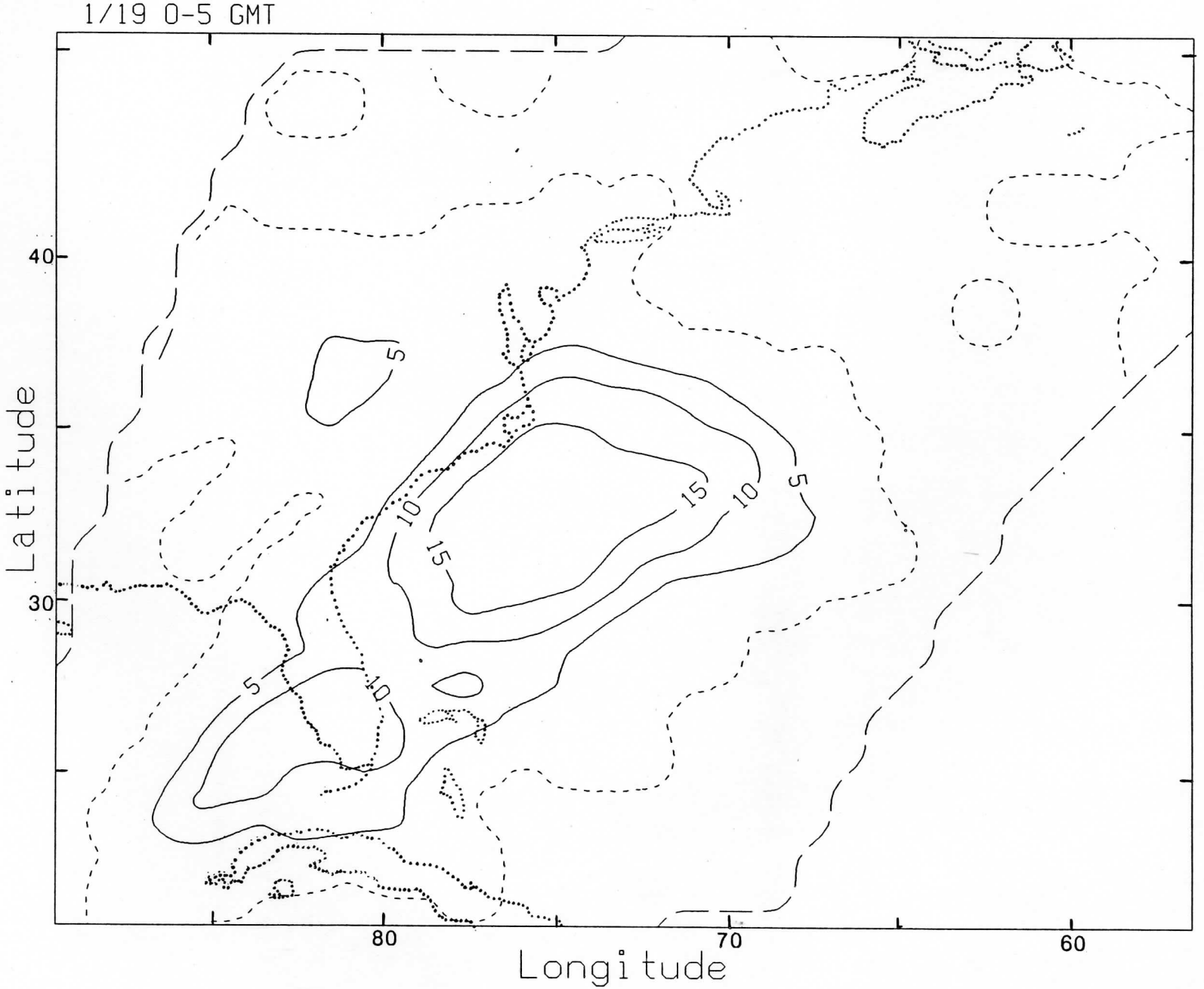
1/19 0-5 GMT
40
30
Latitude
80
70
60
Longitude
5
10
15
10
5
15
5
10

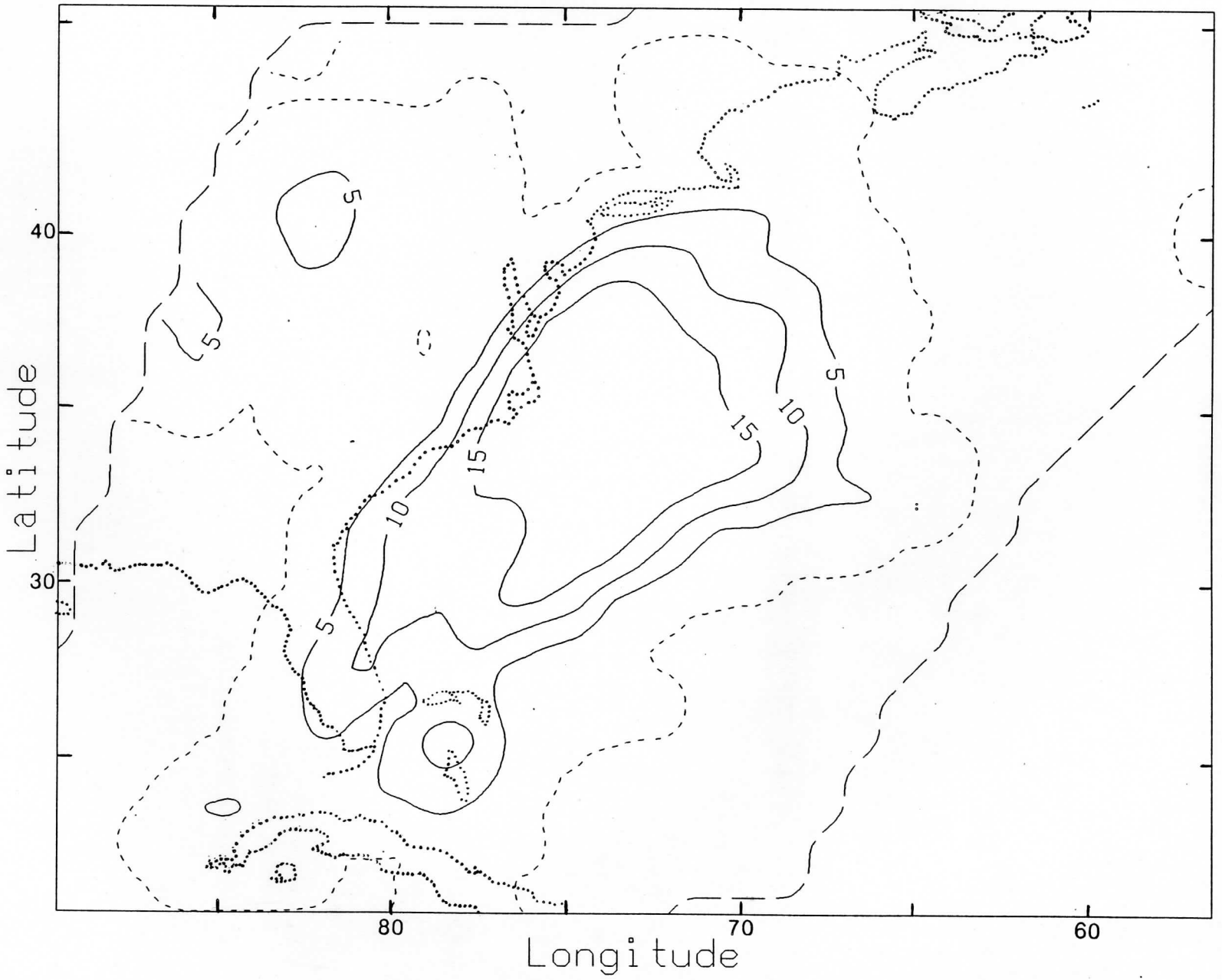
1/19 6-11 GMT
40
30
Latitude
80
70
60
Longitude
5
5
5
10
15
15
10
5
0

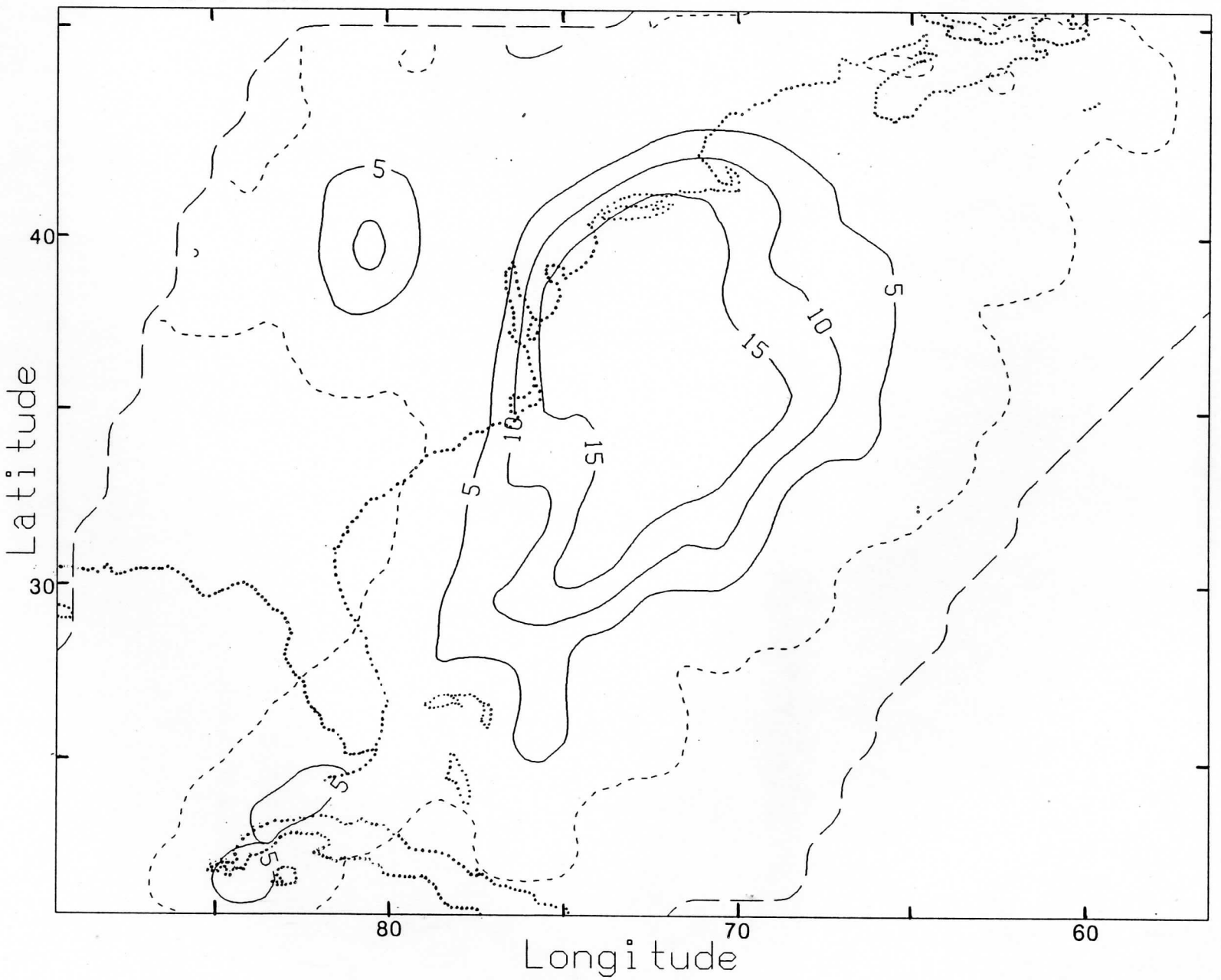
1/19 12-17 GMT
40
30
80
70
60
Latitude
Longitude
5
10
15
5
10
15
5
5

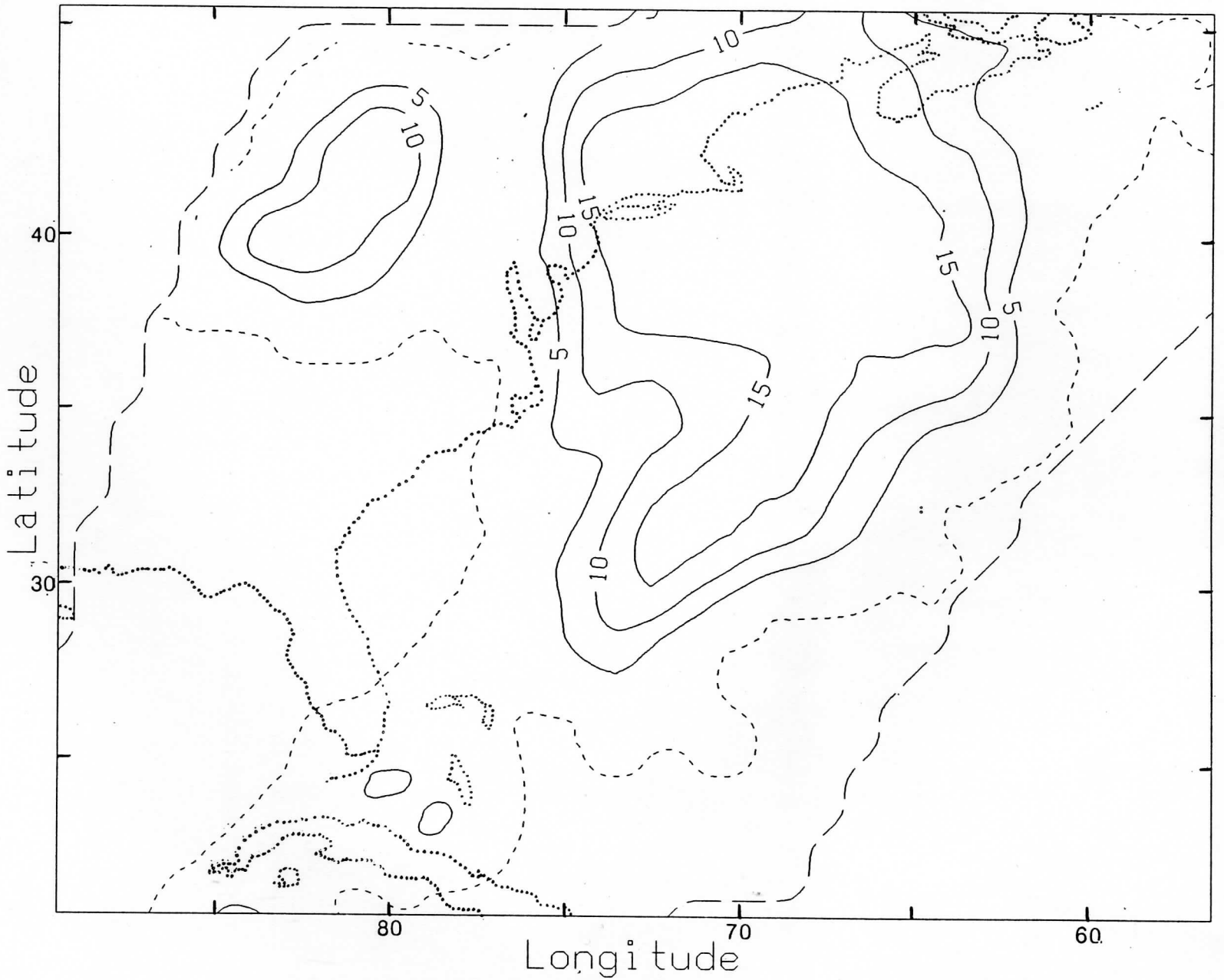
1/19 18-23 GMT
Latitude
40
30
80
70
60
Longitude
5
10
15
10
5
15
10
5
10
15

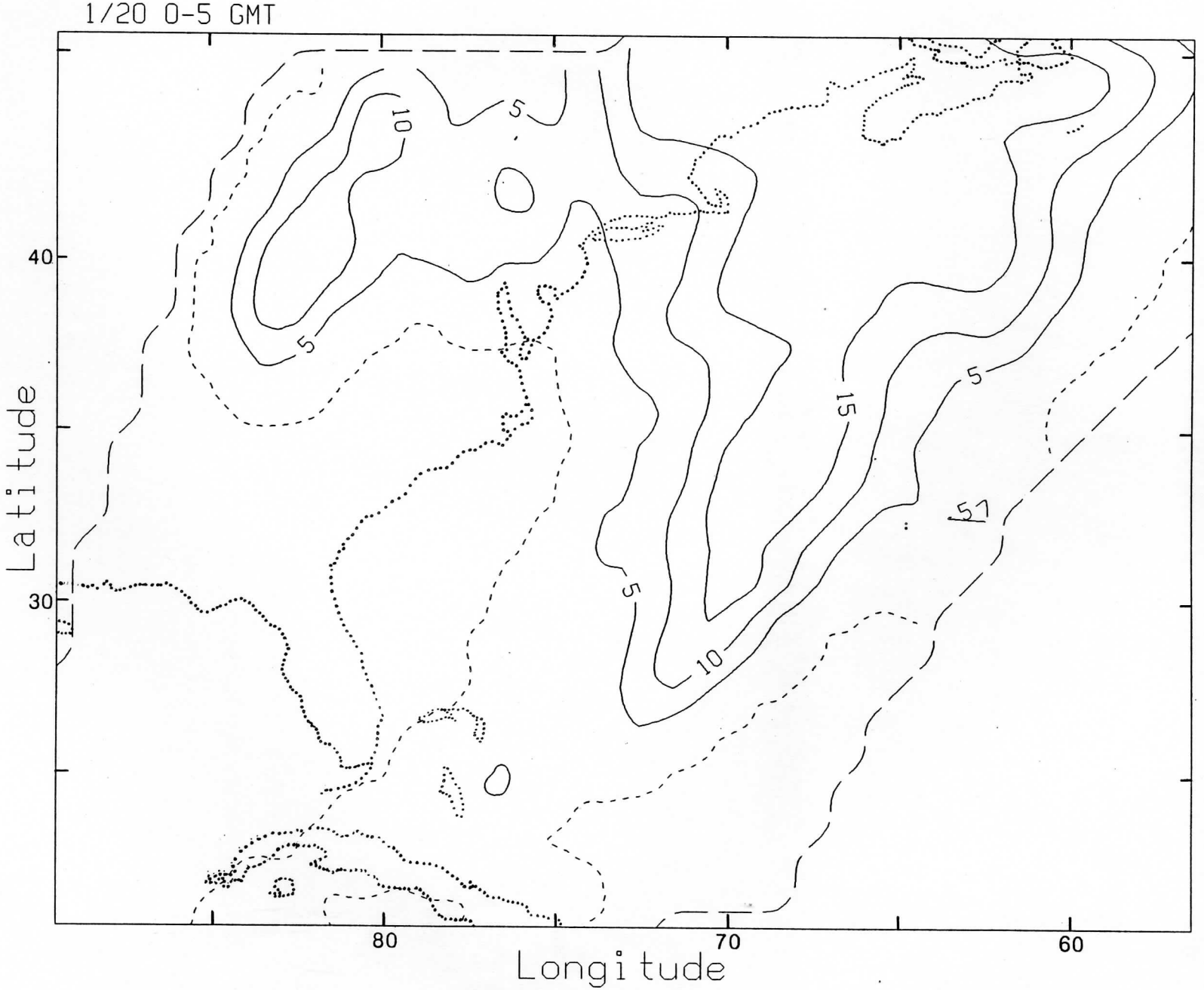
1/20 0-5 GMT
40
30
Latitude
80
70
60
Longitude
10
5
5
5
15
5
10
5
0
0

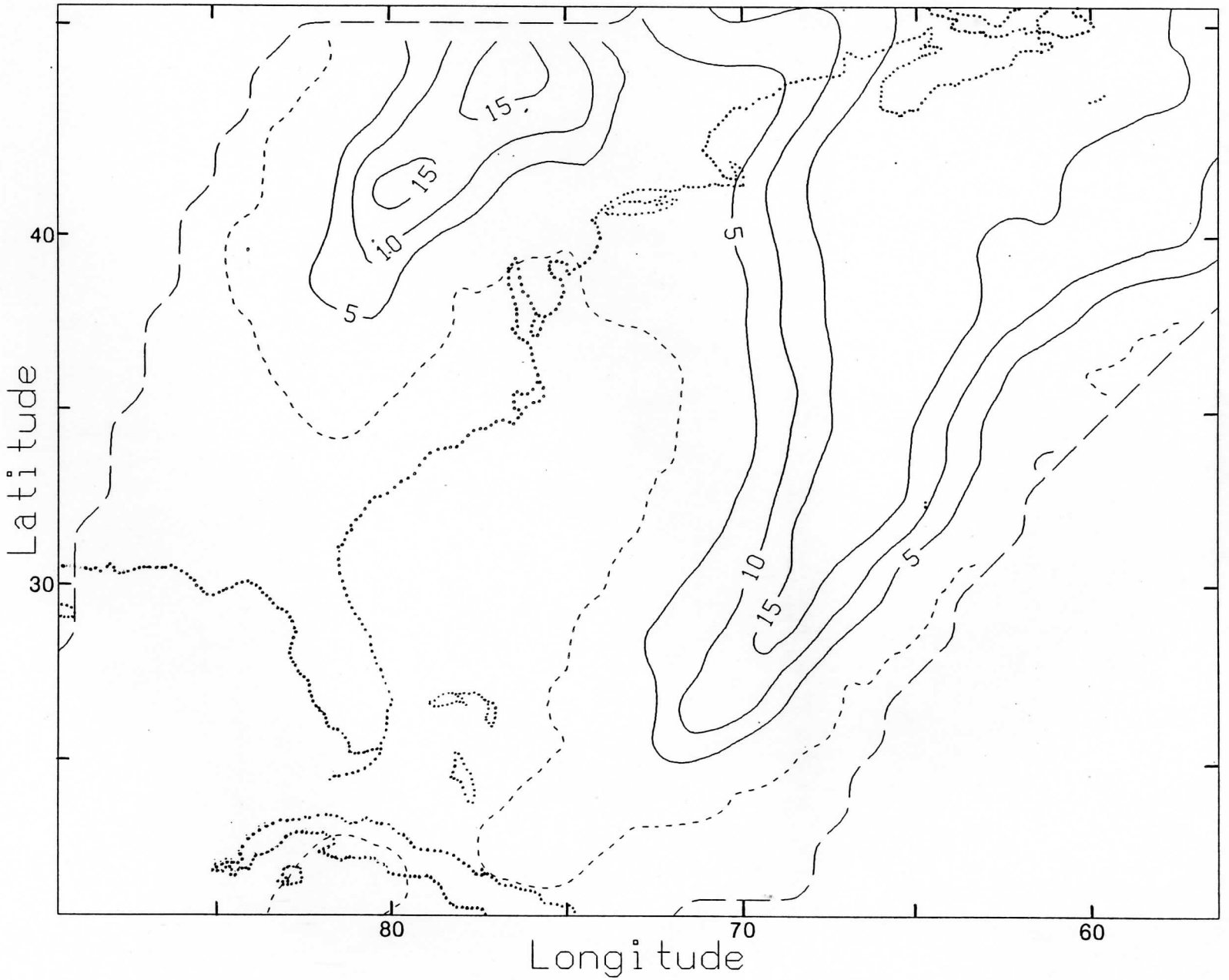
1/20 6-11 GMT
40
30
Latitude
80
70
60
Longitude
5
10
15
15
10
5
5
10
15
5

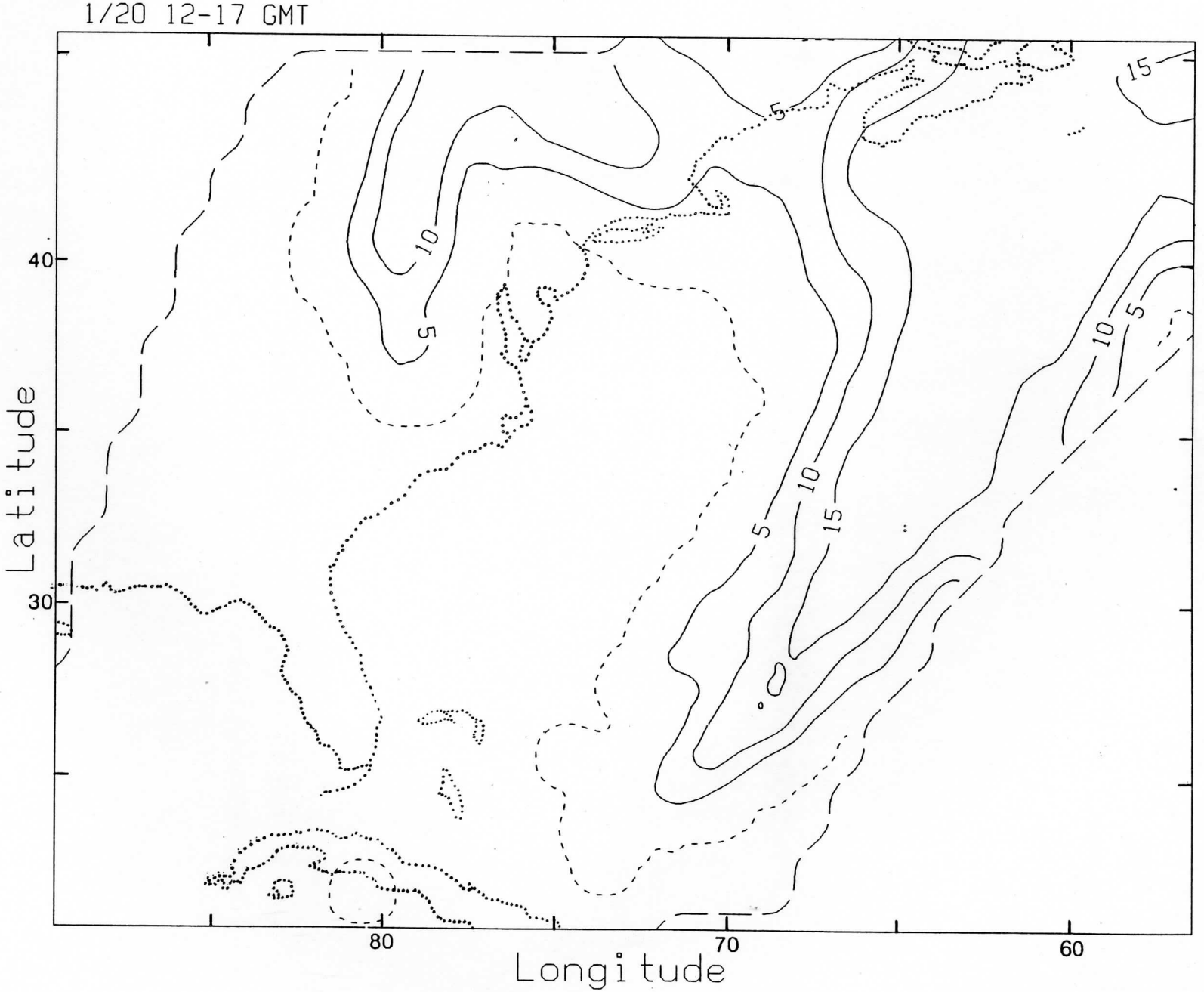
1/20 12-17 GMT
40
30
Latitude
80
70
60
Longitude
5
10
15

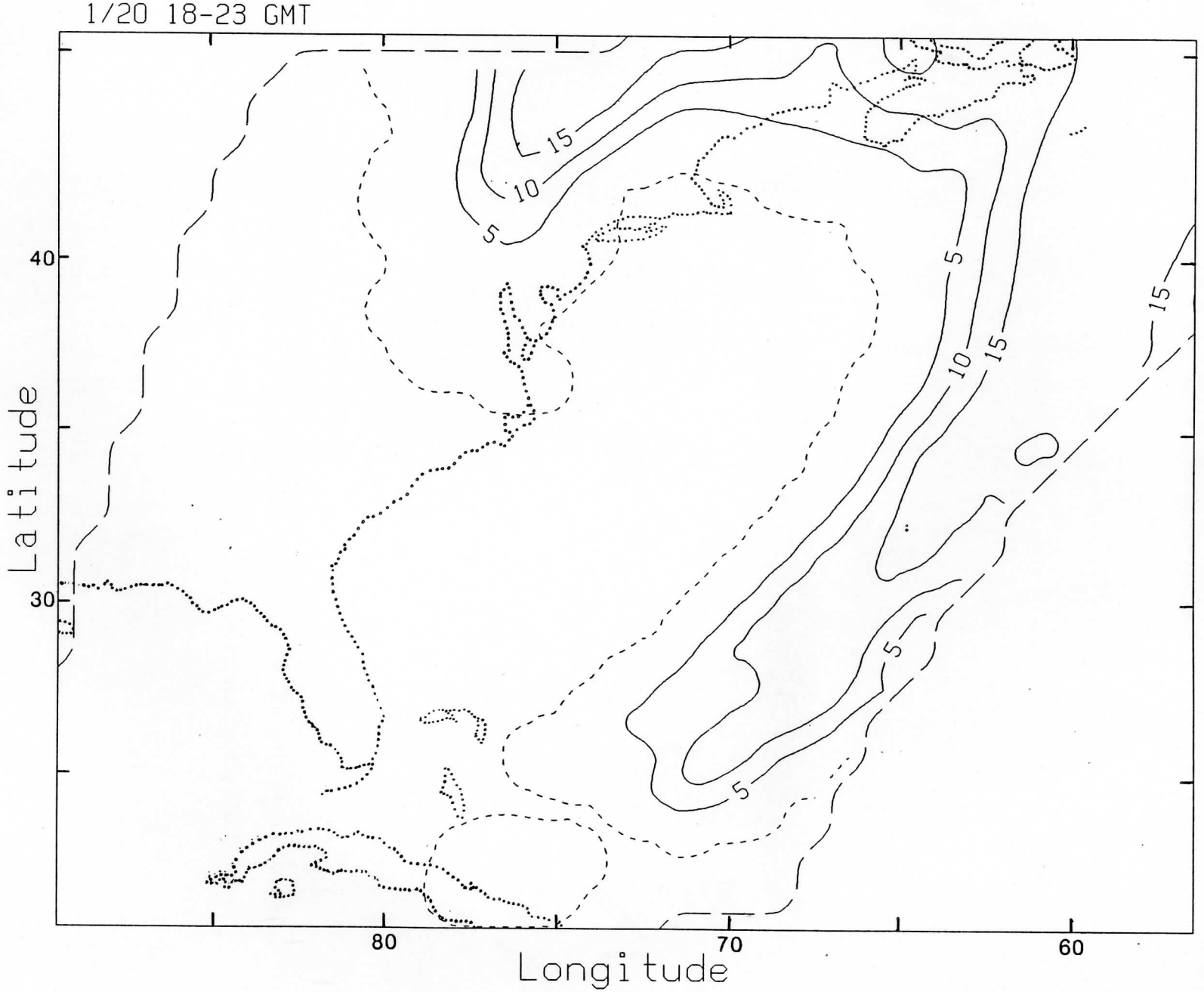
1/20 18-23 GMT
40
30
Latitude
80
70
60
Longitude
5
10
15
5
10
15
15
5
5
0

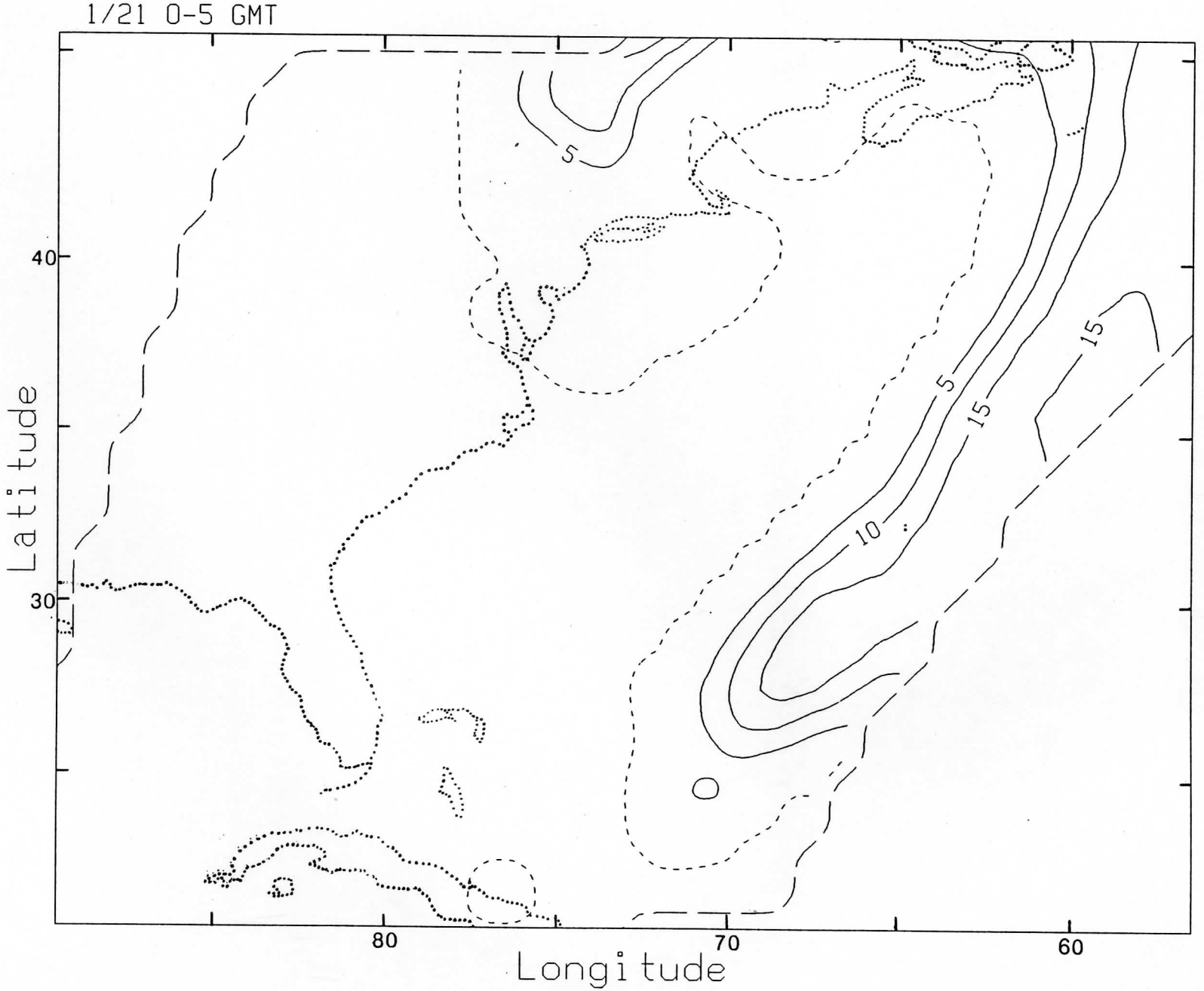

67

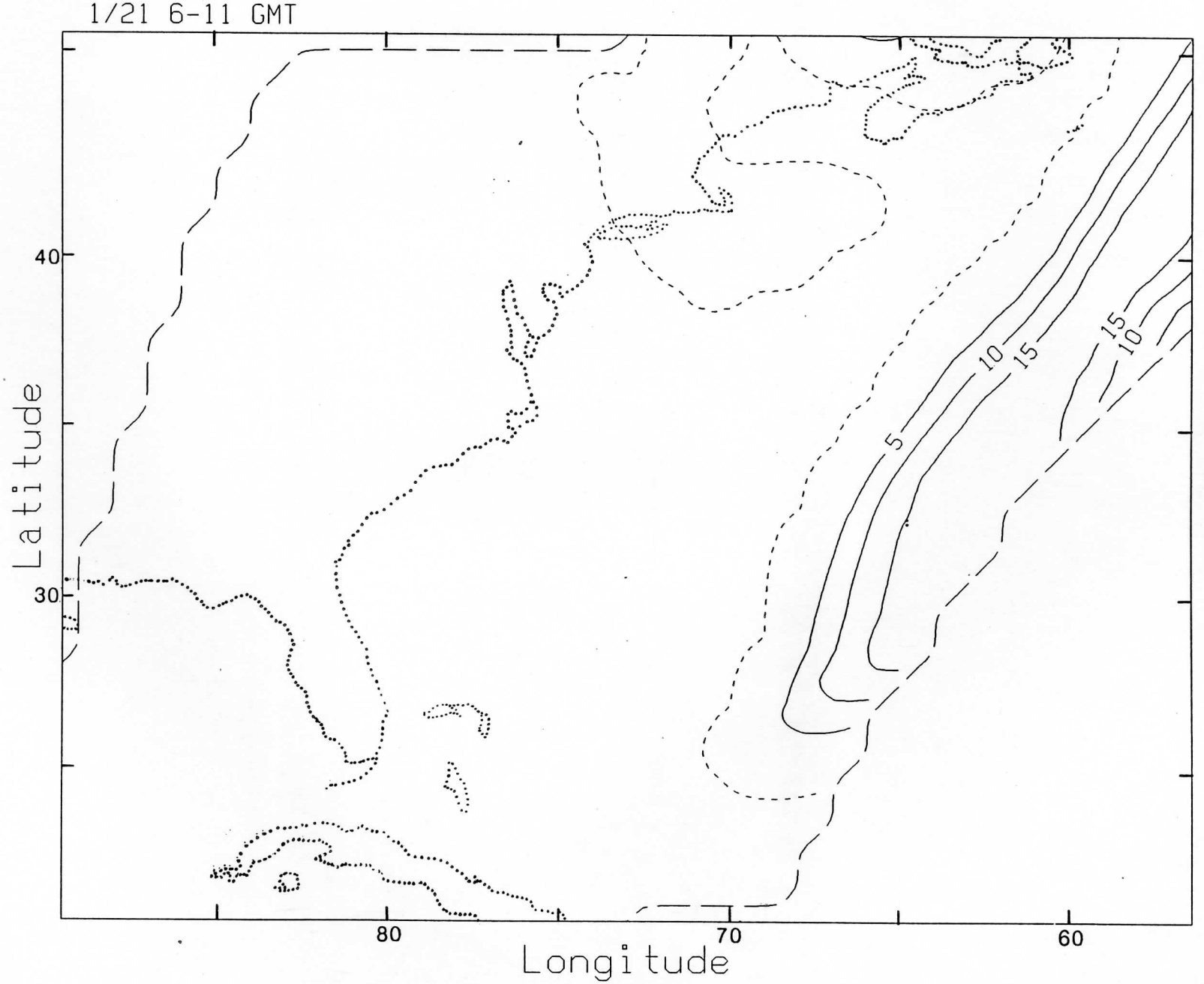
1/21 6-11 GMT
40
30
Latitude
80
70
60
Longitude
5
10
15
15
10

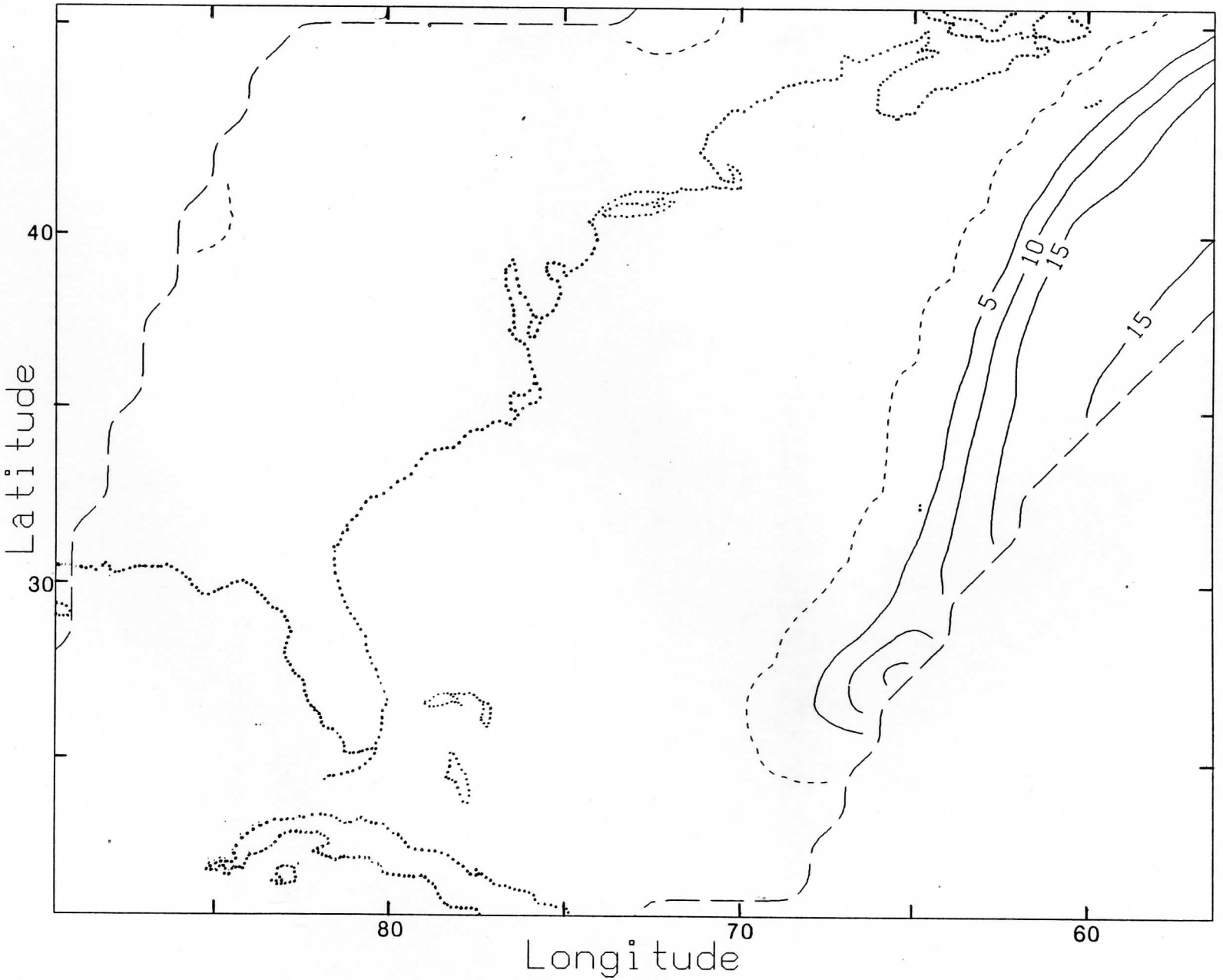
1/21 12-17 GMT
40
30
Latitude
80
70
60
Longitude
5
10
15
15

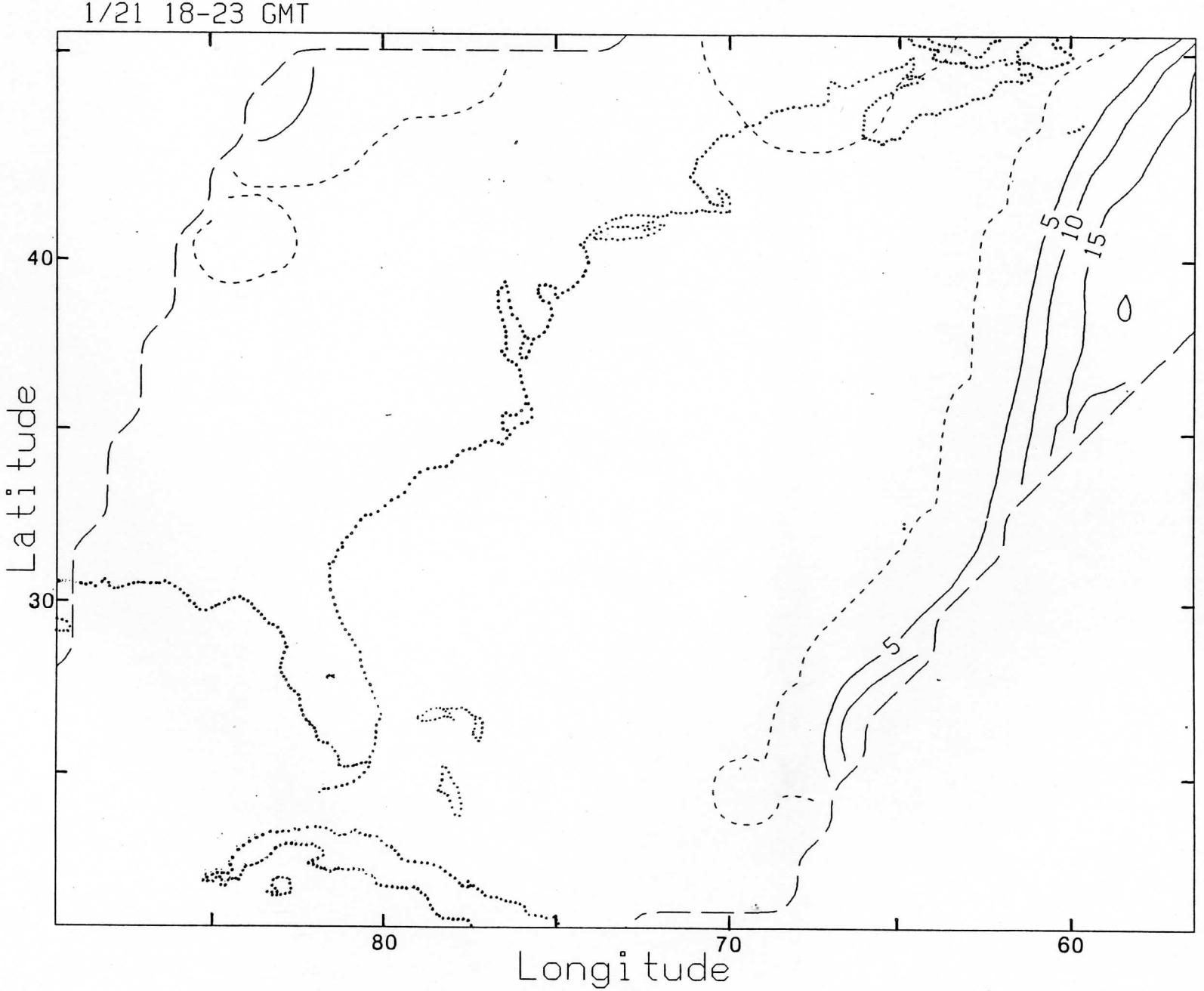
1/21 18-23 GMT
40
30
Latitude
80
70
60
Longitude
5
10
15
5
0

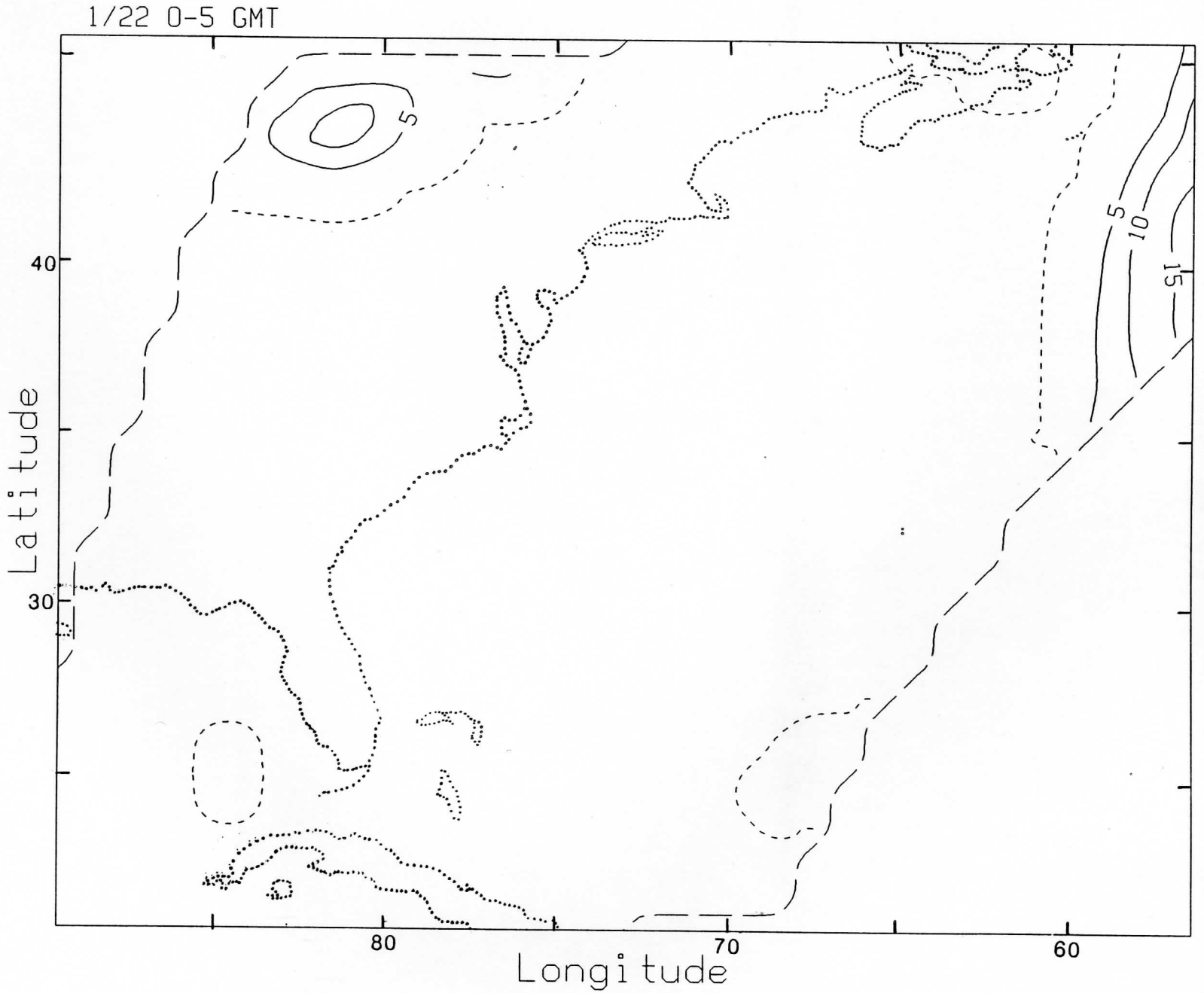

16

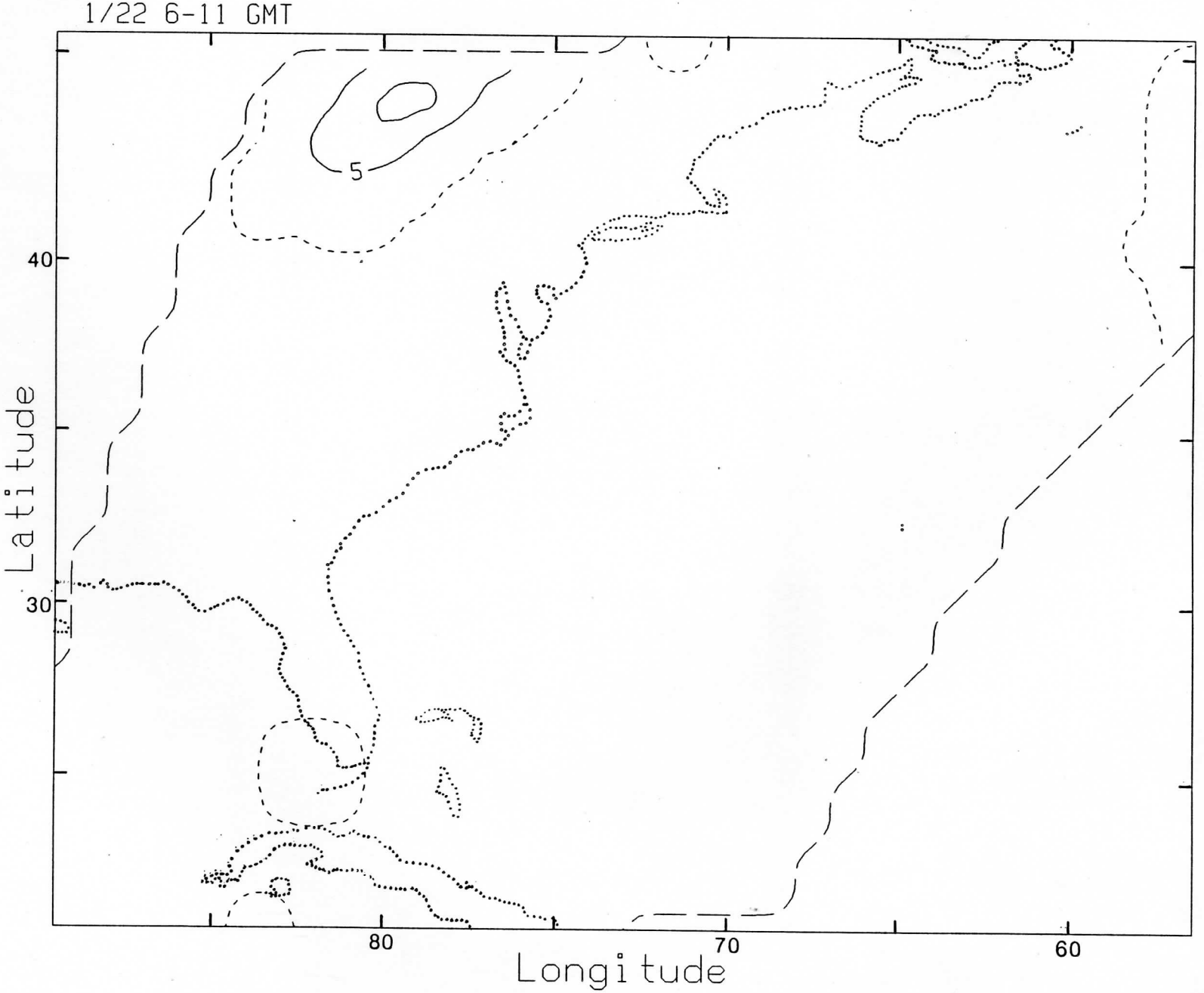
1/22 6-11 GMT
5
40
30
Latitude
80
70
60
Longitude

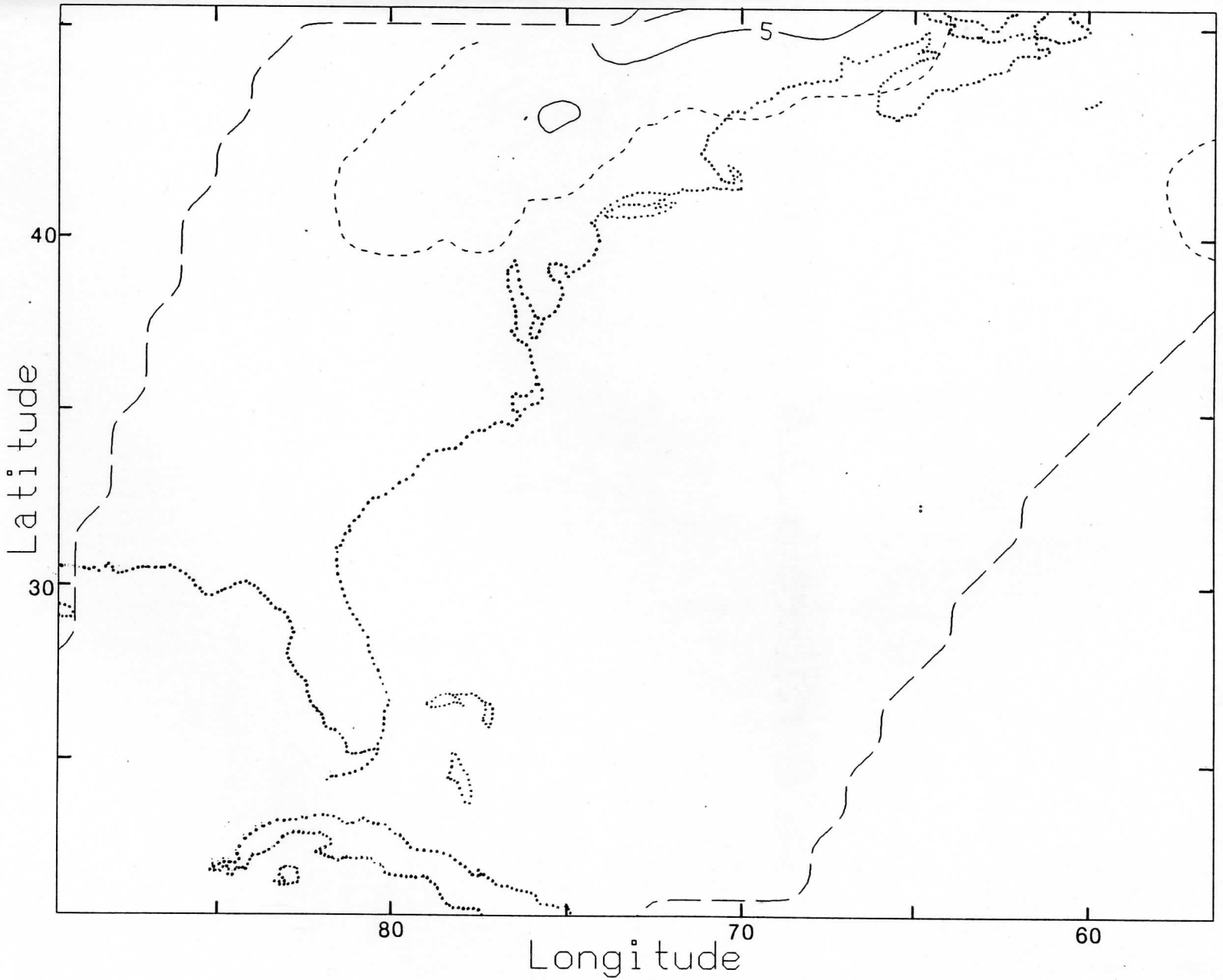
1/22 12-17 GMT
5
40
30
Latitude
80
70
60
Longitude

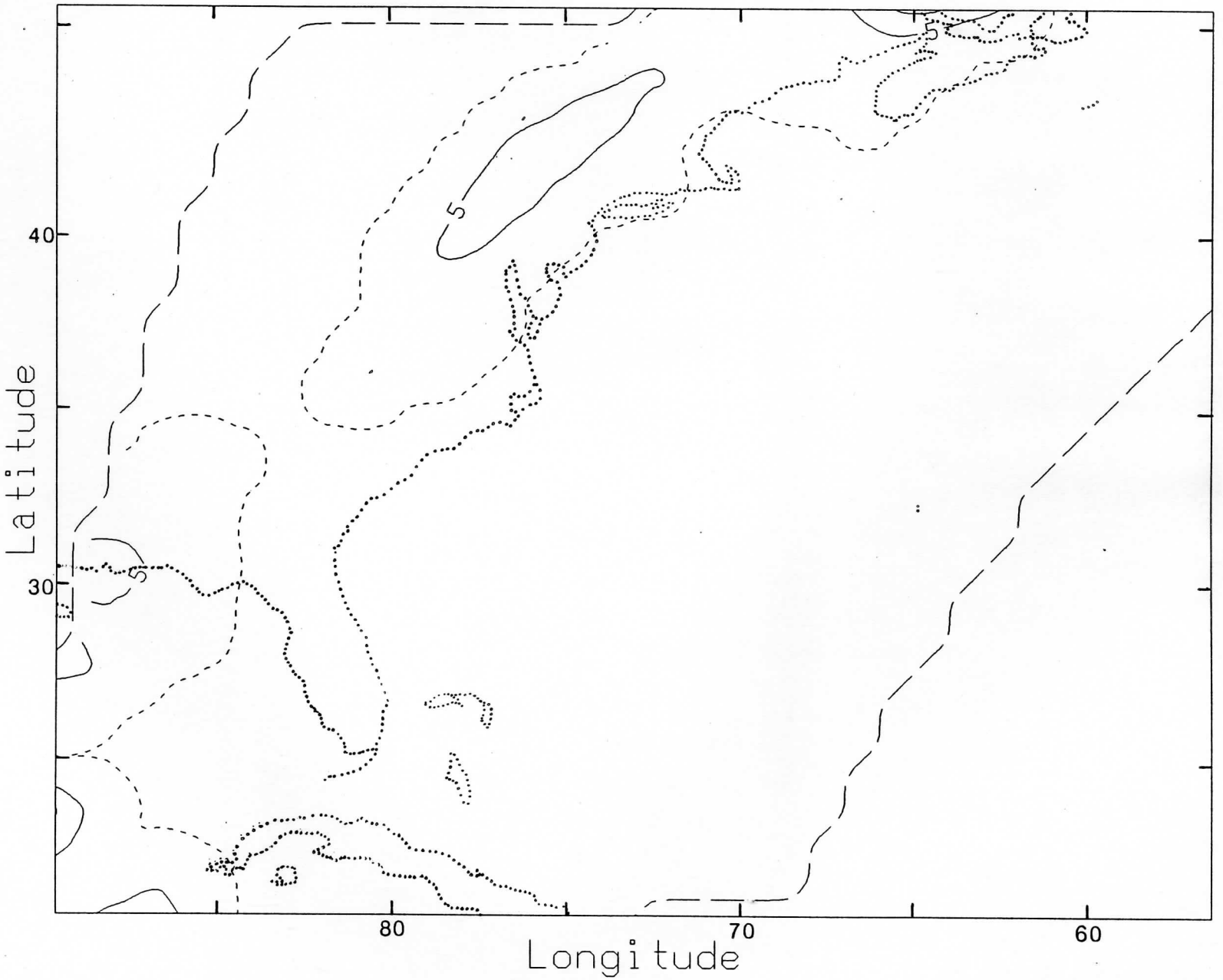
1/22 18-23 GMT
5
5
5
40
30
Latitude
80
70
60
Longitude

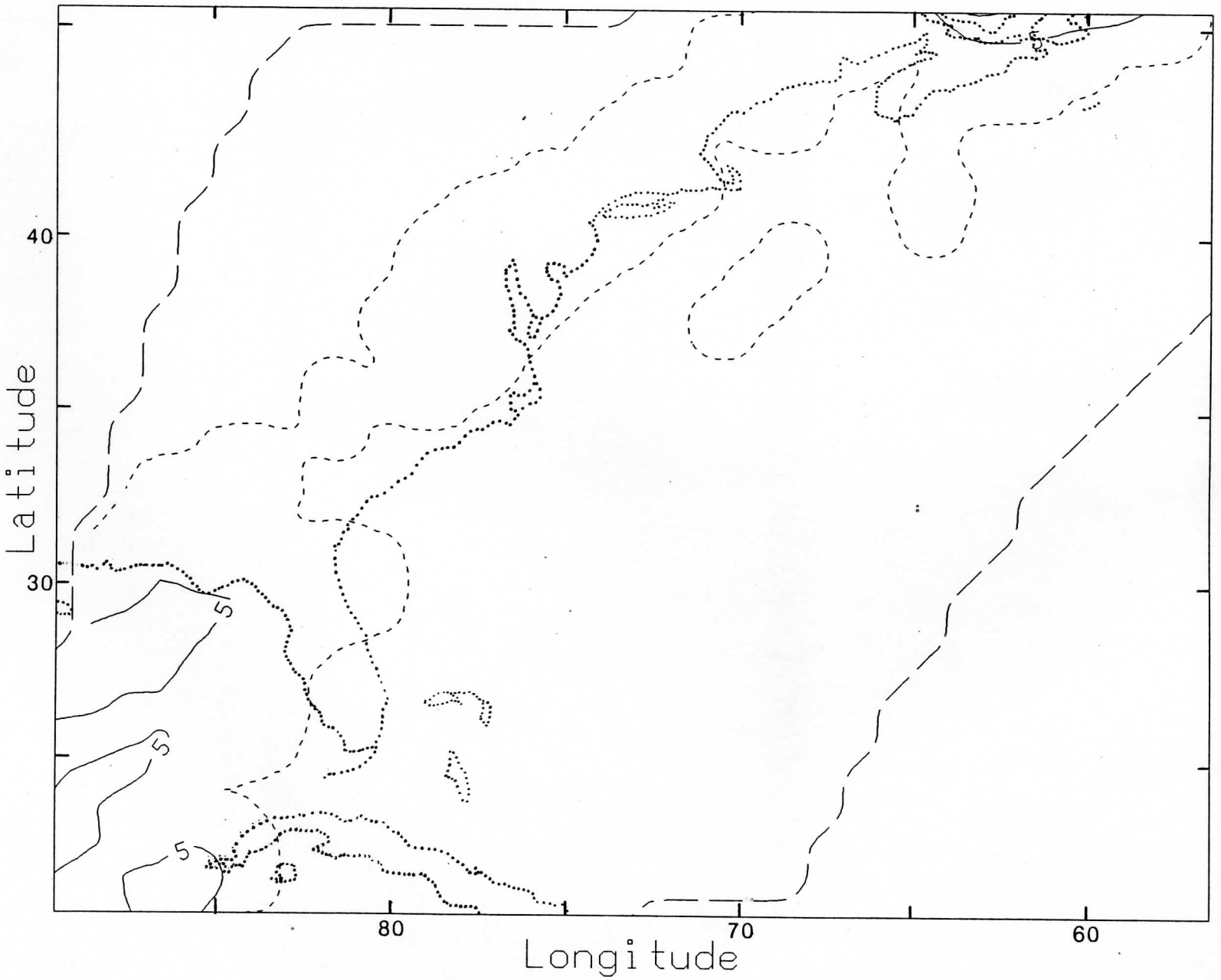
1/23 0-5 GMT
40
30
Latitude
80
70
60
Longitude
5
5
5

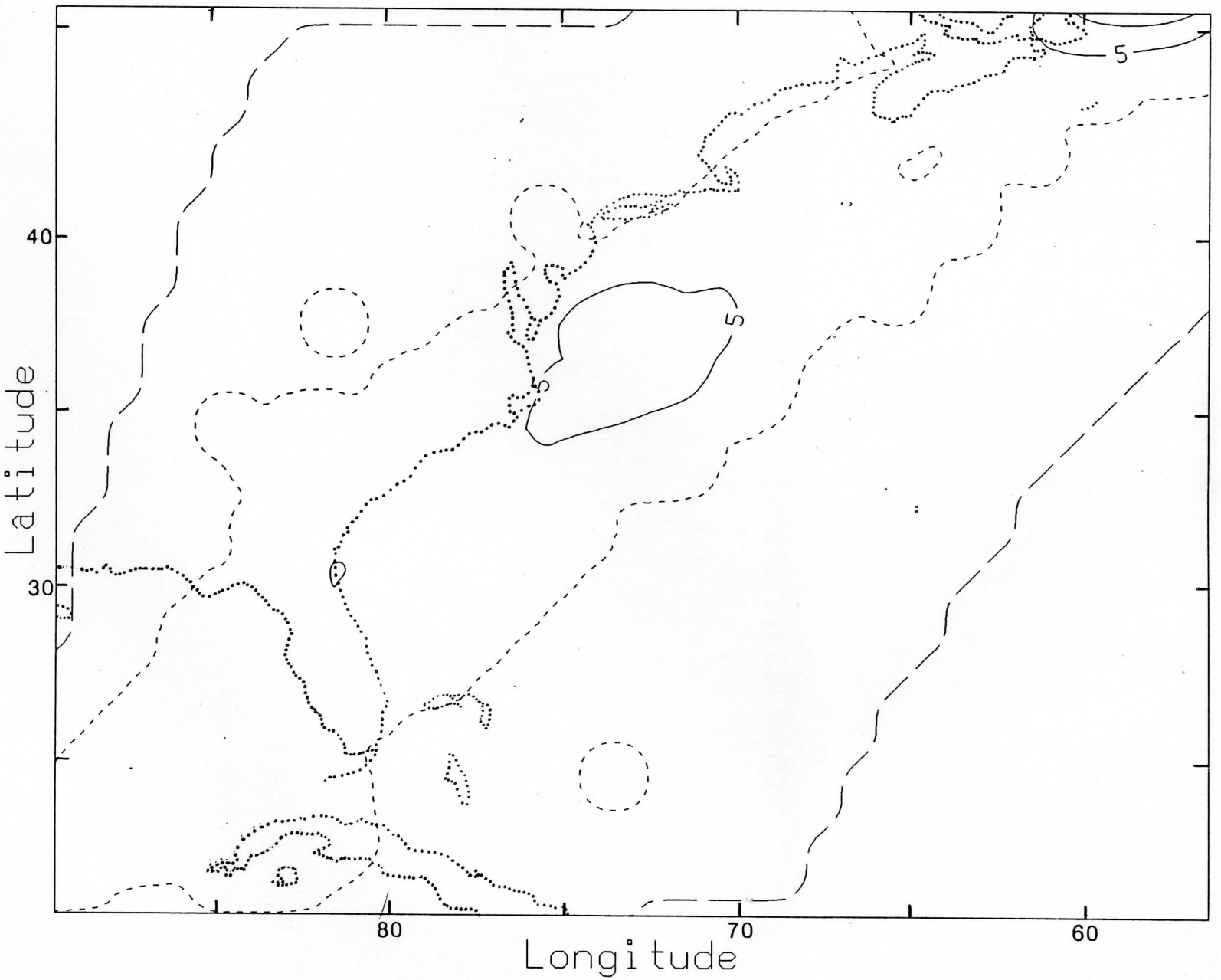
1/23 6-11 GMT
5
5
5
40
30
80
70
60
Latitude
Longitude

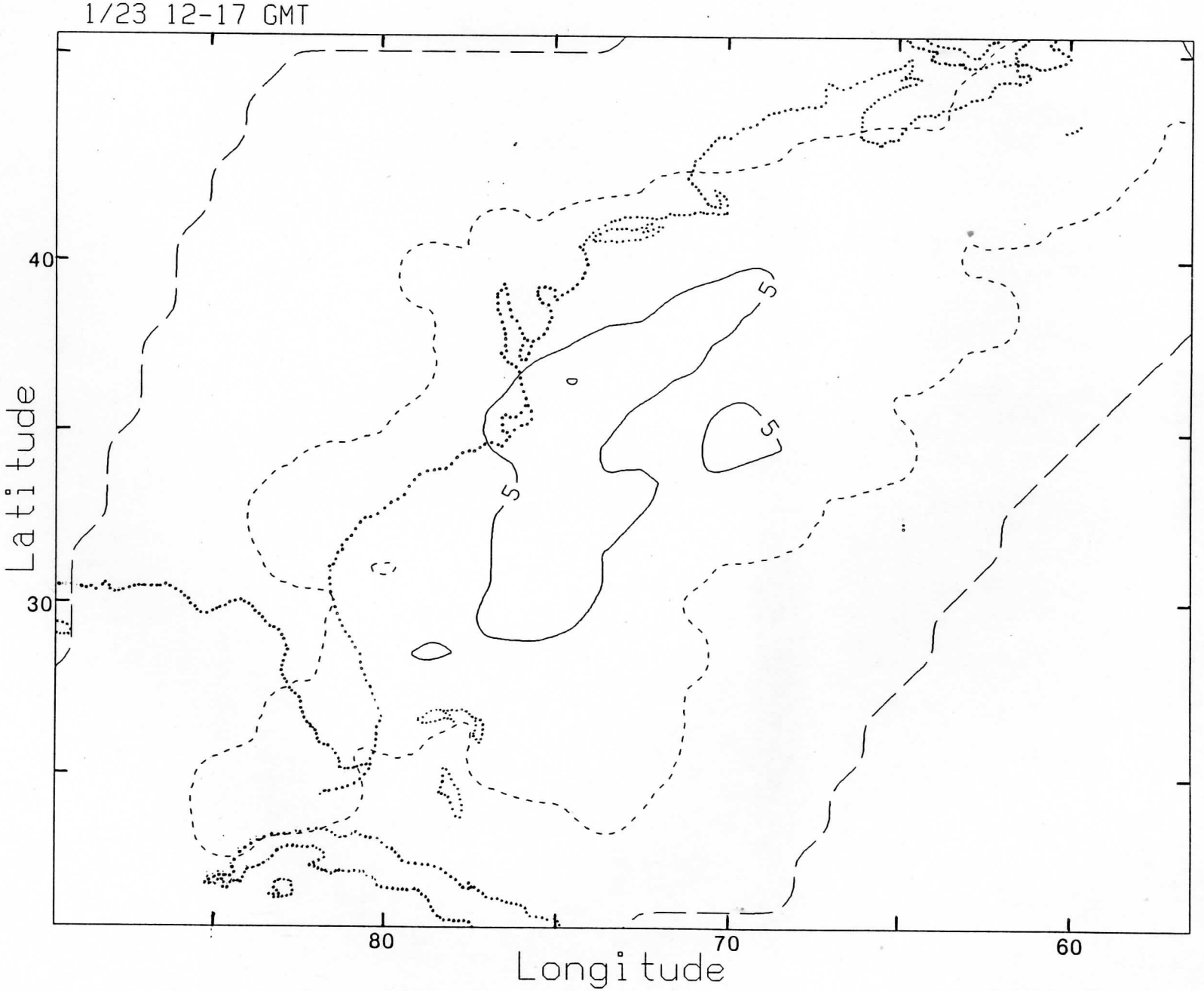
1/23 12-17 GMT
40
30
Latitude
80
70
60
Longitude

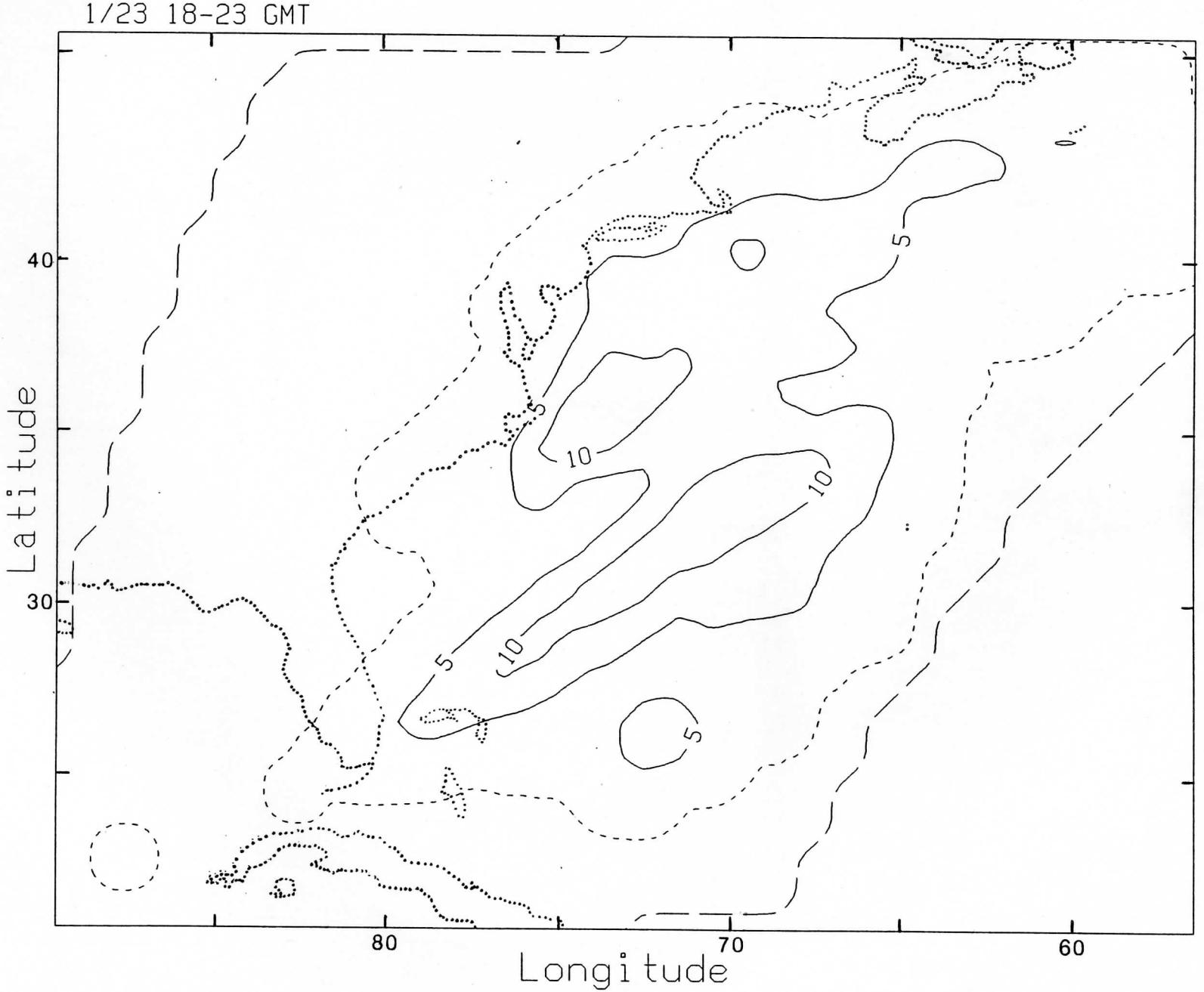
1/23 18-23 GMT
40
30
Latitude
80
70
60
Longitude
0
5
10
5
10
10
5
5

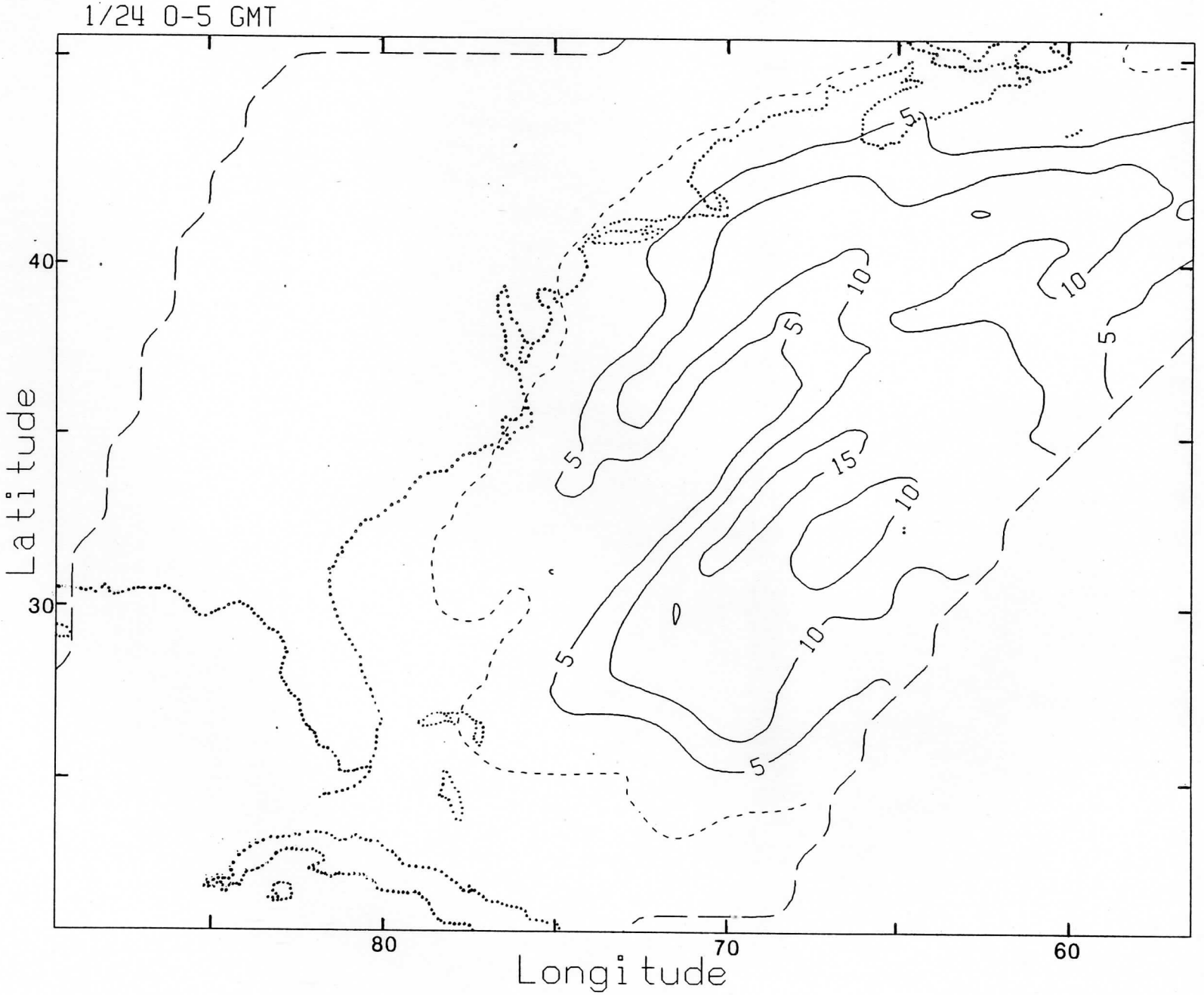
1/24 0-5 GMT
40
30
Latitude
80
70
60
Longitude
5
10
15

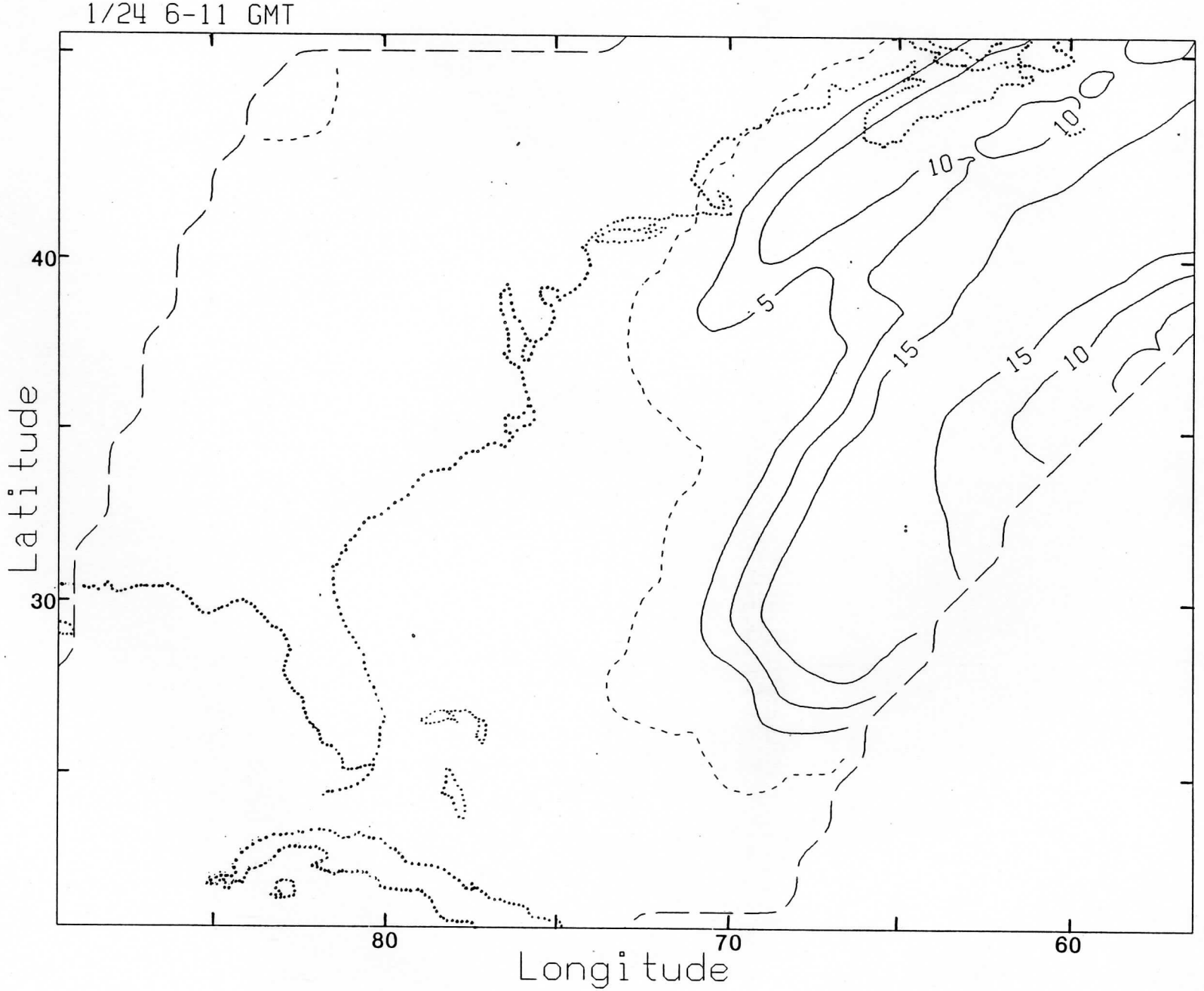
1/24 6-11 GMT
40
30
Latitude
80
70
60
Longitude
5
10
10
10
15
15
10

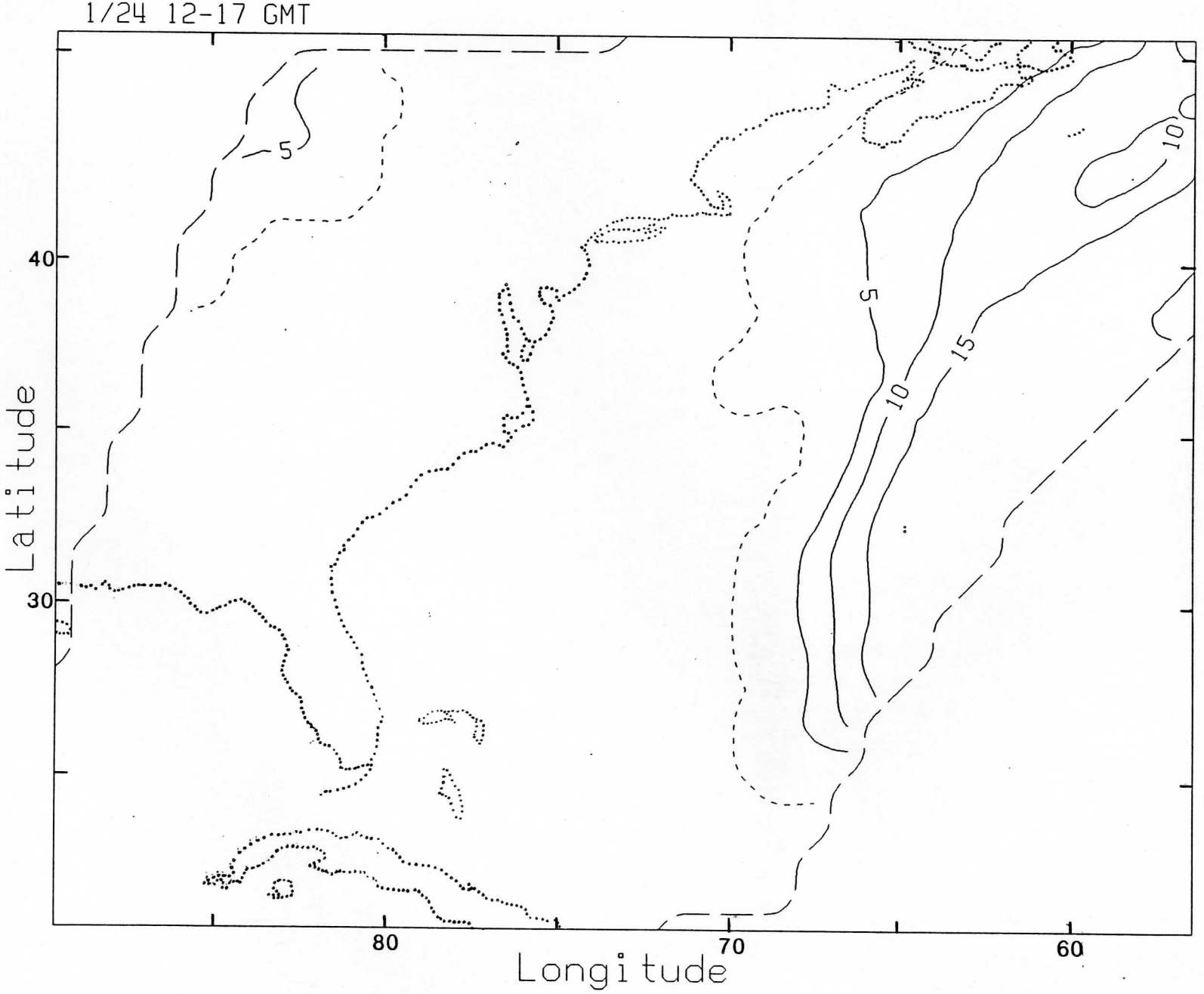
1/24 12-17 GMT
5
10
5
10
15
40
30
Latitude
80
70
60
Longitude

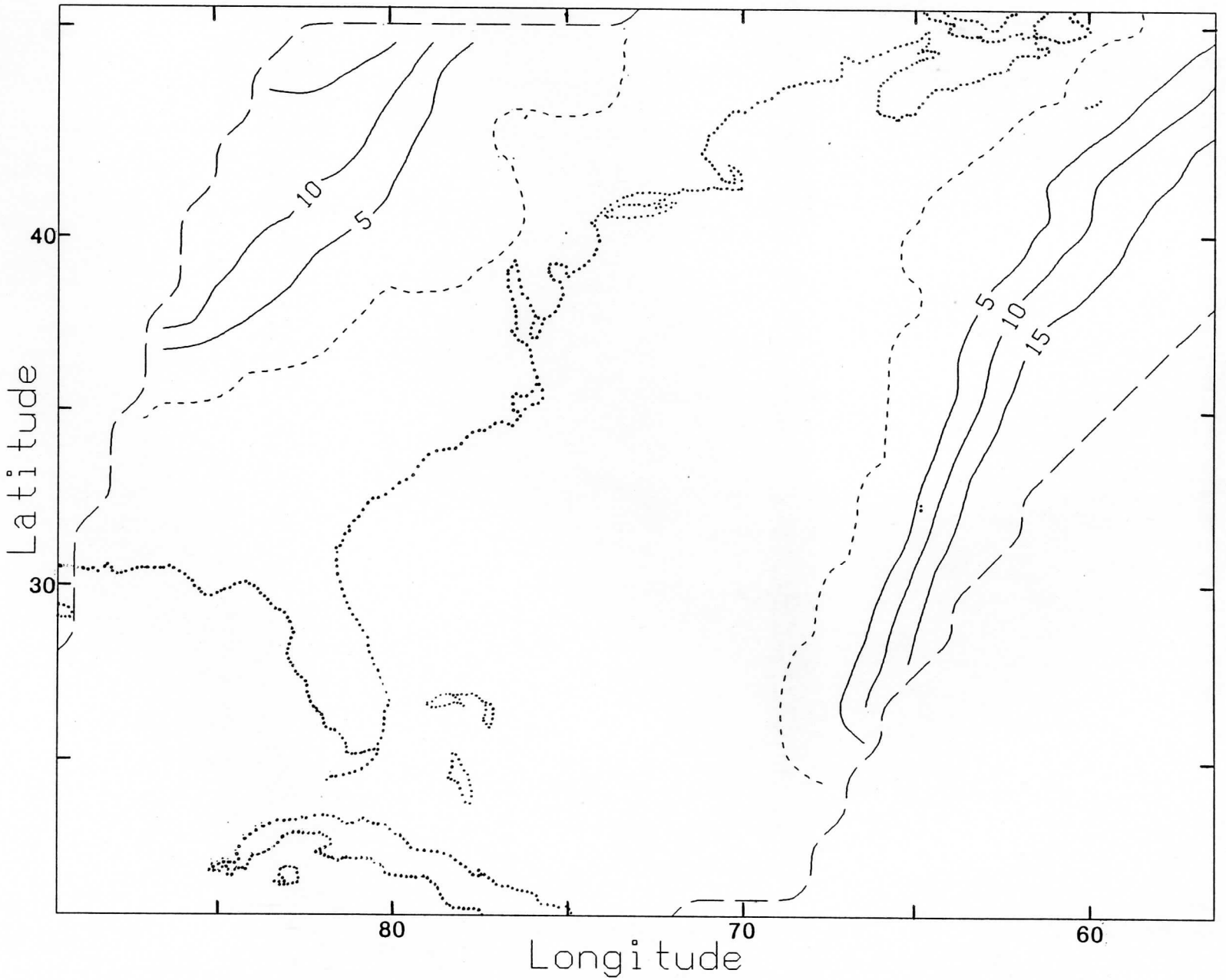
1/24 18-23 GMT
10
5
5
10
15
40
30
Latitude
80
70
60
Longitude

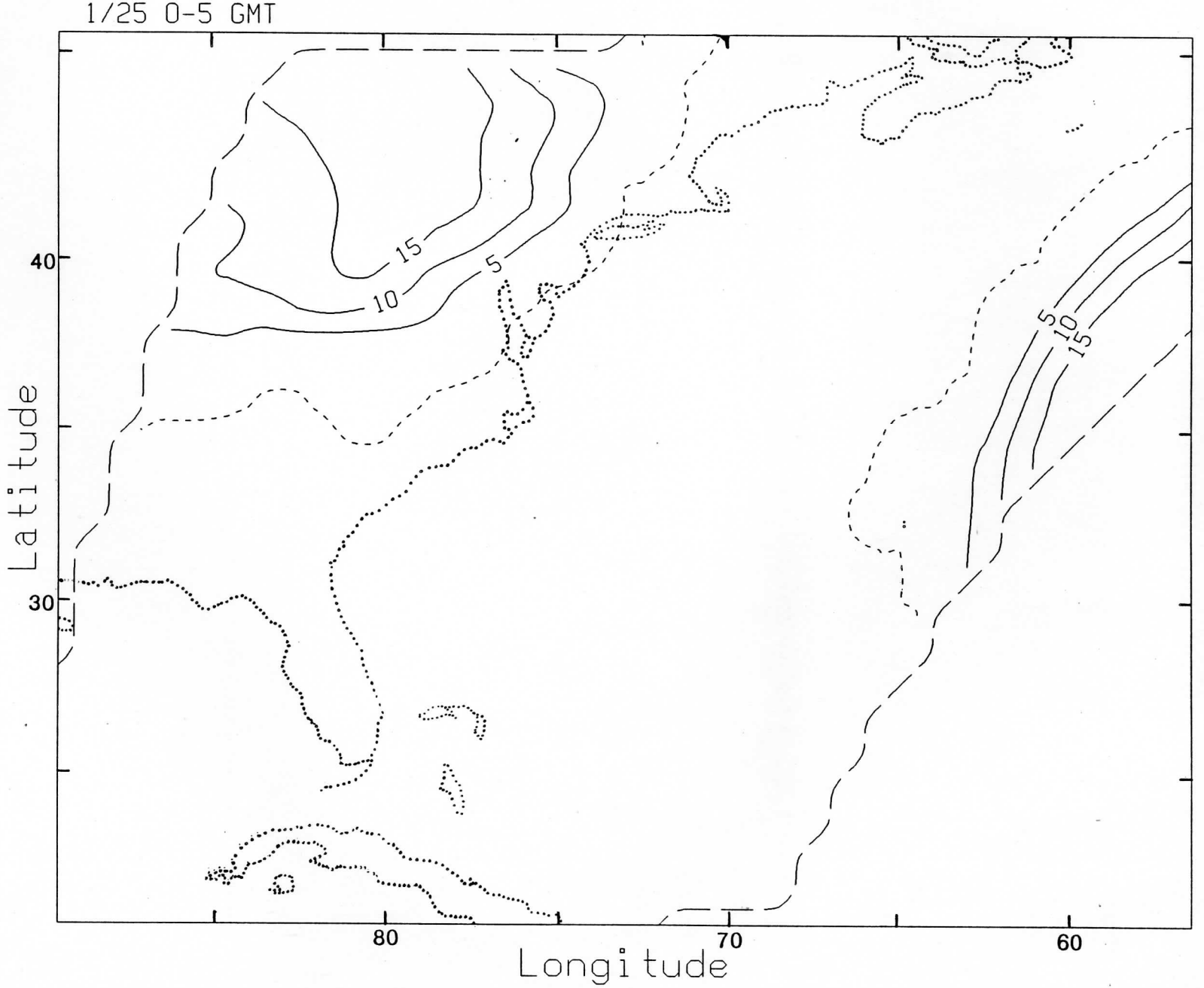
1/25 0-5 GMT
40
30
Latitude
80
70
60
Longitude
15
10
5
5
10
15

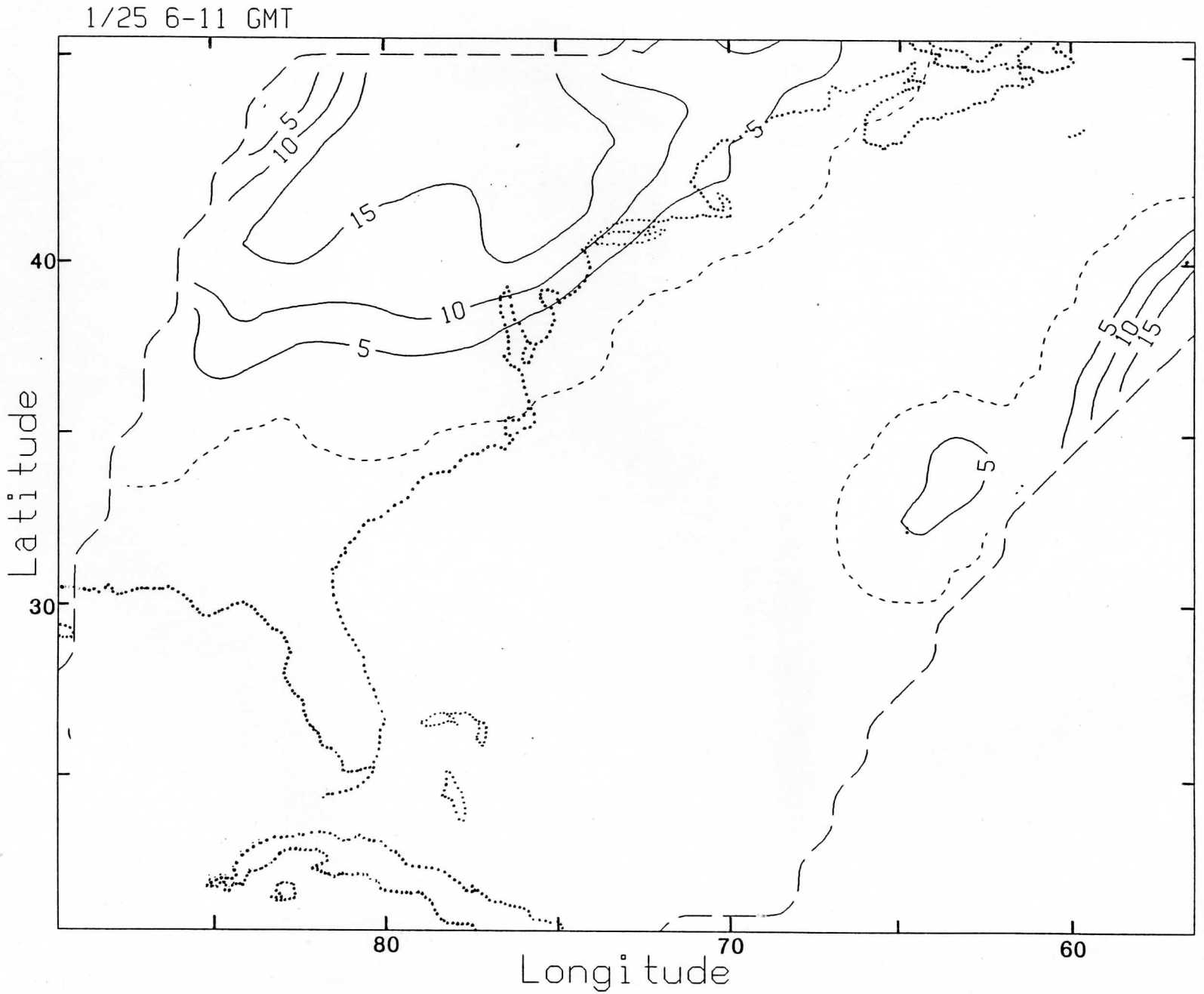
1/25 6-11 GMT
40
30
80
70
60
Latitude
Longitude
5
10
15
5
10
15
5
5
10
15

48

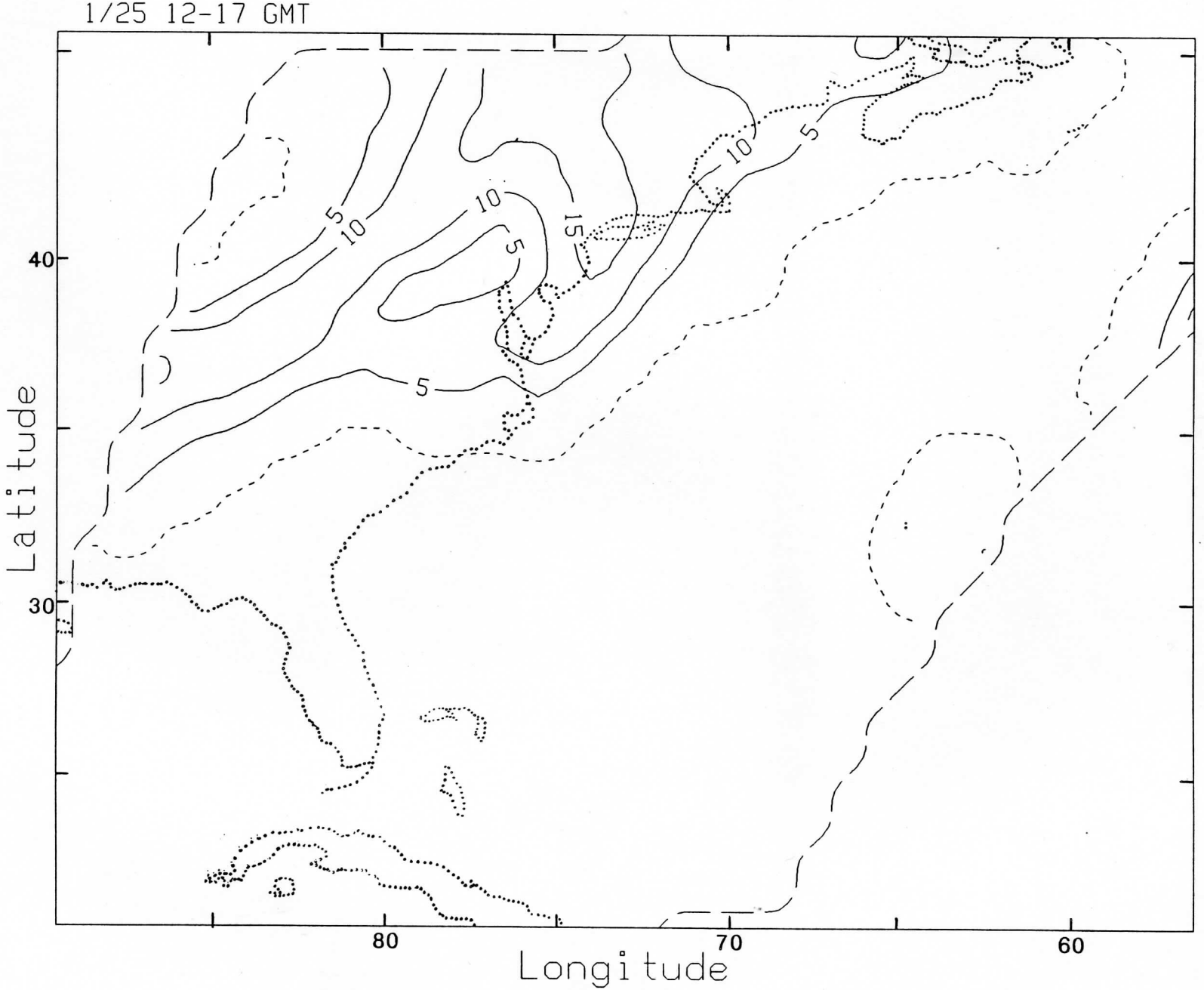
1/25 12-17 GMT
40
30
Latitude
80
70
60
Longitude
5
10
5
10
15
5
10
5

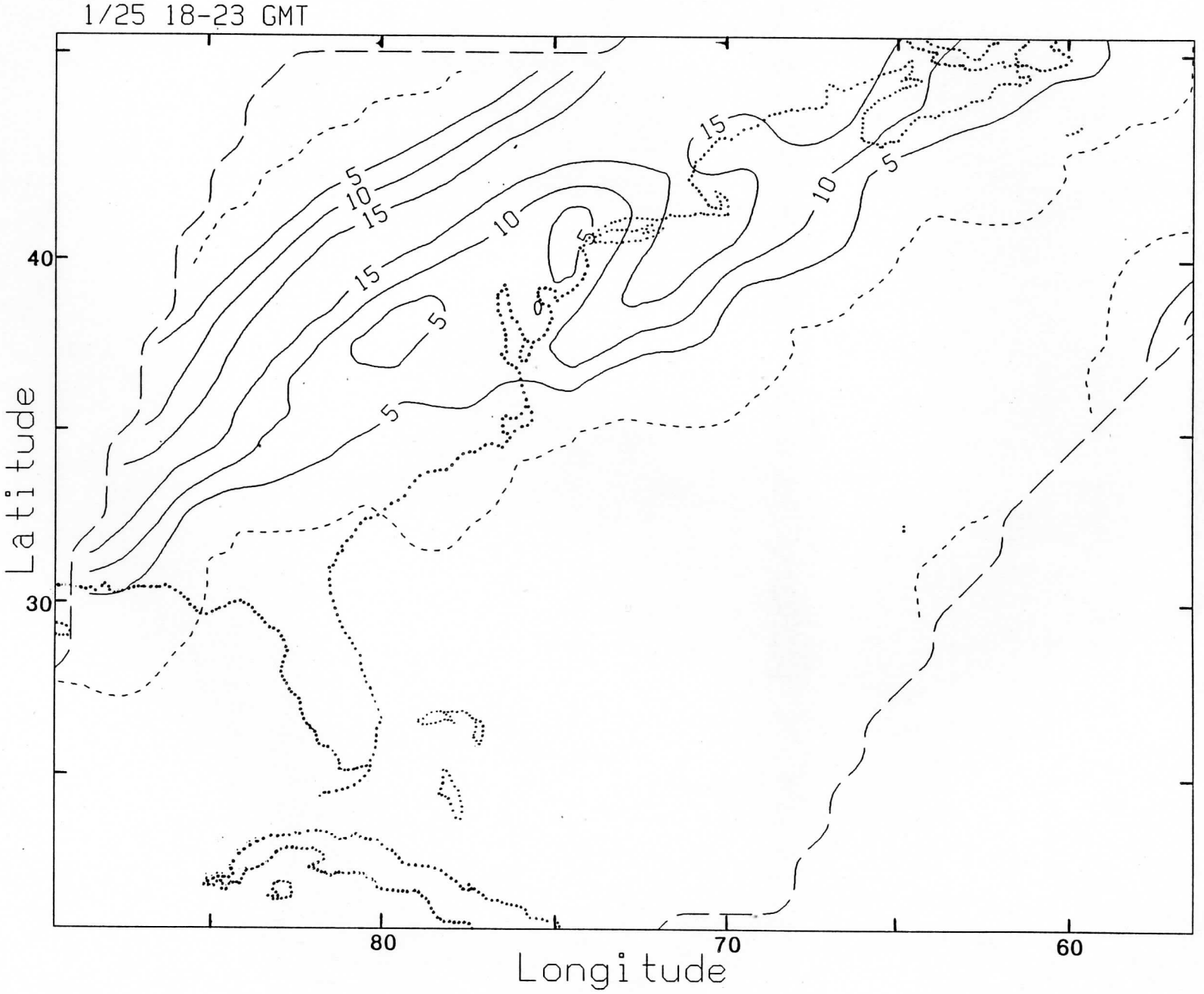
1/25 18-23 GMT
5
10
15
40
30
Latitude
80
70
60
Longitude

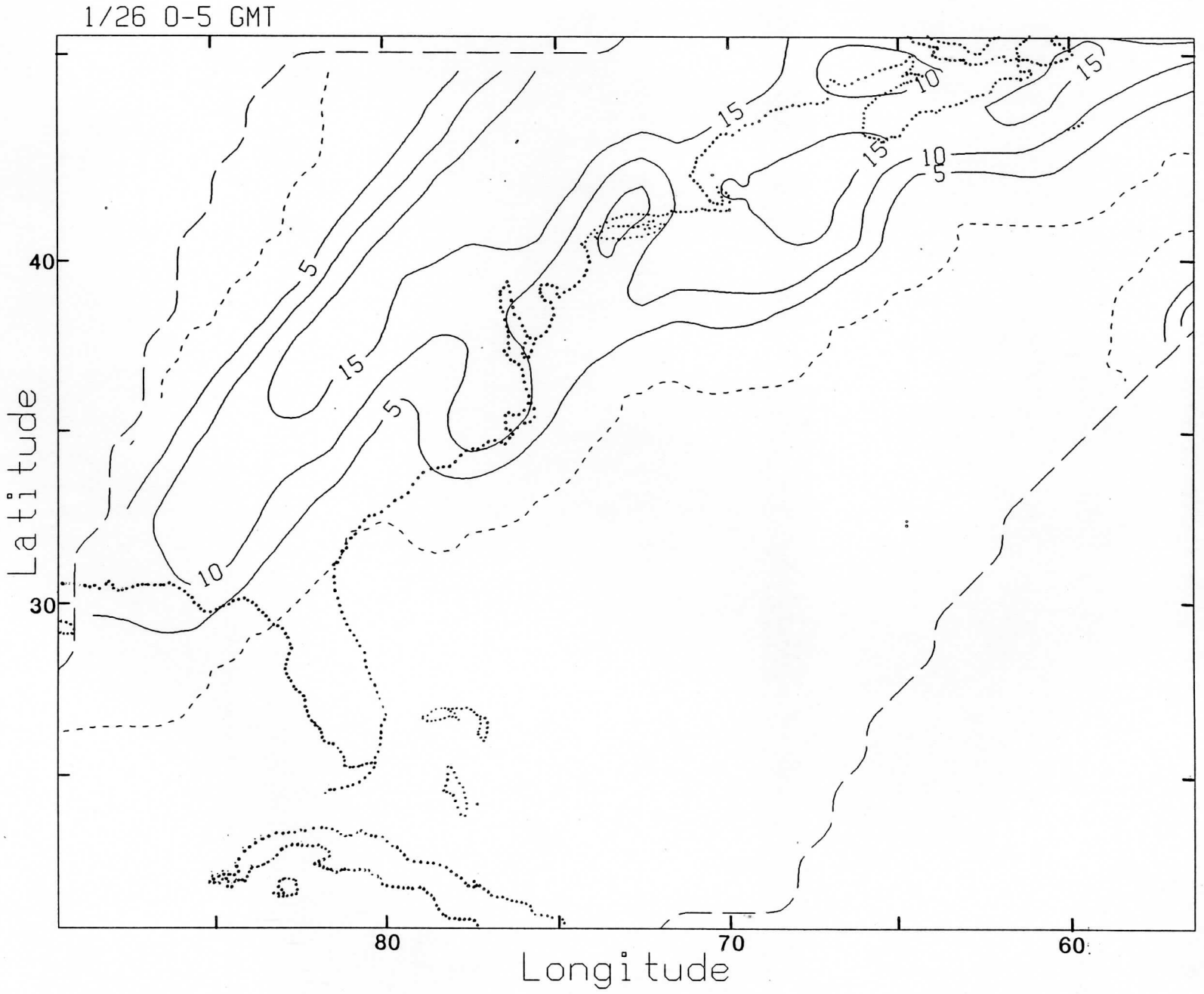
1/26 0-5 GMT
Latitude
40
30
80
70
60
Longitude
5
10
15

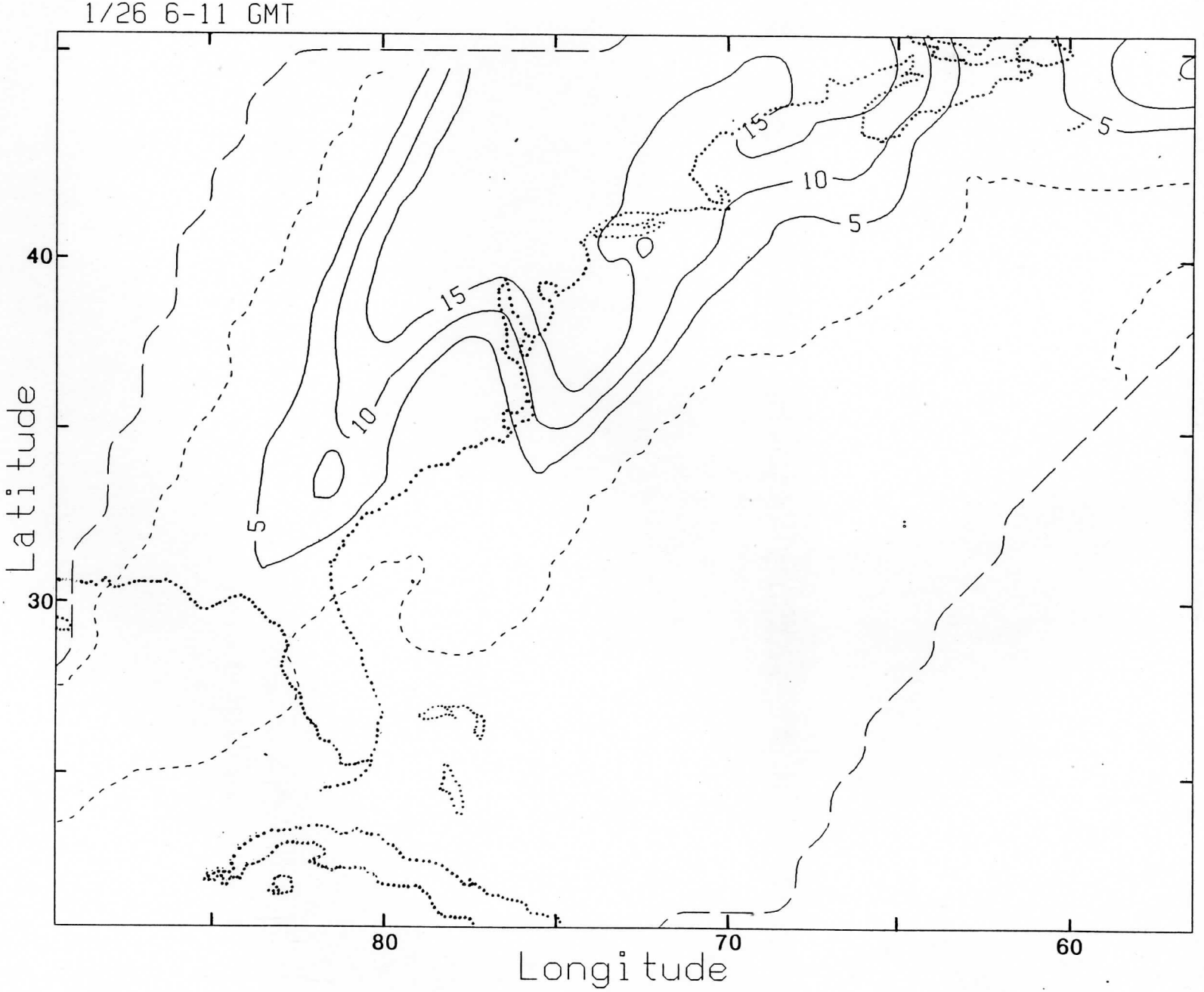
1/26 6-11 GMT
40
30
Latitude
80
70
60
Longitude
15
10
5
0
15
10
5
0
5

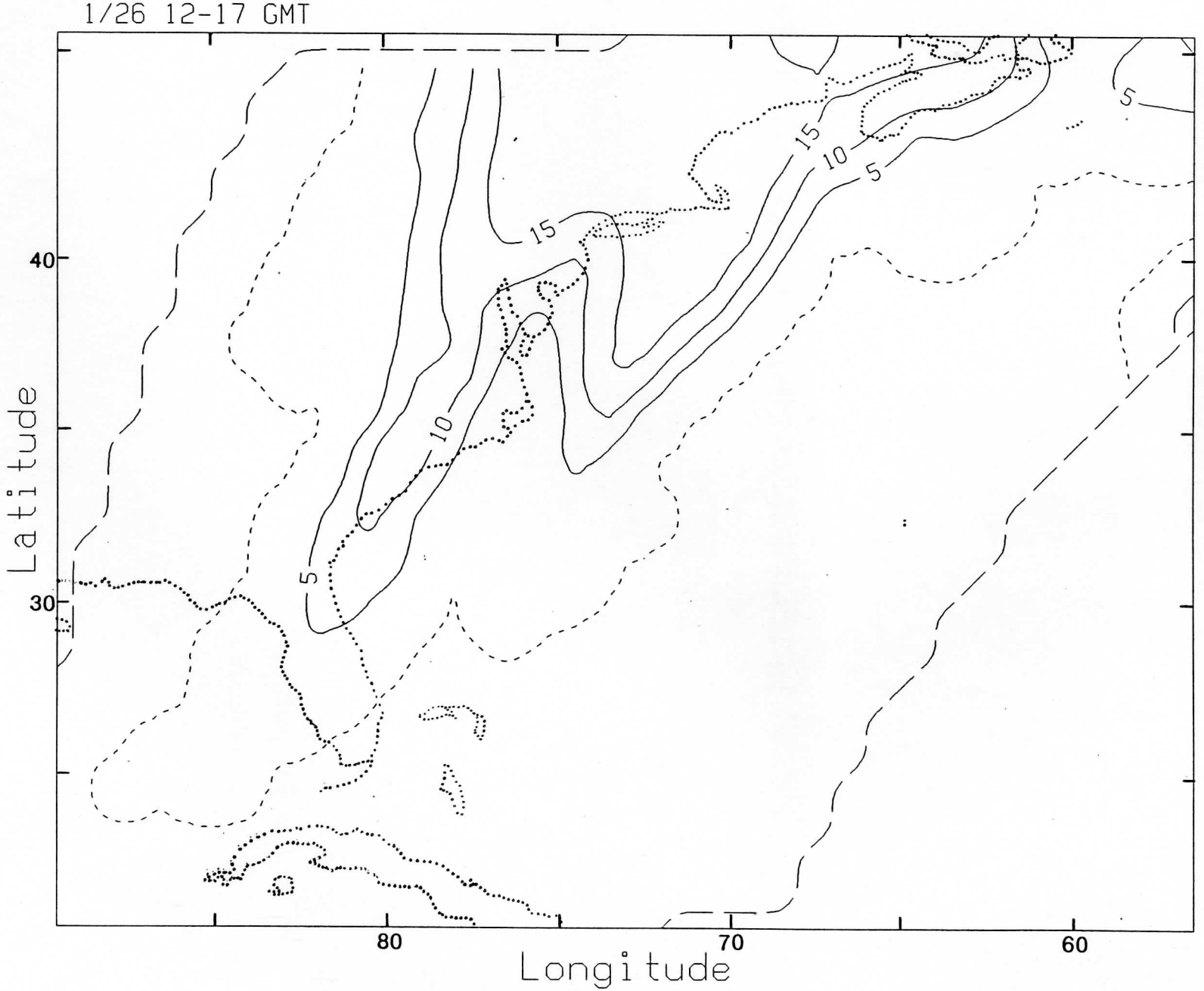
1/26 12-17 GMT
40
30
Latitude
80
70
60
Longitude
5
10
15
5
10
15
5

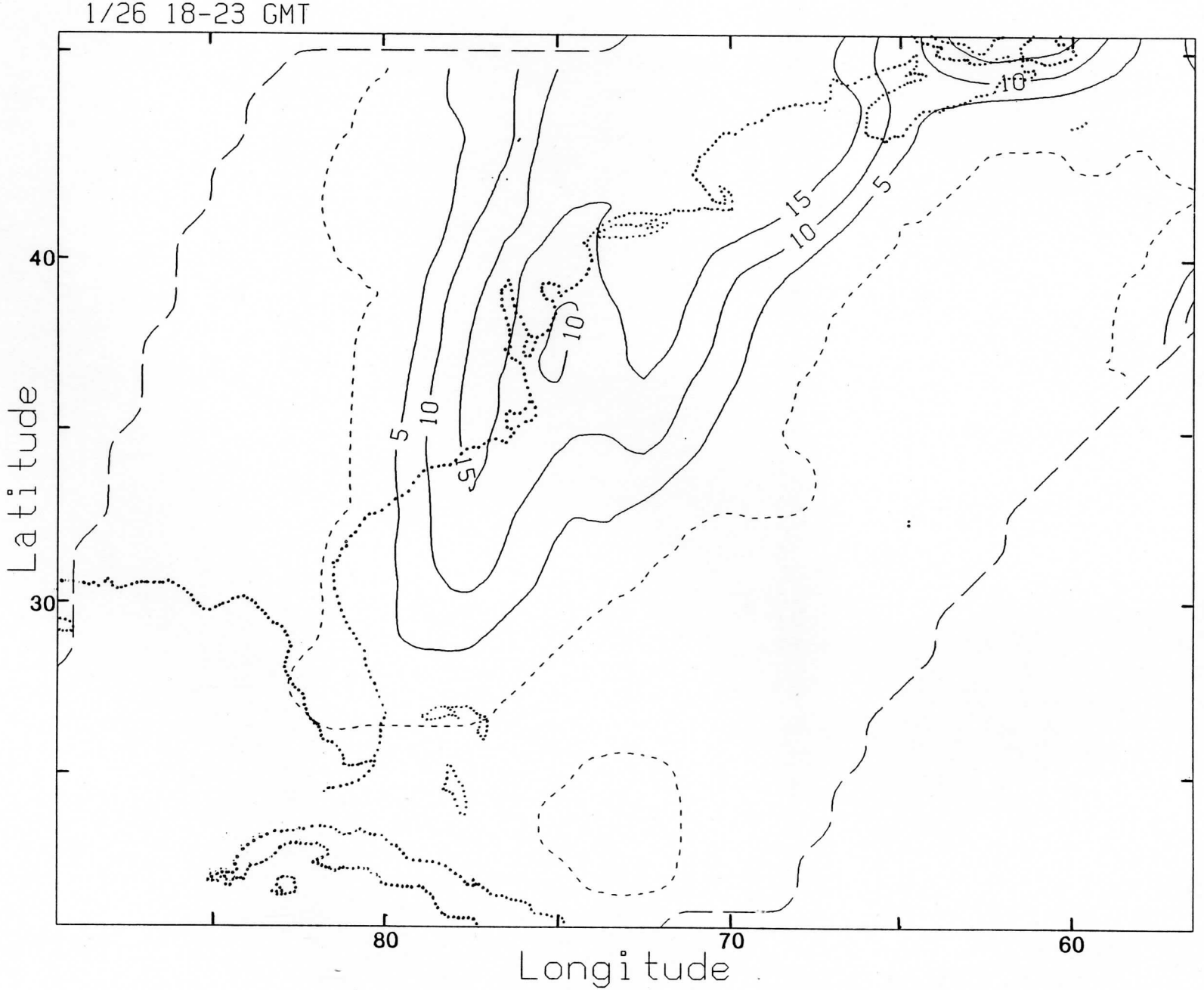
1/26 18-23 GMT
40
30
Latitude
80
70
60
Longitude
5
10
15
10
5
10
10
15

96

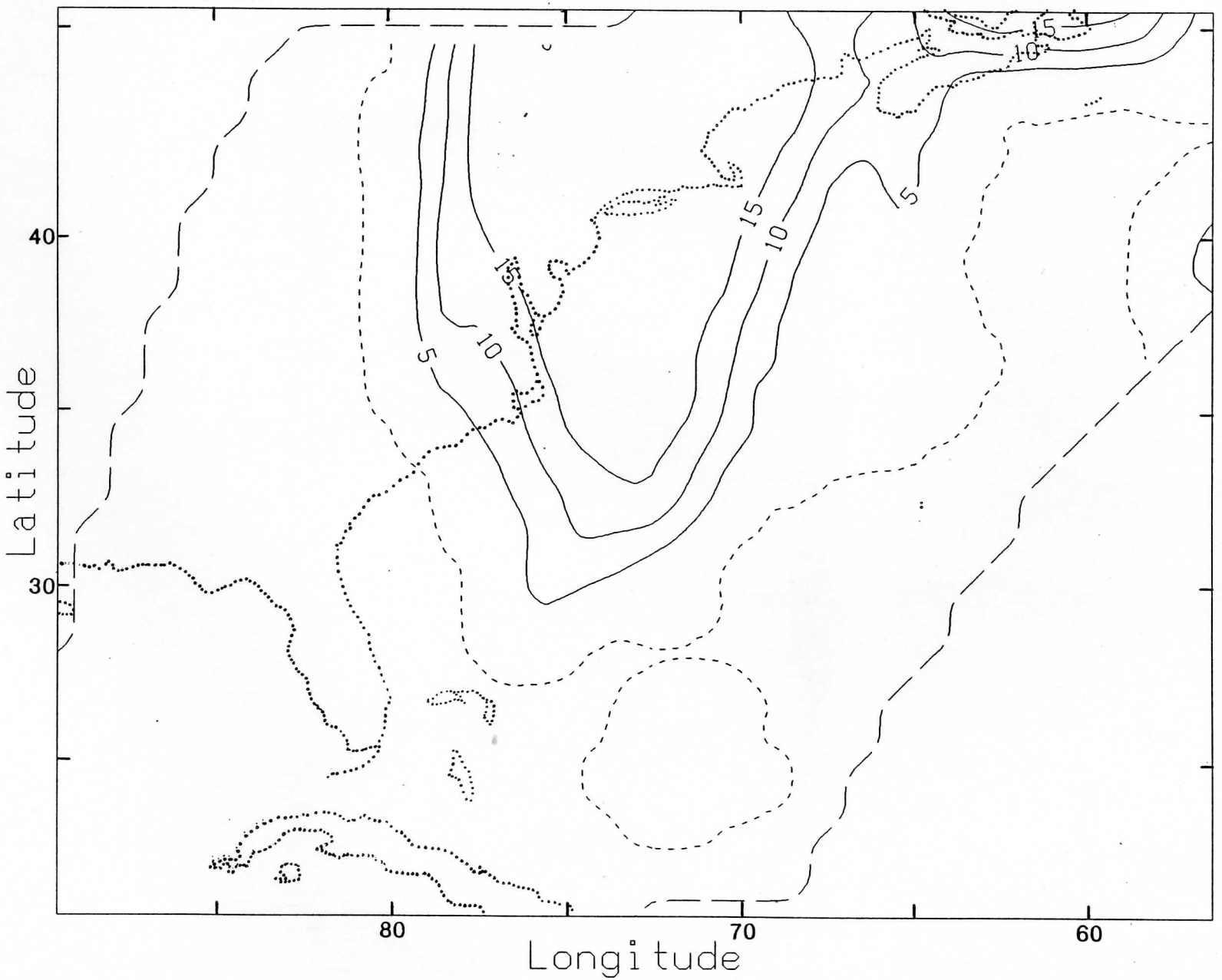
1/27 0-5 GMT
40
30
80
70
60
Latitude
Longitude
5
10
15
5
10
15
5
10
15

16

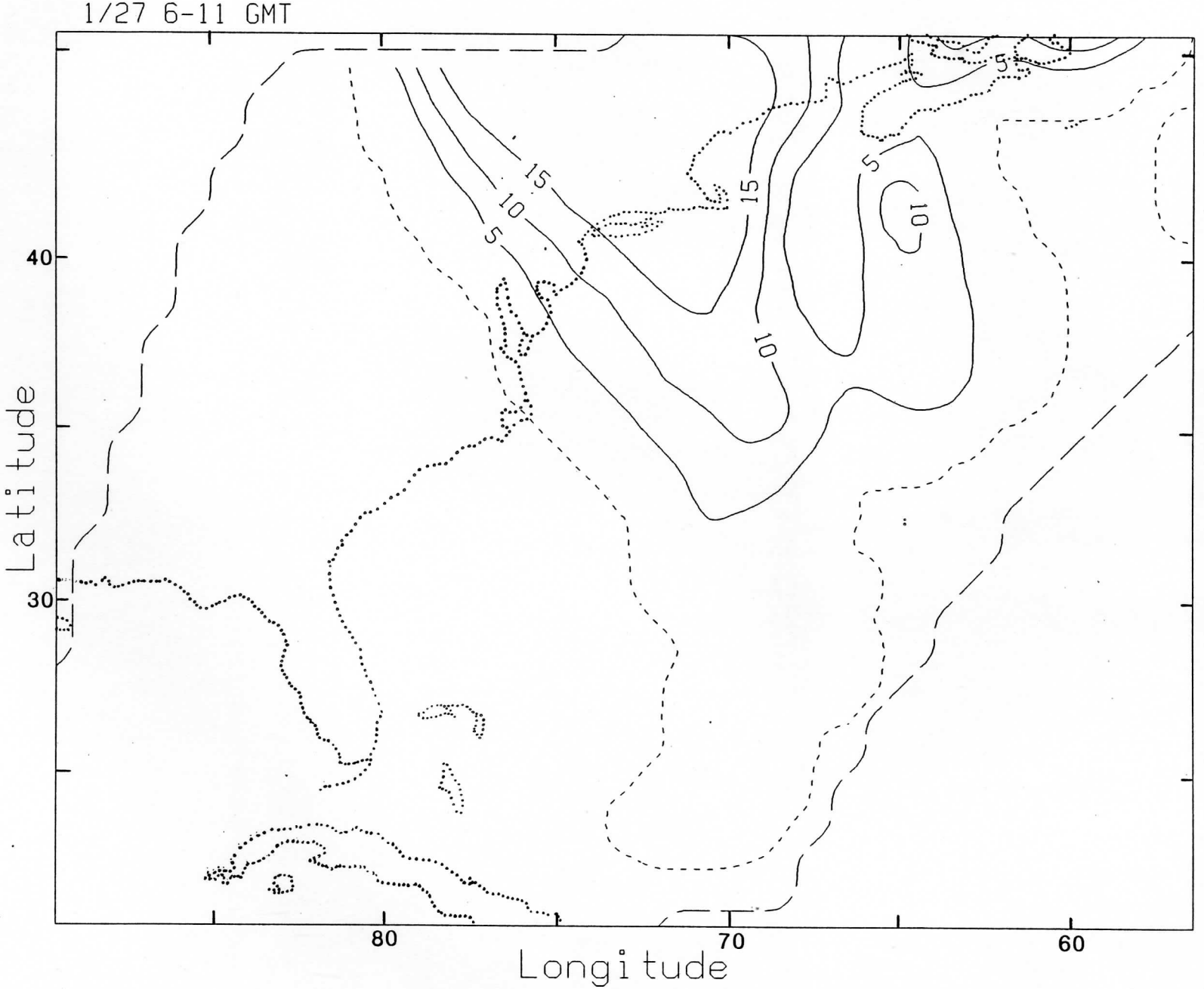
1/27 6-11 GMT
40
30
Latitude
80
70
60
Longitude
15
10
5
15
10
5
5

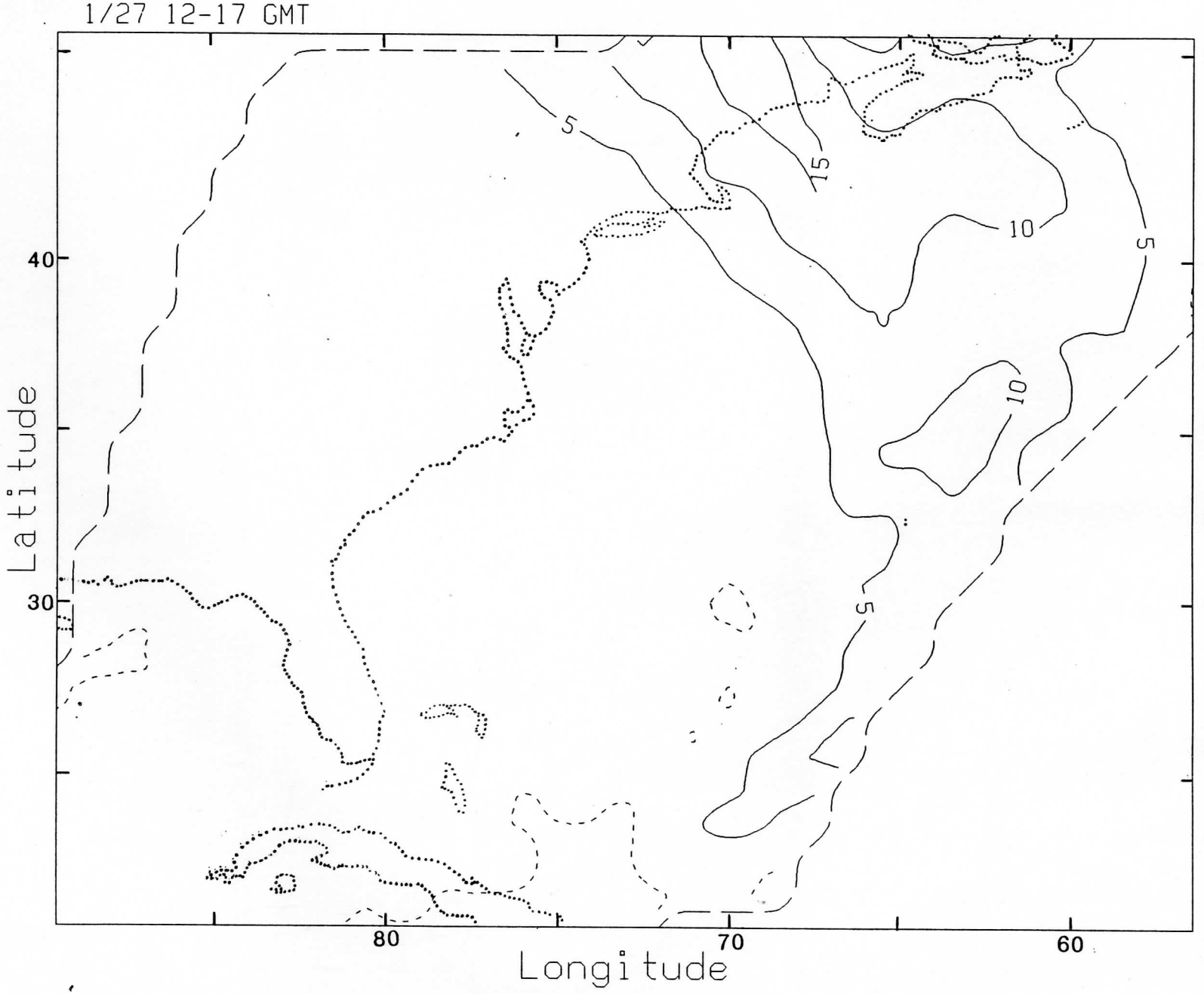
1/27 12-17 GMT
5
15
10
5
10
5
40
30
80
70
60
Latitude
Longitude

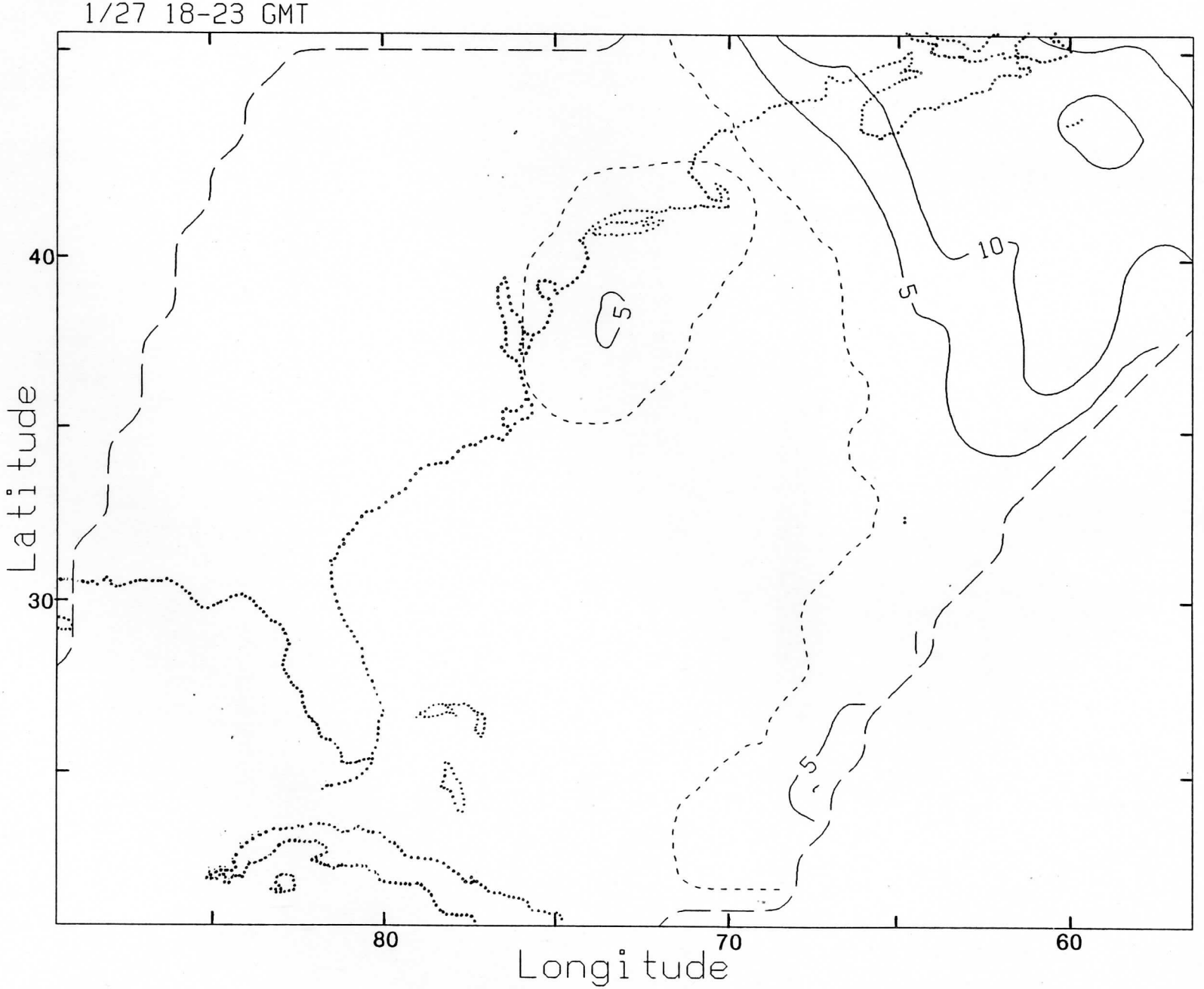
1/27 18-23 GMT
40
30
Latitude
80
70
60
Longitude
5
10
5
5

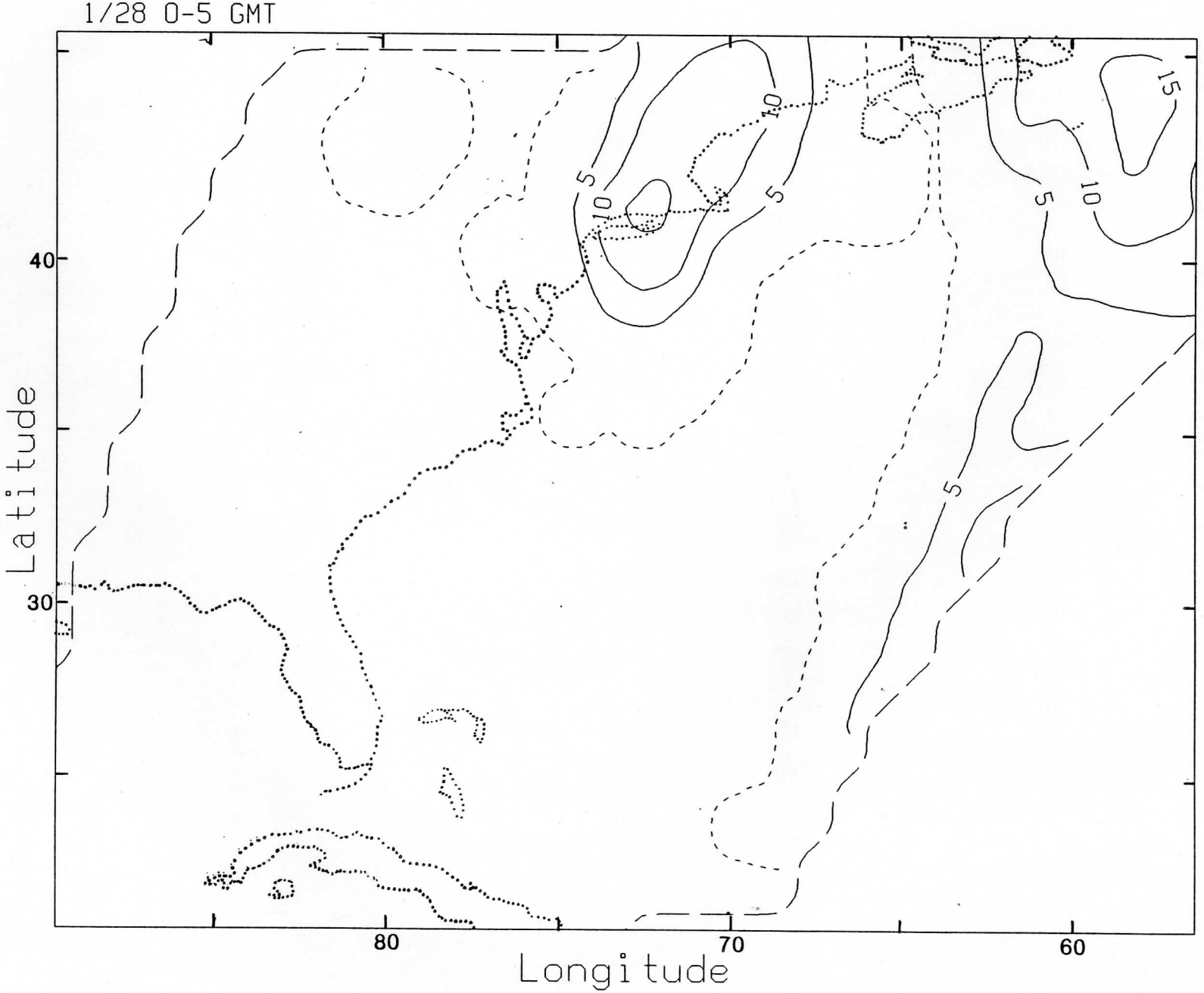
1/28 0-5 GMT
40
30
Latitude
80
70
60
Longitude
5
10
15

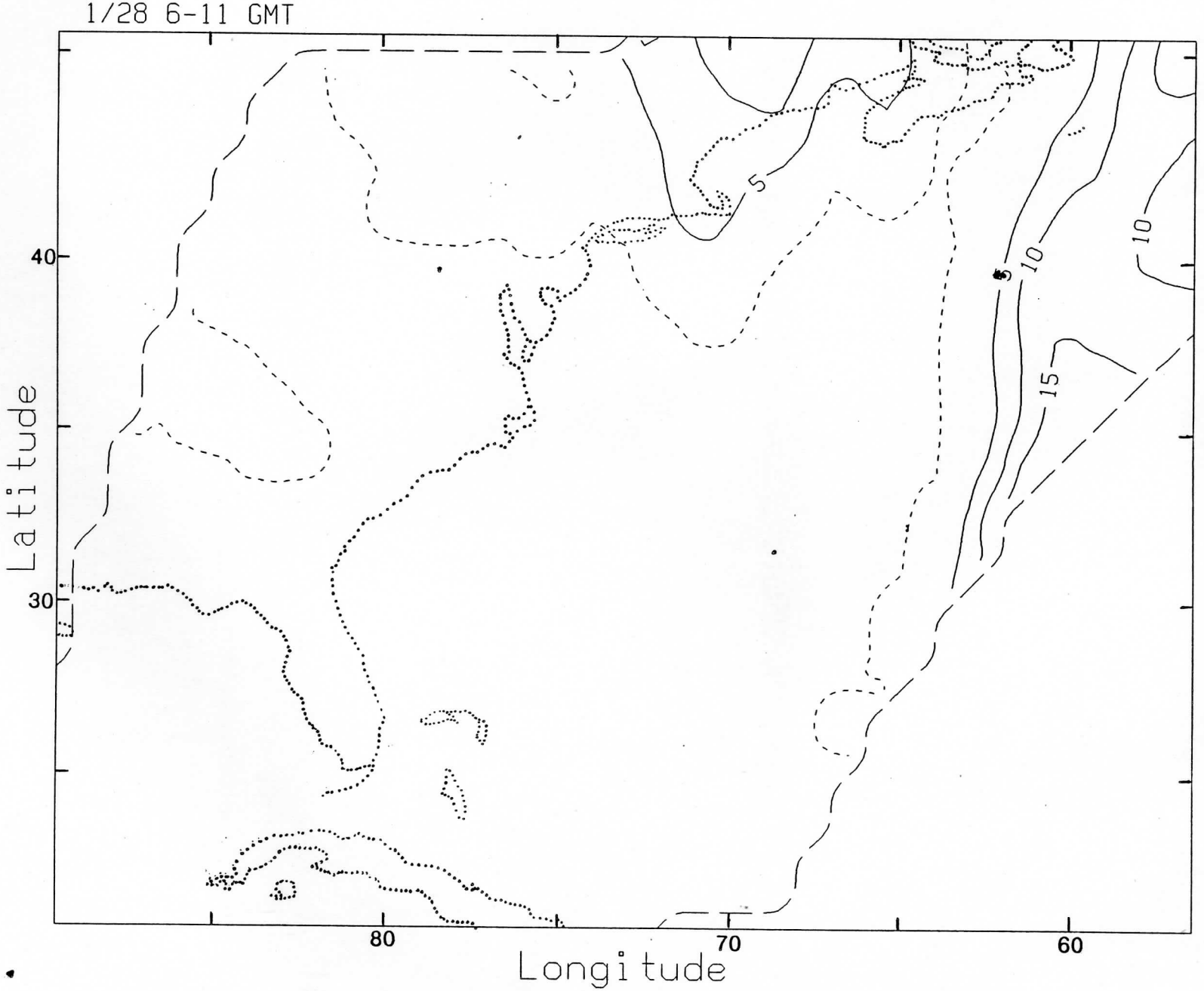

96

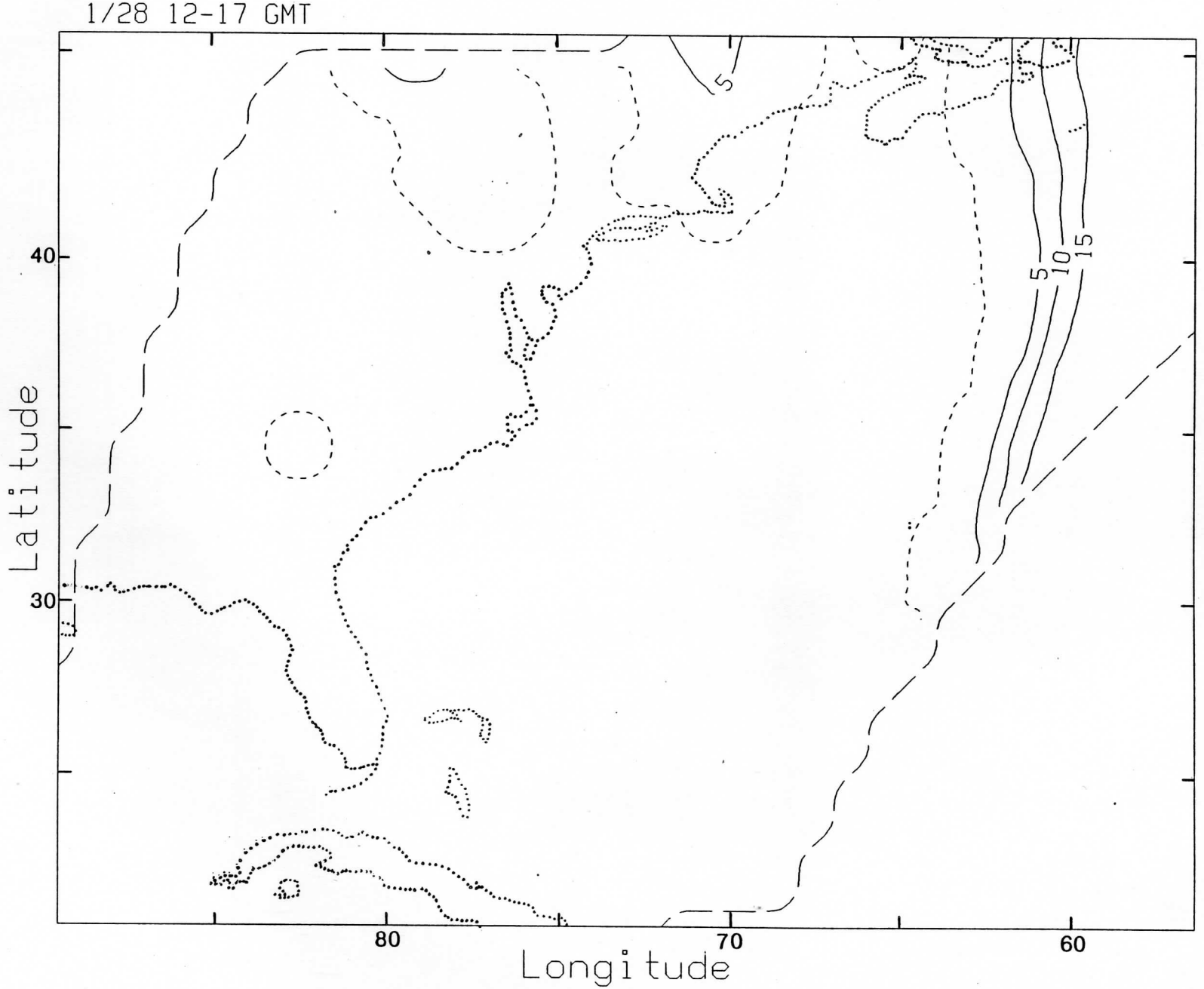
1/28 12-17 GMT
5
5
10
15
40
30
Latitude
80
70
60
Longitude

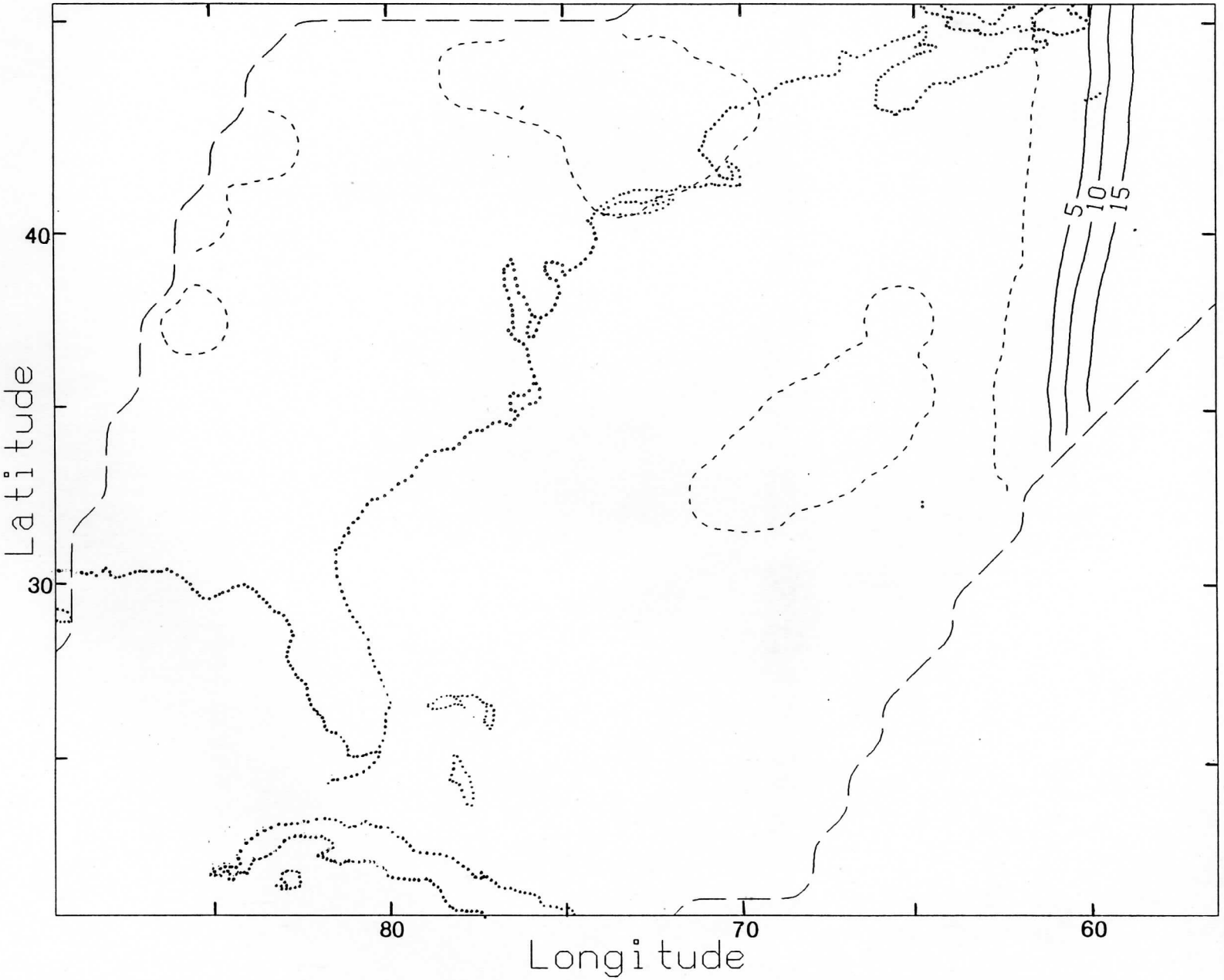
1/28 18-23 GMT
40
30
Latitude
80
70
60
Longitude
5
10
15